

AD-A145 198

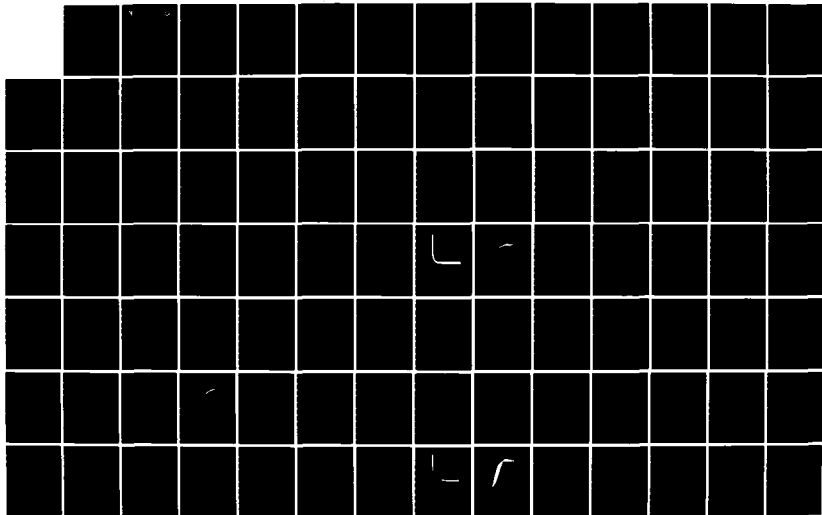
COLLISIONAL EXCITATION CROSS SECTIONS(U) CHEMICAL
DYNAMICS CORP COLUMBUS OH M J REDMON ET AL. AUG 84
AFRPL-TR-84-030 F04611-82-C-0041

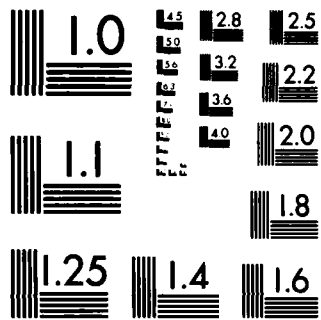
1/2

UNCLASSIFIED

F/G 20/8

NL





MICROCOPY RESOLUTION TEST CHART
NATIONAL BUREAU OF STANDARDS-1963-A



AFRPL TR-84-030

AD:

12

Final Report
for the period
15 June 1982 to
15 April 1984

Collisional Excitation Cross Sections

August 1984

Authors:
M. J. Redmon
L. T. Redmon
B. C. Garrett

Chemical Dynamics
1550 West Henderson Road
Columbus, OH 43220

F04611-82-C-0041

AD-A145 198

Approved for Public Release

Distribution unlimited. The AFRPL Technical Services Office has reviewed this report, and it is releasable to the National Technical Information Service, where it will be available to the general public, including foreign nationals.

DTIC FILE COPY

DTIC
SELECTED
SEP 5 1984

prepared for the:

**Air Force
Rocket Propulsion
Laboratory**

Air Force Space Technology Center
Space Division, Air Force Systems Command
Edwards Air Force Base,
California 93523

84 08 85 024

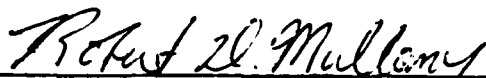
NOTICE

When U.S. Government drawings, specifications, or other data are used for any purpose other than a definitely related Government procurement operation, the Government thereby incurs no responsibility nor any obligation whatsoever, and the fact that the Government may have formulated, furnished, or in any way supplied the said drawings, specifications, or other data is not to be regarded by implication or otherwise, or in any manner licensing the holder or any other person or corporation, or conveying any rights or permission to manufacture, use, or sell any patented invention that may be related there to.

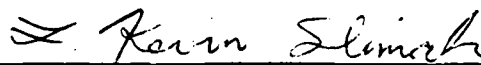
FOREWORD

This final report was submitted by the Chemical Dynamics Corporation, Columbus OH 43220, under Contract No. F04611-82-C-0041, with the Air Force Rocket Propulsion Laboratory, Edwards AFB, California 93523, under Air Force Project Task 305813A1, "Collisional Excitation Cross Sections". This report documents the theoretical calculation of cross sections for vibrational excitation and relaxation of HF, HCl, CO, water, and carbon dioxide upon high velocity collisions with atomic oxygen.

This report has been reviewed and approved for publication in accordance with the distribution statement on the cover and on the DD form 1473.



ROBERT D. MULLANY, A.T., USAF
Project Manager



L. KEVIN SLIMAK
Chief, Interdisciplinary Space Tech Br

FOR THE DIRECTOR



ROBERT L. GEISLER
Chief, Propulsion Analysis Division

REPORT DOCUMENTATION PAGE

1a. REPORT SECURITY CLASSIFICATION UNCLASSIFIED		1b. RESTRICTIVE MARKINGS	
2a. SECURITY CLASSIFICATION AUTHORITY		3. DISTRIBUTION/AVAILABILITY OF REPORT Approved for Public Release; Distribution Unlimited	
2b. DECLASSIFICATION/DOWNGRADING SCHEDULE			
4. PERFORMING ORGANIZATION REPORT NUMBER(S)		5. MONITORING ORGANIZATION REPORT NUMBER(S) AFRPL-TR-84-030	
6a. NAME OF PERFORMING ORGANIZATION Chemical Dynamics	6b. OFFICE SYMBOL (If applicable)	7a. NAME OF MONITORING ORGANIZATION Air Force Rocket Propulsion Laboratory	
6c. ADDRESS (City, State and ZIP Code) 1550 West Henderson Road Columbus, Ohio 43220		7b. ADDRESS (City, State and ZIP Code) AFRPL/DYSO (Stop 24) Edwards AFB, California 93523	
8a. NAME OF FUNDING/SPONSORING ORGANIZATION	8b. OFFICE SYMBOL (If applicable)	9. PROCUREMENT INSTRUMENT IDENTIFICATION NUMBER F04611-82-C-0041	
8c. ADDRESS (City, State and ZIP Code)		10. SOURCE OF FUNDING NOS.	
		PROGRAM ELEMENT NO. 62302F	PROJECT NO. 3058
		TASK NO. 13	WORK UNIT NO. AI
11. TITLE (Include Security Classification) Collisional Excitation Cross Section (U)			
12. PERSONAL AUTHOR(S) Redmon, Michael J.; Redmon, Lynn T.; Garrett, Bruce C.			
13a. TYPE OF REPORT Final	13b. TIME COVERED FROM 82/06/15 to 84/04/15	14. DATE OF REPORT (Yr., Mo., Day) 84/08	15. PAGE COUNT 114
16. SUPPLEMENTARY NOTATION			
17. COSATI CODES		18. SUBJECT TERMS (Continue on reverse if necessary and identify by block number)	
FIELD	GROUP / SUB. GR.	Cross sections Rocket plumes	
07	04	Reaction kinetics Infrared signatures	
20	10	Potential energy surfaces Advanced propellants (over)	
19. ABSTRACT (Continue on reverse if necessary and identify by block number) First principles calculations are reported of high velocity vibrational excitation and relaxation processes in several molecules of importance in plume technology. These involve collisions of atomic oxygen with HF, HCl, CO, water, and carbon dioxide. Cross sections for vibrational excitation and relaxation are reported, along with vibrational relaxation rate constants. The effect of chemical reaction channels in these systems is discussed, and is relatively unimportant except at the highest velocities considered. Translational energies were studied up to 6 eV.			
20. DISTRIBUTION/AVAILABILITY OF ABSTRACT UNCLASSIFIED/UNLIMITED <input checked="" type="checkbox"/> SAME AS RPT. <input type="checkbox"/> DTIC USERS <input type="checkbox"/>		21. ABSTRACT SECURITY CLASSIFICATION	
22a. NAME OF RESPONSIBLE INDIVIDUAL Lt Robert Mullany		22b. TELEPHONE NUMBER (Include Area Code) (805) 277-5244	22c. OFFICE SYMBOL AFRPL/DYSO

Block 18: Halogen oxidizers
Thermochemistry
Vibrational excitation

Molecular collisions
Quantum chemistry
Collision dynamics

Accession For	
NTIS GRA&I	<input checked="" type="checkbox"/>
DTIC TAB	<input type="checkbox"/>
Unannounced	<input type="checkbox"/>
Justification	
By	
Distribution/	
Availability Codes	
Dist.	Avail and/or Special
A/1	



EXECUTIVE SUMMARY

This document reports the results of a program to predict, from first-principles theoretical techniques, vibrational excitation cross sections for HF, HCl, and CO colliding with atomic oxygen and to study vibrational relaxation in these systems and in H₂O and CO₂. This work follows the previous AFRPL contract to obtain theoretical predictions for excitation of H₂O and CO₂ (AFRPL-TR-81-27). The goal of these efforts is to provide reliable theoretical predictions of important kinetic data required as input by plume modelling codes.

Vibrational excitation cross sections have been obtained for these systems over a relative velocity range of 4-10 km/sec. The cross sections are generally small below seven km/sec, but rise exponentially above 10 km/sec to values on the order of 10^{-16} cm². Calculations were done for three different initial angular momenta, and the cross sections are found to be rather insensitive to initial molecular rotation. The final rotational distributions of the diatomics are hot, with the average J being approximately 10 for HF and HCl, and 20 for CO. Chemical reaction results in vibrationally excited OH at the higher velocities. The O+CO exchange reaction leads to considerable vibrational excitation of CO. The rate of vibrational relaxation of the asymmetric stretch mode of H₂O rises to 3×10^{-11} cm³/mol-sec above 10000 K, while the corresponding CO₂ rate is less than 5×10^{-13} . Thus, radiation from the latter process is relatively unimportant in modelling plume intensities for the 4.3 micron band, and combination bands involving asymmetric stretch quanta must be considered.

CONTENTS

<u>Section</u>		<u>Page</u>
1	INTRODUCTION	7
2	TECHNICAL DISCUSSION	9
	2.1 Potential Energy Surfaces	9
	2.2 Fitting Potential Energy Surfaces	13
	2.3 Cross Section Calculations	17
	2.4 The Calculation of Chemical Reaction Rates	22
3	O + HF COLLISIONS	28
	3.1 Potential Energy Surface	28
	3.2 Analytical Fit of the O + HF Potential Surface	35
	3.3 Cross Sections for Excitation of HF by O(³ P).....	46
	3.4 Chemical Reaction in O(³ P) + HF Collisions	55
	3.5 Vibrational Relaxation in O(³ P) + HF Collisions	56
4	O + HCl COLLISIONS	60
	4.1 Potential Energy Surface	60
	4.2 Analytical Fit of the O + HCl Potential Surface	60
	4.3 Cross Sections for Excitation of HCl by O(³ P).....	69
	4.4 Chemical Reaction in O(³ P) + HCl Collisions	69
	4.5 Vibrational Relaxation in O(³ P) + HCl Collisions	74

CONTENTS (Cont.)

5	O + CO COLLISIONS	79
	5.1 Potential Energy Surface	79
	5.2 Analytical Fit of the O + CO Potential Surface	81
	5.3 Cross Sections for Excitation of CO by O(³ P)	88
	5.4 Chemical Reaction in O(³ P) + CO Collisions	88
	5.5 Vibrational Relaxation in O(³ P) + CO Collisions	93
6	DYNAMICAL STUDIES OF O(³ P) + CO ₂ COLLISIONS	96
7	DYNAMICAL STUDIES OF O(³ P) + H ₂ O COLLISIONS	99
8	CONCLUSIONS	103
9	REFERENCES	107

ILLUSTRATIONS

<u>Figure</u>	<u>Page</u>
1 HF Potential Curves for a DZ Basis Set	29
2 Basis Set Effects on HF Potential Curves	30
3 O+HF Potential Surface II for R=1.733 at a CM Angle of 60 Degrees	42
4 O+HF Potential Surface II for R=3.0 at a CM Angle of 60 Degrees ..	43
5 A Contour Plot of the 0-degree O+HF Surface II	44
6 A Perspective Plot of the 0-Degree O+HF Surface II	45
7 A Comparison of 3D versus IOS Cross Sections for O+HF Surface I ..	49
8 Cross Section for v=1 Excitation of HF(J=10) on Surface II	54
9 Cross Sections for Relaxation of HF(v=1) to HF(v=0)	58
10 Rate Constant for Relaxation of HF(v=1) to HF(v=0)	59
11 HCl Potential Curves for a DZ Basis Set	61
12 O+HCl Potential Surface for R=2.465 at a CM Angle of 30 Degrees ..	65
13 O+HCl Potential Surface for R=3.4 at a CM Angle of 0 Degrees	66
14 A Contour Plot of the 0-degree O+HCl Surface	67
15 A Perspective Plot of the 0-Degree O+HCl Surface	68
16 Cross Sections for Vibrational Excitation of HCl(J=10)	73
17 Reactive Cross Sections to Form OH From O + HCl(v=1)	76
18 Cross Sections for Vibrational Relaxation of HCl(v=1)	77
19 Rate Constant for Relaxation of HCl(v=1) to HCl(v=0)	78
20 CO Potential Curve for a DZ Basis	80

ILLUSTRATIONS (continued)

<u>Figure</u>	<u>Page</u>
21 O+CO Potential Surface for R=2.2 at a C.M. Angle of 90 Degrees ...	84
22 O+CO Bond Angle Bending Potential for R(CO)=2.2, R=4.0	85
23 O+CO Surface Contour Plot for a Bond Angle of 127 degrees	86
24 A Perspective Plot of the 127-Degree O+CO Surface	87
25 Cross Section for v=1 Excitation of CO(J=10)	92
26 Cross Section for Vibrational Relaxation of CO(v=1)	94
27 Rate Constant for Relaxation of CO(v=1)	95
28 Rate Constant for relaxation of CO (001)	98
29 Cross Sections for Vibrational Energy Transfer in H ₂ O(001)	101
30 Rate Constant for Relaxation of H ₂ O(001)	102

TABLES

<u>Table</u>	<u>Page</u>
1	Transmission Coefficients for Collinear Reactions at 300 K 24
2	Parameters for O+HF Potential Energy Surface I 37
3	Parameters for O+HF Potential Energy Surface II 38
4	Cross Sections for Excitation of HF($v=0$) to HF($v=1$) on Potential Energy Surface I 47
5	Cross Sections for Excitation of HF($v=0$) to HF($v=2$) on Potential Energy Surface I 47
6	Cross Sections for Excitation of HF($v=0$) to HF($v=3$) on Potential Energy Surface I 48
7	Cross Sections for Excitation of HF($J=0$) on Surface II 51
8	Cross Sections for Excitation of HF($J=5$) on Surface II 52
9	Cross Sections for Excitation of HF($J=10$) on Surface II 53
10	Parameters for O+HCl Potential Energy Surface I 62
11	Cross Sections for Excitation of HCl($J=0$) on Surface I 70
12	Cross Sections for Excitation of HCl($J=5$) on Surface I 71
13	Cross Sections for Excitation of HCl($J=10$) on Surface I 72
14	Parameters for O+CO Potential Energy Surface I 83
15	Cross Sections for Excitation of CO($J=0$) on Surface I 89
16	Cross Sections for Excitation of CO($J=5$) on Surface I 90
17	Cross Sections for Excitation of CO($J=10$) on Surface I 91

Section 1

INTRODUCTION

At altitudes above 90 km, the principal source of infrared radiation from rocket plumes is hyperthermal (4-10 km/sec) collisions of exhaust gas molecules with ambient air species, most importantly $O(^3P)$. These collisions cause increases in the populations of infrared-active molecular states of the exhaust gases, leading to enhancement of the infrared signature.¹ Kinetic information about these processes is generally unavailable, and, as a result, several experimental programs have been funded by USAF and DARPA during the past decade to measure collisional excitation cross sections of two of the processes thought to be important contributors to the plume intensity, the relaxation of the asymmetric stretch bands of H_2O (2.3 microns) and of CO_2 (4.3 microns). In spite of the considerable effort expended, the experimental results to date are sparse,² indicating the difficulty of obtaining data of this type.

To augment the experimental programs, which employed shock tube and molecular beam methods, AFRPL in 1979 sponsored a theoretical program to employ state-of-the-art methods of computational chemistry to obtain the required asymmetric stretch cross sections for H_2O and CO_2 .³ These studies were based on ab-initio (first-principles) methods that evolved during the last decade into predictive tools of high reliability. This 12 month program demonstrated that the cross sections of interest could be obtained for modest cost from theoretical techniques.

As an added bonus, such calculations yield predictions for most energetically accessible processes, information not likely to be forthcoming from experimental programs because of the difficulty in resolving collision

induced transitions among high-lying states. Not only is a theoretical approach useful for rapidly obtaining data for collisional excitation, relaxation and recombination, but once obtained, the wealth of detail in the results is of value in the interpretation of experimental information as it becomes available and it aids in decisions concerning the selection of future experiments.

This report describes the results of a program to extend the application of the theoretical methods to the prediction of cross section data for other systems thought to contribute to the plume signatures, namely $O(^3P)$ colliding with HF, HCl, and CO. Computational studies of vibrational relaxation of these species is also reported, along with a discussion of the effect of chemical reaction channels on predicted excitation/relaxation rates. The latter has to date been largely ignored. New results for H_2O and CO_2 are presented. Also, results of quantum mechanical calculations for high velocity oxygen atom collisions are reported.

The body of this report is divided into seven parts, the first being an overview of the technical aspects of the theoretical methods employed. This is followed by five sections describing the results of the present studies for collisional excitation of HF, HCl, CO, CO_2 and H_2O . The final section provides a summary of the program, along with an assessment of the capability of the methods employed to contribute to the understanding of fundamental collision processes of importance in the dynamics of high altitude plumes.

Section 2

TECHNICAL DISCUSSION

The theoretical prediction of collisional excitation cross sections consists of three parts:

- (1) calculation of ab-initio data points on the relevant Potential Energy Surface (PES) or Surfaces;
- (2) determination of functional forms suitable for fitting the PES data;
- (3) dynamical calculations and analysis to determine the cross sections.

The reliability of the predicted cross sections is a function of the accuracy of each phase.

This section gives a general description of the methods considered for and employed in this project, including those used to obtain the potential energy surfaces, fit the ab-initio potential data to analytical functions, compute the cross sections, and obtain reaction rates. In our studies we have attempted to first establish the potential capabilities of each of the methods, and then to assess the accuracy of the calculations performed. Most of this examination was done using the O + HF system as an example. In particular, HF (diatomic) potential energy curves were calculated in several different ways and compared, and different dynamical methods were applied to a preliminary OHF surface. These studies are described in the section on OHF.

2.1 POTENTIAL ENERGY SURFACES

Calculations of the dynamical interactions between atoms and molecules usually begin from a knowledge or assumption of the relevant adiabatic potential energy surfaces (PES); i.e., the total electronic energy(ies) of

the system as a function of its nuclear geometry. Over the years many theoretical methods have been employed to obtain the PES. Before the development of high-speed computers, researchers often resorted to semi-empirical methods in order to afford the large number of calculations required, particularly for larger systems since the number of degrees of freedom is $3N-6$ where N is the number of nuclei. However, it is generally accepted that these methods parameterized from atomic data yielded surfaces of limited accuracy.

Most quantitative theoretical studies today are based on ab-initio methods, which can be pursued to increasing levels of accuracy, thereby providing useful estimates of the errors at preceding levels. The most well-known ab-initio method is the LCAO-SCF or Hartree-Fock (H-F) method.⁴ In this procedure the wavefunction for the system is expressed as a determinant of one-electron orbitals formed from linear combinations of orbitals centered on each of the nuclei. The Hartree-Fock solution is a "variational" one; i.e., for a given set of atomic orbitals ("basis set"), it yields the lowest energy possible for a single-determinant wavefunction. A given calculation can be improved by enlarging the basis set. In principle, this process can be repeated until there no longer is a significant lowering of the energy and the "H-F limit" is obtained. Although this is often not practical, the magnitude of the effects of a given change can be a useful measure of accuracy.

The range of applicability of single-determinantal methods can be extended somewhat by use of the Unrestricted-Hartree-Fock (UHF) method. UHF assumes that the orbitals for alpha and beta electrons are not the same spatially and optimizes them separately. This usually permits the

calculation of improved potential energy curves for the breaking of single bonds. However, since a single determinant is not generally capable of describing spin states correctly, the UHF solution is often "spin-contaminated"; i.e., it is actually a linear combination of different multiplets. Because this mixture of states can vary as the geometry of the molecule changes, the resultant PES can have an incorrect shape, even though the calculation is variational. Thus, there can be two types of deficiency in the PES: that from the use of a finite basis set and that from the neglect of correlation.

Theoretically, the correlation energy is defined to be the difference between the Hartree-Fock energy and the exact one (within the basis).⁵ This difference arises from the probabilistic nature of the true wavefunction. When a method allows for the possibility that the electrons might at times occupy orbitals other than those of the H-F configuration, it introduces correlation. This flexibility in the description of the wavefunction results in a lowering of the total electronic energy from the SCF energy.

The conventional method of obtaining correlated electronic PES's is the configuration interaction (CI) method.⁶ When increasing numbers of determinants of orbitals representing excited states, usually with respect to the SCF determinant, are included in the description of the wavefunction, the CI method converges monotonically (from above) to the basis-set-limited exact electronic energy (i.e., the "full CI" limit). The rate and/or manner of convergence is a function of the orbitals used. The incompleteness of the basis set is an additional problem.

Other methods, such as diagrammatic many-body perturbation theory (MBPT)⁷, can also be used to obtain correlated surfaces. As higher-order

perturbations are included, the energy (for systems for which a single determinantal starting point is adequate) converges to the same (full CI) limit, although not usually monotonically since the MBPT energy does not include certain spurious positive terms present in nonfull CI energies that are cancelled as the full CI is reached and are responsible for the monotonic convergence. However, recognition of these terms makes it possible to approximately correct and improve the nonfull CI energies.⁸ Like CI calculations, the convergence of perturbation calculations is dependent on the orbitals used. Hartree-Fock orbitals have the property of reducing the number of diagrams to be evaluated, but they may be poor zeroth-order descriptors for many systems. At the present, perturbative methods based on more than a single determinant are being developed.⁹ However, they are not at a stage readily applicable for calculating entire PES's.

The main advantage of multideterminantal methods is that proper spin eigenfunctions and, thus, correct separated atomic and molecular limits of the PES may be obtained for systems which are not amenable to SCF calculations. Also, in this process, correlation is introduced, and more reliable potentials may be obtained. In addition to CI, another method with this ability is the multiconfiguration-SCF (MCSCF) method.¹⁰ In this procedure, both the orbital coefficients and the correlation coefficients within a limited CI space are varied and iterated to convergence. I.e., within the basis set, the orbitals used for the CI are the optimal ones. Because of its multideterminantal feature and its optimal variational character, the MCSCF method is particularly well suited for the description of reactive systems and was selected as the primary method for our calculations.

2.2 FITTING POTENTIAL ENERGY SURFACES

Once the adiabatic potential energy surface has been computed, it is necessary to obtain an accurate analytical representation suitable for dynamics calculations. This is a difficult problem, since the surfaces are multidimensional in the nuclear coordinates. The shapes of the surfaces can vary drastically from one region of geometric space to another, particularly near a saddle point.

Simple functional forms with only a few adjustable parameters, such as LEPS functions, are widely used in dynamical calculations.¹¹ The ordinary LEPS function can be expressed as

$$V_L = Q_1 + Q_2 + Q_3 - \left(\frac{1}{2} [(U_1 - U_2)^2 + (U_1 - U_3)^2 + (U_2 - U_3)^2] \right)^{\frac{1}{2}} \quad (1)$$

where Q_i and U_i are "coulomb" and "exchange" terms, terminology left over from the original application to three monovalent atoms. For such a system, these integrals can be expressed in terms of the lowest singlet and triplet diatomic potential curves

$$\begin{aligned} Q_i &= \frac{1}{2} ({}^1E_i + \Delta_i {}^3E_i) \\ U_i &= \frac{1}{2} ({}^1E_i - \Delta_i {}^3E_i) \end{aligned} \quad (2)$$

The parameter Δ_i is referred to as the Sato parameter, and is a function of the overlap between atomic orbitals on the two centers

$$\Delta_i = (1 - S_i) / (1 + S_i) \quad (3)$$

The overlap integral S_i theoretically varies from 0 to +1, although when used as an adjustable parameter negative values are sometimes seen. In its simplest form, S_i is taken as constant with internuclear distance.

The singlet and triplet curves are usually represented by Morse and antimorse functions since they can be constructed from just a few pieces of experimental data, namely the dissociation energy, the equilibrium

internuclear separation, and the harmonic force constant. These curves are usually written in the following form:

$$\begin{aligned} {}^1E(\Delta r) &= D_0 \{ \exp(-2\alpha\Delta r) - 2 \exp(-\alpha\Delta r) \} \\ {}^3E(\Delta r) &= D_0 \{ \exp(-2\alpha\Delta r) + 2 \exp(-\alpha\Delta r) \} \end{aligned} \quad (4)$$

where $\Delta r = r - r_0$, r_0 being the diatomic equilibrium distance. This form of the LEPS parametrization is not sufficiently flexible for representing ab initio data since only the three triplet curve parameters and the Sato parameter are available for adjustment. (The singlet curve parameters are fixed by the requirement that the potential surface dissociate to the correct diatomic fragments). However, the LEPS functional form can be made more useful by representing the triplet curves and three Sato parameters with more flexible functional forms as will be discussed below.

New and different analytical functions, continually being tested for the representation of potential surface data, must satisfy several requirements. Such expressions must possess continuous first and second derivatives in order to be compatible with dynamical methods used to compute cross sections. They must not be so complicated that their evaluation is inordinately costly. They should be sufficiently flexible that the ab initio potential data can be reproduced to within 1 or 2 kcal/mole, yet they must not produce unphysical features in regions where potential data is not available. In fact, all energetically accessible regions of the surface must be physically correct. Obviously, the simultaneous satisfaction of all of these requirements is one of the more difficult aspects of this program.

Close collaboration of the scientists computing the potential surfaces and those doing the fitting is important, since considerable experience is

required to select the grid of ab initio points so that the number of expensive ab initio calculations is kept to a minimum.

During the last AFRPL program, the present investigators made several contributions to fitting potential energy surfaces.¹²⁻¹⁴ The H₂O 3-atom surface and the O(³P) + H₂O 4-atom surface are among the first examples of attempts to accurately represent a complete ab initio potential surface. The systems studied during the present program offer opportunities to extend and refine these techniques.

For the systems reported here, a suitable starting point for representing the ab initio data is an extended LEPS function. Instead of the simple diatomic curves used above, we write the ground state potential as

$${}^1E(\Delta r) = -D_0 \{ 1 + b_1 \Delta r + b_2 (\Delta r)^2 + b_3 (\Delta r)^3 \} \exp(-b_1 \Delta r) \quad (5)$$

The "triplet" function is expressed as

$${}^3E(r) = a_1 \{ 1 + a_2 r + a_3 r^2 \} \exp(-a_4 r) \quad (6)$$

The Sato parameter offers another opportunity to increase the flexibility of the LEPS. It can be made angle-dependent by expressing it in terms of Legendre polynomials:

$$S(\mu) = \Delta_0 \{ 1 + d_1 P_1(\mu) + d_2 P_2(\mu) + d_3 P_3(\mu) \} \quad (7)$$

where $\mu = \cos \theta$, and Δ_0 is the angle-independent Sato parameter. The use of an angle-dependent Sato function is particularly useful when a molecule has a stable, bent intermediate, or a nonlinear minimum energy path, as does the A'' state of OCO.

A long range term representing the interaction of an open shell atom with a dipole can be added to the LEPS function. It has the form

$$V_{LH} = C_4 \{ 1 - \exp[-\gamma_4(R-R_4)] \} \cos \theta / R^4 - C_6 \{ 1 - \exp[-\gamma_6(R-R_6)] \} / R^6 \quad (8)$$

The exponential part of this expression assures that the LEPS function will not need to offset a large, unphysical attraction for small R .

All of the parameters in the extended LEPS function are optimized with a nonlinear Levenberg-Marquardt algorithm¹⁵. This allows the simultaneous optimization of only a few of the nonlinear parameters at a time; otherwise numerical instabilities result. Thus the fitting of the LEPS requires painstaking iteration to optimize the many nonlinear parameters. Through experience, it is possible to group certain parameters together for simultaneous optimization.

To augment the extended LEPS function, a polynomial 3-body term is employed. It is fit to the difference between the LEPS fit and the ab initio data, and thus represents an error function for the LEPS. This polynomial is represented by the expansion

$$V_3(s_1, s_2, s_3) = \left[\sum_i c_i P_i(s_1, s_2, s_3) \right] \prod_{j=1}^3 \chi_j(s_j) \quad (9)$$

This function is conveniently written in terms of the displacements from some reference point $s_i = R_i - R_{i0}$. The product is a damping function consisting of components

$$\chi_i(s_i) = (1 - \tanh(\alpha_{i0} s_i)) \exp(-\beta_{i0} R_i^2) \quad (10)$$

The linear parameters c_i are adjusted by weighted linear least squares, while the nonlinear parameters in the damping function are individually varied to obtain a smooth 3-body term that goes to zero asymptotically.

2.3 CROSS SECTION CALCULATIONS

The most useful tool for obtaining theoretical cross sections for high energy collision processes is the classical trajectory method. This is the primary approach in the present calculations. However, the most accurate method available for obtaining information about energy transfer in molecular collisions is the quantum-mechanical close-coupling method. In this approach, the wave function for the system is expanded in partial waves (total angular momentum representation), with each term represented as an expansion in products of functions of internal motion, parametric in the scattering coordinate, and translational functions of the scattering coordinate. Because of the rapid growth in the number of coupled equations with energy and system reduced mass, this approach is practical (at present) only for light 3-atom systems at relatively low energies. In spite of this, a number of methods have been developed for handling these coupled equations (some by the present investigators), and at some laboratories the close-coupling method, with its decoupling approximations, is a common research tool. Approximate decoupling methods which greatly reduce the number of rotational channels needed in a calculation have been developed.¹⁶⁻²⁵ The j_z -conserving centrifugal sudden approximation¹⁸⁻¹⁹ assumes that the orbital angular momentum is conserved and that the centrifugal potentials for the orbital motion are degenerate. The energy sudden approximation²¹⁻²² assumes that rotational angular momentum is conserved and that the centrifugal potentials for the rotational motion are degenerate. In the rotational infinite-order-sudden approximation²⁶ (IOS) these two approximations are combined to completely decouple the rotational motion from the vibrational and translational motions. The assumptions inherent in IOS are most valid

for systems in which the relative translational energy is much larger than the energy spacing between rotational states.

The IOS approximation can also be formulated within a purely classical framework²⁷; we will call this the classical infinite-order-sudden approximation (CIOS). Although the computational effort saved by CIOS over the full classical treatment is less than the savings of the quantum mechanical infinite-order-sudden method (QIOS) over full quantum, the classical IOS method is useful for comparative purposes. Since the CIOS and QIOS methods employ the same dynamical approximations (except that one method is quantum mechanical and the other is classical) comparison of inelastic cross sections calculated by the two methods will give a direct estimate of the importance of quantum mechanical effects.

Most previous applications of the IOS method have been to study rotationally inelastic processes (with no change in vibrational state). However, in the current study we are interested in calculating vibrationally inelastic cross sections in atom-diatom collisions. These cross sections are for a specific initial rotational state but are summed over all final rotational states. For this case the cross section can be expressed (quantum mechanically) as a sum over the orbital angular momentum ℓ of opacity functions

$$\sigma_{nn'}^j = \frac{\pi}{k_{jn}^2} \sum_{\ell} (2\ell + 1) P_{nn'}^{j\ell} \quad (11)$$

The opacity function for each value of j and ℓ is obtained by an angular average

$$P_{nn'}^{j\ell} = \frac{1}{2} \int_0^\pi d\gamma \sin\gamma \left| \delta_{nn'} - S_{nn'}^{j\ell}(\gamma) \right|^2 \quad (12)$$

where the S-matrix for each j , ℓ , and γ is obtained by standard techniques of quantum mechanical scattering. In particular, we use the R-matrix

propagation method²⁸ for solving the coupled-channel equations.

Classically, the CIOS cross section is the average over impact parameters of the classical opacity function

$$\sigma_{nn'}^j = 2\pi \int_0^{b_{\max}} db b P_{nn'}^j(b) \quad (13)$$

Comparing equations 11 and 13 gives the relationship between the impact parameter, b , and the orbital angular momentum, ℓ ,

$$\ell(\ell + 1) = 2\mu E_{\text{rel}} b^2 / \hbar^2 \quad (14)$$

where μ is the reduced mass for the relative translational motion, E_{rel} is the relative translational energy, and \hbar is Planck's constant. The classical opacity function is also obtained from an angular average

$$P_{nn'}^j(b) = \frac{1}{2} \int_0^\pi d\gamma \sin\gamma P_{nn'}^j(b, \gamma) \quad (15)$$

where the classical transition probability for fixed b and γ can be obtained from standard quasiclassical trajectory methods.²⁹ We consider two methods of determining $P_{nn'}^j(b, \gamma)$. The first is the standard histogram method in which each trajectory is given unit transition probability for the transition to state n if the final action variable is between $n\hbar$ and $(n+1)\hbar$ (\hbar is Planck's constant divided by 2π) and zero otherwise. The transition probability $P_{nn'}^j(b, \gamma)$ is obtained by an average of this histogram probability over the initial vibrational phase of the diatomic molecule.

The second method employs information-theoretic moments.³⁰ In this method powers of the difference between the final and initial vibrational actions are averaged over the initial vibrational phase of the diatomic molecule; these averaged moments are then used to construct $P_{nn'}^j(b, \gamma)$. The probabilities are obtained by fitting the averaged moments $\langle \Delta^m \rangle$ to the form

$$\langle \Delta^m \rangle = \sum_{n=0}^N (n - n_1)^m P_{nn_1}, \quad m = m_0, \dots, M \quad (16)$$

subject to the constraint

$$\sum_{n=0}^N P_{nn_1} = 1 \quad (17)$$

The probabilities are chosen to be those with the least-biased distribution (in an information theoretic sense) and are expressed as

$$P_{nn_1} = \exp\left(-\sum_{m=m_0}^M \lambda_m (n - n_1)^m\right) \quad (18)$$

For initial vibrational action n_1 we use the first two moments (i.e., $m_0=1, M=2$) and for $n_1 > 0$ we use the first four moments (i.e., $m_0=1, M=4$). Given $\langle \Delta^m \rangle$, equations 16-18 are solved for λ_m for a fixed value of N . The values of λ_m are then converged with respect to increasing N . Equations 16-18 do not necessarily have solutions for a given set of moments. If no solution is found, the number of moments used is decreased by one and a solution is sought for a reduced set of moments. When only one moment is used, we use the second moment (i.e., $m_0=2, M=2$). For this case a solution can always be found.

For processes in which the classical transition probabilities are large, the histogram and moment methods should agree; however for cases where the histogram probabilities are identically zero, the moment methods can give finite probabilities comparable with quantum mechanical transition probabilities. It is for these threshold values of the transition probabilities that we use the moment methods. Comparison of classical moment extrapolations with accurate quantal cross sections within the IOS approximation allows us to eliminate quantal effects for high energy collisions considered in this project (see Section 3.3).

The three-dimensional atom-diatomic molecule collision calculations were performed using the method of Porter, Raff and Miller³¹. In this approach, classical trajectories are integrated using standard techniques; we use a variable step hybrid Gear method to solve Hamilton's equations. However, action variables are calculated by assuming the diatomic molecule is represented by a Morse oscillator. A transformation is made to good action-angle variables to analyze initial and final conditions. Although our potential fits give more accurate representations of the diatomic fragments than do Morse curves, the Morse representations are sufficiently good for these systems that they can be used to analyze the results of trajectory calculations. We do have numerical techniques to determine actions for the exact diatomic fragments, and actually used them for the classical IOS calculations where we needed essentially exact classical results for comparison with the quantal calculations. The classical method used in the four-atom calculations is described in Reference 3, and will not be discussed here.

2.4 THE CALCULATION OF CHEMICAL REACTION RATES

Gas-phase chemical reactions occurring in the flame immediately above the surface of a condensed-phase propellant or explosive play an important role in the combustion of such materials.³¹ The gas-phase reactions control the release of heat from the gas-phase into the surface and thereby greatly influence the initiation of the chemical decomposition of energetic materials. Gas-phase reactions can also occur in high-velocity collisions associated with molecules in rocket exhaust plumes. Information about the overall gas-phase rate constant and heat release can be obtained from experiments; however, the experiments are restricted to those temperature and pressure regimes physically attainable. The modelling of the gas-phase process enables these experimental results to be extended to wide ranges of temperature and pressure. Theoretical methods can provide a means of obtaining thermal rate constants for elementary reaction steps over an extended temperature range, even for reactants which are hard to handle experimentally. In particular, variational transition state theory (VTST) can be used to accurately predict thermal rate constants for gas-phase chemical reactions.³²

The two limiting factors in the accuracy of a calculated rate constant are:

- (1) the accuracy of the potential energy surface (PES);
- (2) the accuracy of the dynamical theory used.

In this discussion we address the accuracy of VTST rather than the accuracy of the PES. Therefore, in all of our comparisons of calculated to experimental rate constants we use a "chemically accurate" PES and for those cases where an accurate PES is not known we compare our approximate

theoretical rate constants to accurate quantum mechanical ones for the same PES.

The two major deficiencies of conventional transition state theory (TST) are:

- (1) the breakdown of the fundamental dynamical assumption of TST;
- (2) uncertainties in the manner in which quantum mechanical effects are included in the theory.

The fundamental dynamical assumption of TST can be stated in classical mechanical terms as follows: any classical trajectory which has flux in the product direction at the transition state will be a reactive trajectory. The conventional choice of the transition state is a dividing surface separating reactants from products, which passes through the saddle point of the PES. Breakdown of the fundamental assumption leads to recrossing of the dividing surface and subsequent overestimation of the reaction rate. In VTST an effort is made to find the dynamical bottleneck of the reaction (i.e., the dividing surface that minimizes the rate constant) and thereby obtain a better estimate of the rate constant.

Canonical variational transition state theory (CVT) is a form of VTST in which an optimized dividing surface is located for each temperature at which the thermal rate constant is calculated.³²⁻³⁴ The ratio of the conventional TST rate constant $k^{\text{TST}}(T)$ to the CVT rate constant $k^{\text{CVT}}(T)$ gives an estimate of the amount of classical recrossing at the conventional dividing surface and offers an estimate of the improvement that can be obtained from variationally locating the dividing surface. This ratio is always larger than or equal to one, and has been found to be as large as a factor of 10,000 for some model systems³⁴ and a factor of 100 for an atom-

transfer reaction on an accurate ab initio PES.³⁵

For systems involving hydrogen atoms at low temperatures (typically 200 to 600 K), quantum mechanical tunneling effects are very important. A consistent method for including tunneling effects in VTST is the vibrationally adiabatic model; this method is valid for systems in which the reaction-path curvature is small.³⁶ The reaction-path curvature is a measure of the amount of bending the reaction coordinate exhibits in going from reactants to products. Reactions involving the transfer of a light atom between two heavy atoms exhibit large reaction-path curvature and for this type of system the vibrationally adiabatic approximation breaks down. A large-curvature tunneling method has been developed which is appropriate for this type of system.³⁵ The vibrationally adiabatic model

TABLE 1. TRANSMISSION COEFFICIENTS FOR COLLINEAR REACTIONS AT 300 K.

System	LAG	accurate
H + BrH	3.8	5.3
H + Cl ₂	1.2	1.2
H + H ₂	7.3	8.7
O + H ₂	7.5	9.4
Cl + H ₂	2.3	3.5
Cl + HCl	9.9	15.9

and large-curvature tunneling method have been unified using a least action principle³⁷; the resulting least-action ground-state (LAG) tunneling method is valid for systems with small, medium, or large reaction-path curvature.

This method has been formulated for polyatomic systems with an arbitrary number of degrees of freedom. To show the validity of the method we compare approximate transmission coefficients to the accurate quantal ones computed on the same PES in Table 1. The transmission coefficient in this case is a multiplicative factor to correct VTST for quantum mechanical tunneling effects.

In summary, variational transition state theory incorporates two important effects which are necessary to accurately predict thermal rate constants:

- (1) Recrossing effects are minimized by variationally locating the dividing surface;
- (2) Quantum mechanical tunneling effects are accurately described by the LAG method.

Both of these effects must be included in the theory to use VTST semiempirically, e.g., to predict high-temperature rate constants from low-temperature ones.

Because of its reliability, VTST was used in this program to obtain reaction rates for oxygen reacting with HF and HCl. These rates were also obtained using classical trajectories, and a comparison of the predicted rates permitted an assessment of the reliability of the trajectory rates; the latter became unreliable at low temperatures for the systems studied during this project.

2.5 THE CALCULATION OF VIBRATIONAL RELAXATION RATES

Rates for excitation and relaxation processes are obtained within the framework of the classical trajectory method by averaging the product of the relative velocity and the cross section over a suitable temperature

distribution function. The methods employed have been reviewed recently by Truhlar and Muckerman for reaction rates²⁹, so we present only a few details here, with modifications of notation to suit our interest in relaxation processes.

The state-selected rate for a collision-induced transition from state (v_i, j_i) to state (v_f, j_f) is given by the multidimensional integral

$$k_{n_i, j_i, n_f, j_f}(T) = \langle v_{rel} \sigma(E_{rel}; n_i, j_i, n_f, j_f) \rangle_T \quad (19)$$

This integral is performed using Monte-Carlo techniques. If we let the collision probability as a function of impact parameter b be represented by the functional

$$P(b) = \int_0^1 d\beta_1 \beta_1 I[\ell(\beta_1)] \quad (20)$$

and relate the orbital angular momentum to a random variable β_1 by the relation

$$\ell = \beta_1 \ell_{max} \quad (21)$$

then the cross section for the process considered is

$$\sigma(E_{rel}; n_i, j_i, n_f, j_f) = \pi b_{max}^2 \frac{1}{N} \sum_{i=1}^N \left(\frac{2\ell_i + 1}{\ell_{max, i}} \right) \sigma_{fi} \quad (22)$$

from which the rate constant is

$$k_{n_i j_i n_f j_f}(T) = \left(\frac{8kT}{\pi \mu} \right)^{1/2} \pi b_{max}^2 \frac{1}{N} \sum \left(\frac{2\ell_{i+1}}{\ell_{max, i}} \right) \sigma_{fi} \quad (23)$$

An analysis of variance gives the following expression for the standard deviation

$$\bar{\sigma} = N^{-1/2} \left\{ \frac{1}{N^2} \left[\sum_{i=1}^N \left(\frac{2\ell_i + 1}{\ell_{\max, i}} \right) \delta_{fi} \right]^2 - \frac{1}{N} \sum_{i=1}^N \left(\frac{2\ell_i + 1}{\ell_{\max, i}} \right)^2 \delta_{fi} \right\}^{1/2} \quad (24)$$

which differs from that obtained with a simple Boolean sampling function for the impact parameter²⁹. Each trajectory is weighted by the factor $(2\ell + 1)/\ell_{\max}$, a form of importance sampling²⁹.

The integral over relative energy is carried out by defining a random variable β_6 as

$$\beta_6 = 1 - (u+1) e^{-u} \quad (25)$$

where $u = E_{\text{rel}}/kT$. This cannot be inverted to yield an analytical expression for u , so the iterative formula

$$u_{i+1} = u_i + \frac{u_{i+1} - (1 - \beta_6) e^{u_i}}{u_i} \quad (26)$$

is derived using a Newton-Raphson method. In practice, we selected the random variable β_6 , iterated Equation 26 to obtain a value of u , and obtained the relative energy for the current trajectory from the relation $E_{\text{rel}} = ukT$.

Section 3

O + HF COLLISIONS

3.1 POTENTIAL ENERGY SURFACE

The basis sets employed for the OHF calculations were based on Dunning's [4s2p] contractions³⁸ of Huzinaga's (11s9p) primitive Gaussian orbitals for second row atoms.³⁹ A [2s]/(4s) contraction was used for H. This basis is referred to as double-zeta (DZ). When polarization functions are added (d's for O or F and p's for H) the basis is called a DZP basis. The exponents for these functions were chosen based on previous experience with correlated calculations.⁴⁰

Figure 1 shows the results of different theoretical methods for determining the potential energy curve for HF using a DZ basis. The trends are similar for DZP. The UHF and UHF-based MBPT curves exhibit humps at intermediate separations. Comparison with experiment shows that these features are not realistic. Potential curves calculated for this system with the MCSCF method exhibit a physically correct shape. Figure 2 demonstrates the effect of polarization functions and the incorporation of electron correlation using the MCSCF method, and shows the capability of obtaining quantitative agreement with experiment.

The MCSCF method gives a realistically shaped curve, even for a DZ basis, although the well-depth is too small. It is important to realize from previous experience that the DZ calculations may also obtain too high an energy for the transition state, for example, for the formation of OH from O + HF. The net result for the difference of these two energies (that of the transition state minus that of the HF equilibrium) can still be a good approximation to the activation energy. Based on this information and

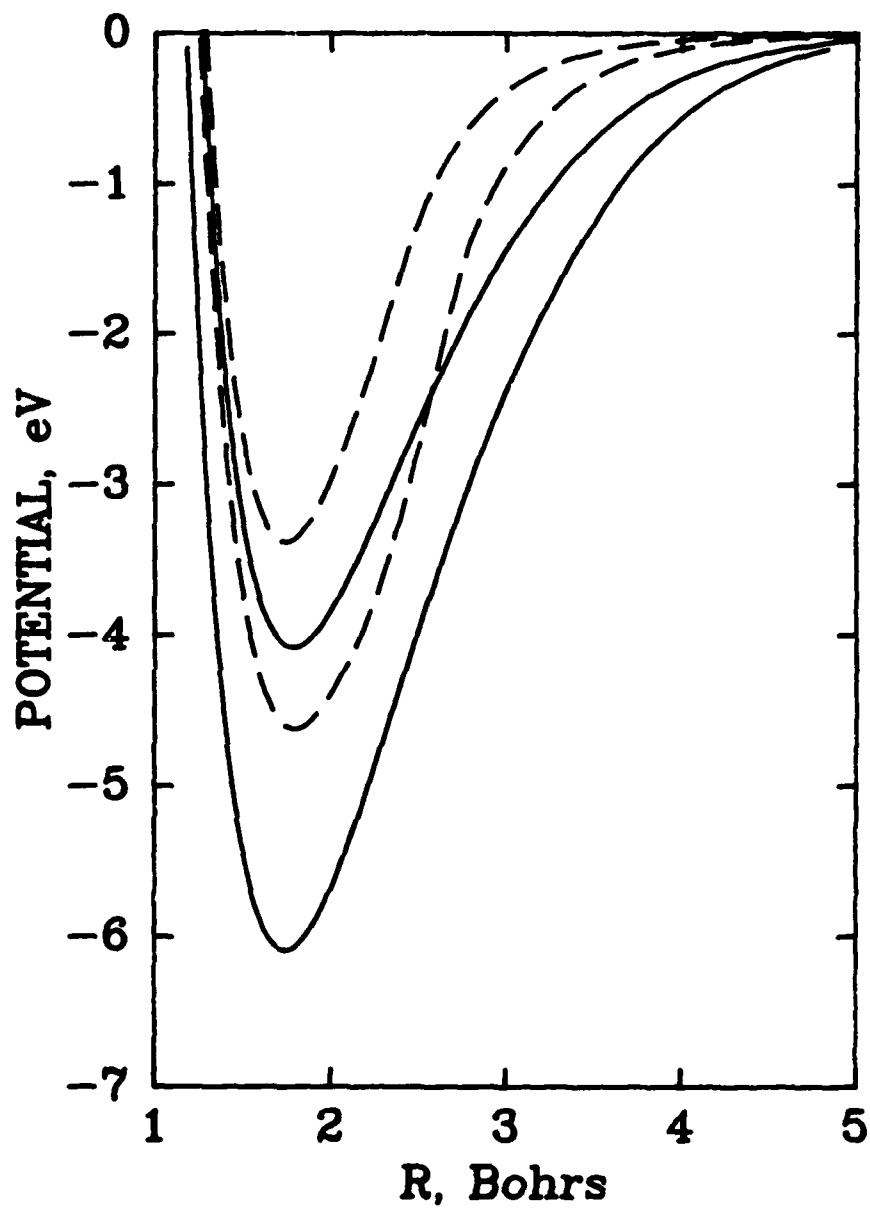


Figure 1. HF Potential Curves for a DZ Basis. The upper and lower Dashed Curves are the UHF and UHF-MBPT Potentials. The upper and lower solid curves are the MC(5) and RKR curves. The ab initio potentials are relative to the respective total energies at $R = 6$.

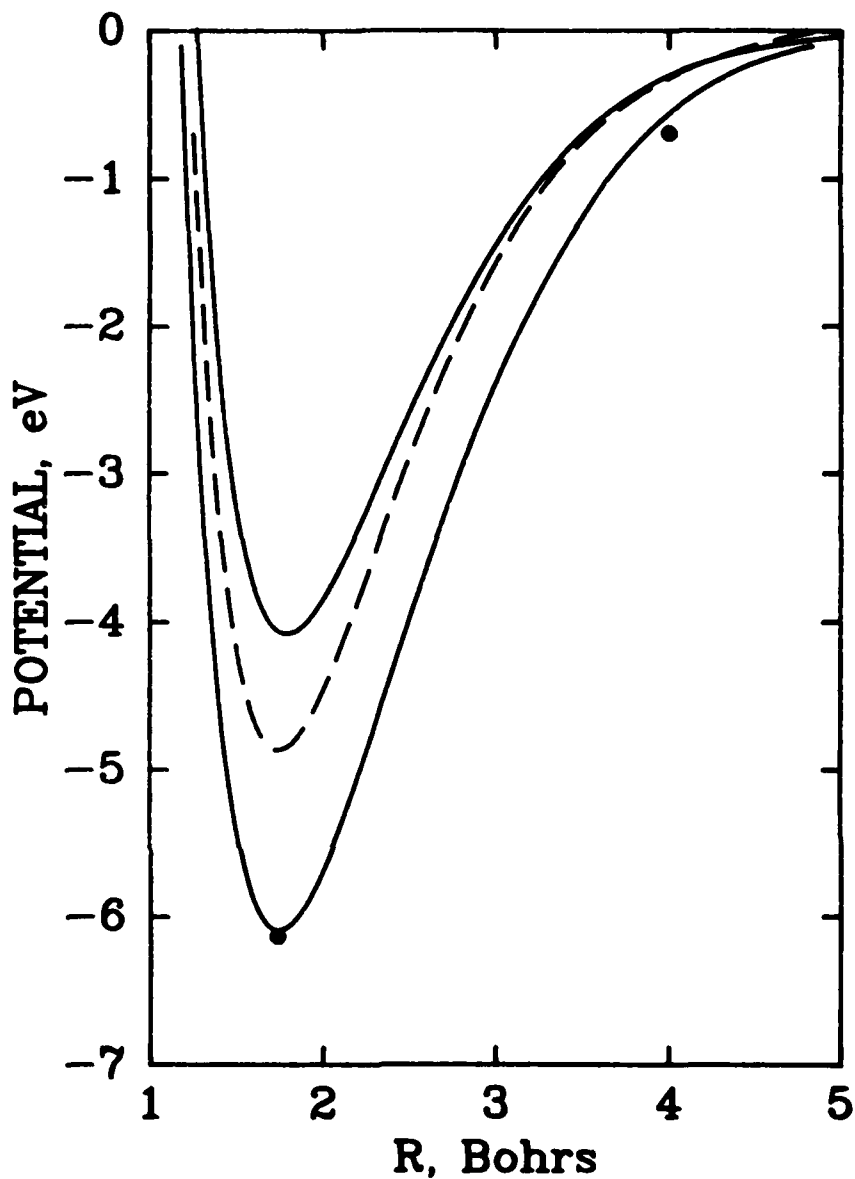


Figure 2. Basis Set Effect on HF Potential Curves. The Dashed Curve Represents the MC(5)-DZP result, while the Upper and Lower Solid Curves are the MC(5)-DZ and RKR Curves. The dots are MCSCF-DZP points obtained using a selection of 21 terms, based on the results of a single and double excitation CI (51 terms) using MC(8)-DZ orbitals. These results show the effect of additional correlation and the potential accuracy of the MCSCF method. The *ab initio* potentials are relative to the respective total energies at $R = 6$.

on a knowledge of the computer requirements of each type of calculation, we decided to compute the OHF surface at the DZ level, eventually using the MCSCF method.

However, the UHF method was considerably faster than the MCSCF method because it did not need to transform the integrals at each iteration or construct the Hessian matrix, as did the MC. Therefore a preliminary OHF DZ surface was first calculated using UHF, so that testing of dynamical methods could get underway. Over 120 data points were calculated for this surface. Five to seven points (equally angularly spaced) were calculated for diatomic HF distances of 1.5, 1.733, 2.1, 2.5, and 3.0 Bohrs and at distances (relative to the diatomic center of mass) of 3.5, 4.0, and 4.5 Bohrs. Additional points for $R = 3.0, 5.0,$ and 6.0 were done for $r = 1.733$. Since the IOS method could not handle reaction and the UHF method was expected to be inferior to the MCSCF method in describing transition states, larger displacements of HF were not included in this data set.

For comparison, a few points were calculated with a DZP basis using the UHF, UHF-MBPT, and a large (308 configuration) MCSCF. These studies involved the O atom approach at 90 degrees, which is basically a repulsive interaction, and a comparison of the repulsion at different angles. A great deal of difficulty was encountered in these MC calculations. One of the main problems was finding adequate starting orbitals for the MC. Apparently, using the alpha orbitals from a UHF calculation is not a good procedure. We have found that these orbitals are, at best, difficult to converge from, and that they can lead to divergence or to the location of relative minima in the MC solution space; i.e., false solutions. Unfortunately, convergence to a local minimum is not directly detectable,

resulting in the necessity of spending a good amount of effort to assure the reliability of the calculations.

We also encountered difficulties which seemed to be associated with employing a configuration space which was restricted to less than a full CI within the orbitals selected for the valence space. Our experience was that the more terms that were omitted, the sooner convergence slowed down to a near standstill. These problems were later linked to possible ill conditions in the calculations (See the discussion in the section on $O + CO$.)

Another restriction was that the amount of program space available on our computer system at that time precluded the simultaneous use of DZP basis sets, large MC configuration spaces, and the exact solution of the MCSCF problem involving orbital coupling. The space problem is no longer a factor, but the execution time involved for such calculations is substantial. Calculation of the orbital coupling etc. can be comparable to or greater than the integral transformation time. Because orbital coupling was not used for the MC308 calculations, and because of difficulties associated with starting orbitals encountered in these and subsequent calculations, it is possible that globally optimal solutions were not obtained in some of the comparative calculations.

Because of these considerations, we decided to do the MCSCF OHF surface using a small but adequate valence orbital space, including the full CI within that space. The minimal space for the OHF system consists of eleven orbitals: the 1s, 2s, and 2p orbitals on O and F, and the 1s orbital of H. When $H(2S)$ and $F(2P)$ interact to form ground state HF (singlet sigma-plus), the H 1s and the singly occupied p-sigma orbital of F interact to form

bonding and antibonding orbitals. At the equilibrium geometry, the bonding orbital becomes doubly occupied, resulting in stabilization. At the separated limit, this electron pair is split up. The proper construction of a spin eigenfunction here requires at least two determinants, because of the potential singlet or triplet coupling of an alpha and a beta electron. The singlet-coupled determinants constitute one configuration. If the electrons in the F 1s and 2s orbitals are not allowed to be excited, a total of 5 configurations can be generated having the proper ground state symmetry. (Of course, configurations of different symmetry are noninteracting.)

The analogous O atom calculation for the minimal orbital space has just one configuration. In calculations of this type, the full spherical symmetry of the atom is not taken into account. The atom is assumed to have D_{2h} symmetry, and whichever p-orbital is doubly occupied will have a lower energy. However, the full symmetry of the atom would be broken by the interaction with HF anyway. We have done both MC and UHF-MBPT calculations at several geometries for both the lowest singlet A' and A'' symmetries. Although the energy differences were small, the A'' surface seems to be the lower one at all of the points examined with either method. This surface is the one that corresponds to oxygen having one unpaired electron in the p-orbital perpendicular to the plane of the OHF molecule (usually labelled p_z in C_s symmetry) and one in an in-plane orbital. (The p_x and p_y orbitals will mix in C_s symmetry.)

The MC calculations for the OHF system using these 11 orbitals result in 56 configurations of A'' symmetry if five orbitals are required to remain doubly occupied, and 110 if only four are so restricted. Most of the points on the OHF surface were calculated using 56 terms. The first points were

selected similarly to those of the DZ-UHF surface. In moving around on the surface, starting each successive point with varying angle, R, or r value, from a neighboring one, we happened to discover that the first few points calculated, which ultimately had been started from UHF orbitals were locally optimal solutions. The sequence of steps was retraced, recalculating data points, until the new solutions merged back into the previous ones. This self-consistency should indicate that the potential surface is reliable, even though there is no way to guarantee that it is globally optimal. Next, extra points were added to locate the saddle points, or transition state regions, for OH formation at 0 degrees and for OF formation at 180 degrees. In all, over 173 data points were calculated at this level.

Additional calculations using 110 configurations were done at selected points to determine if the reduction to 56 terms made a significant difference. In the process of checking this, we found that the previously determined solutions in the OH saddle point region were relative minima. The first sign was that the MC110 calculations were lower in energy here. When these orbitals were used as starting orbitals for the MC56 calculation, it converged to essentially the MC110 result. Therefore we recalculated several points in an expanding region about the saddle point with both MC56 and MC110, starting from the newly obtained solutions, until no energy difference from the previous results was obtained.

After the DZ points were fit, MCSCF calculations in C_{2v} symmetry with 315 configurations using a DZP basis set were performed for selected geometries along the DZ reaction path for hydrogen abstraction. The barrier to reaction on the fitted DZ surface is 1.95 eV. The DZP calculations predicted a slightly higher barrier, 2.36 eV. However, this value is an

upper limit to the true DZP barrier height since the DZP transition state geometry was not optimized. These DZP calculations indicate that the fitted DZ surface describes the reaction path barrier reasonably well.

We fully expect that the DZ basis is inadequate in some regions of the surface. In particular, the formation of OF is not accurately described. OF is barely bound in these calculations, making the exact determination of the transition state for its formation difficult, as well as unreliable. However, since OF is significantly less stable than HF, we know that a considerable activation energy is required for its formation and that the cross section for this process will be small. Therefore, since our surface reflects this, it should model the system fairly well.

3.2 ANALYTICAL REPRESENTATION OF THE O + HF POTENTIAL SURFACE

The O + HF potential surface calculations were carried out at the UHF level. A set of 101 of these points was selected for fitting, and a simple sum-of-pairs fit was made, rather than a fit to the LEPS function of Equation 1. This fit was improved with the addition of a 3-body term of the form of Equation 9, with the exception that the gaussian decay functions were eliminated (i.e., the gamma parameters were set to zero). This sum-of-pairs is adequate to represent the ab initio data since only small displacements from the vibrational equilibrium distance of HF were considered. The two-body term is expressed as

$$V_2(R_1, R_2, \Delta R_3) = A_1 \exp(-\alpha_1 R_1) + A_2 \exp(-\alpha_2 R_2) + D_0 \{ \exp(-\alpha_0 \Delta R_3) - 1 \}^2 \quad (27)$$

where $\Delta R_3 = R_3 - R_0$, R_0 being the vibrational equilibrium separation of HF. R_1 and R_2 represent the distances of the F and H atoms from the O(³P) atom, respectively. R_3 is the HF vibrational coordinate.

The O + HF UHF potential surface, which we call Surface I, is given as the sum of Equations 9 and 27:

$$V(R_1, R_2, R_3) = V_2(R_1, R_2, R_3 - R_0) + V_3(R_1, R_2, R_3) \quad (28)$$

The parameters for this fit are given in Table 2. This fit, although valid only for relatively small vibrational displacements of HF, is useful for studying pure inelastic transitions in HF, and in particular for comparing various dynamical methods.

The MCSCF calculations sample not only the geometries spanned by the UHF points of Surface I, but reactive geometries as well. Thus we use the LEPS function of Equation 1 for our 2-body term, since it has the physically correct dissociation channels to form OH and OF. The diatomic curves used in the LEPS function are given by Equations 5 and 6. The Sato parameter is set to unity, because the "a" parameter of the triplet function in Equation 6 is varied independently, and a constant Sato parameter becomes redundant. The ground state diatomic curves were fit to ab initio data obtained in the same basis as the full O+HF surface. This was necessary in order to obtain a good fit in all 3 reaction channels.

All 36 nonlinear parameters in the LEPS function were iteratively varied, several at a time, until the rms error was constant to 3 significant figures. The Levenberg-Marquardt algorithm of Reference 15 proved to be essential to this procedure. The final rms error for the LEPS term is .146 eV (3.37 kcal/mole) over the 173 points used in the fit. This is excellent, since the energy range spanned by the data set is from zero to 10.3 eV. The extended LEPS function is an excellent starting point for the OHF system.

After adjustment of the LEPS function, the 3-body parameters were determined. The 3-body term of Equation 9 is expanded to order 4, providing

TABLE 2. PARAMETERS FOR O + HF ($^3A''$) POTENTIAL ENERGY SURFACE I

TWO-BODY TERM

	OF	OH
	$A_1 = 2397.93$	$A_2 = 155.145$
	$\alpha_1 = 2.44667$	$\alpha_2 = 2.26002$
	HF Molecule	
	$D_0 = 6.1255$	$R_0 = 1.7325 \quad \alpha_0 = 1.1800$

THREE-BODY TERM

n	Term	Coefficient	n	Term	Coefficient
1	1.0	-.441971 E+1	6	S_2^2	-.903517 E+0
2	S_1	.763740 E+1	7	$S_1 S_2$.101847 E+1
3	S_2	.628959 E+0	8	$S_1 S_3$	-.269458 E+1
4	S_3	-.332277 E+1	9	$S_2 S_3$.405814 E+1
5	S_1^2	-.287412 E+1	10	S_3^2	-.113327 E+1

OF:	$\alpha_{10} = 0.50$	$R_{10} = 2.000$
OH:	$\alpha_{20} = 0.50$	$R_{20} = 1.500$
HF:	$\alpha_{30} = 0.50$	$R_{30} = 1.738$

* Units of energy are eV, units of distance are Bohrs.

TABLE 3. PARAMETERS FOR O + HF ($^3A''$) POTENTIAL ENERGY SURFACE II

	<u>TWO-BODY TERM</u>		
	OF	OH	HF
D ₀	.5131226 E+0	.3090920 E+1	.4258568 E+1
R ₀	.2862152 E+1	.1890991 E+1	.1783464 E+1
b ₁	.2239155 E+1	.2684080 E+1	.2523759 E+1
b ₂	-.1333435 E+1	.1804630 E+1	.1519809 E+1
B ₃	-.1055436 E+1	.7921508 E+0	.7479872 E+0
a ₁	.6312840 E+3	.2976630 E+3	.1154460 E+3
a ₂	.1964170 E+1	-.7577960 E+0	.1764394 E+1
a ₃	-.4781260 E+0	.4296480 E+0	-.2499930 E+0
a ₄	.2002340 E+1	.2203390 E+1	.1922920 E+1
	C ₄	.1901832 E+3	
	R ₄	.4157720 E+1	
	Y ₄	.9500000 E+0	
	C ₆	.3742970 E+3	
	R ₆	.4589850 E+1	
	Y ₆	.7500000 E+0	

* Units of energy are eV, units of distance are Bohrs.

TABLE 3 (cont.) PARAMETERS FOR O + HF (³A") POTENTIAL ENERGY SURFACE II

THREE-BODY TERM

n	Term	Coefficient	n	Term	Coefficient
1	1.0	.160383 E+2	19	S ₂ S ₃ ²	-.113042 E+2
2	S ₁	-.563400 E+2	20	S ₃ ³	.300013 E+1
3	S ₂	-.766557 E-1	21	S ₁ ⁴	.620537 E+1
4	S ₃	-.187122 E+2	22	S ₂ ⁴	-.277431 E+0
5	S ₁ ²	.811656 E+2	23	S ₁ ³ S ₂	.463748 E+0
6	S ₂ ²	.773517 E+1	24	S ₁ ² S ₂ ²	-.515063 E+1
7	S ₁ S ₂	-.245761 E+2	25	S ₁ S ₂ ³	.314642 E+1
8	S ₁ S ₃	-.353516 E+2	26	S ₁ ³ S ₃	-.447866 E+1
9	S ₂ S ₃	.618313 E+2	27	S ₁ ² S ₂ S ₃	-.313769 E+1
10	S ₃ ²	.243478 E+2	28	S ₁ S ₂ ² S ₃	.391074 E+1
11	S ₁ ³	-.409414 E+2	29	S ₂ ³ S ₃	-.315996 E+1
12	S ₂ ³	-.292658 E+1	30	S ₁ ² S ₃ ²	-.231433 E+1
13	S ₁ ² S ₂	.117959 E+2	31	S ₂ ² S ₃ ²	.628215 E+1
14	S ₁ S ₂ ²	.282815 E+1	32	S ₁ S ₂ S ₃ ²	.168579 E+1
15	S ₁ ² S ₃	.383789 E+2	33	S ₁ S ₃ ³	.326780 E+1
16	S ₂ ² S ₃	-.233417 E+2	34	S ₂ S ₃ ³	-.100540 E+2
17	S ₁ S ₂ S ₃	-.262869 E+2	35	S ₃ ⁴	.169200 E+1
18	S ₁ S ₃ ²	-.245761 E+2			

OF: α₁₀ = 0.34 R₁₀ = 2.360 β₁₀ = 0.037
 OH: α₂₀ = 0.59 R₂₀ = 1.390 β₂₀ = 0.045
 HF: α₃₀ = 0.24 R₃₀ = 1.578 β₃₀ = 0.042

35 linear parameters for adjustment. A weight of unity was used in the least squares procedure. This automatically biases the fit toward higher energies, but that is the energy region we are primarily interested in. The nonlinear parameters in the 3-body term were individually optimized. They essentially control the range of the 3-body term, ensuring that it dies out for large R.

Parameters for Surface II are given in Table 3. As usual, energy units are electron volts, and distances are in Bohrs. This fit to the MCSCF data has an rms error of .071 eV (1.6 kcal/mole). This is almost down to the 1 kcal/mole error range usually considered to be required for "chemical accuracy", and is certainly sufficiently accurate for the high energy collision processes studied here. It is also superior to most other fits in the literature.

The OH product valley is well described. The transition state for forming OH is linear, and our surface predicts a barrier of 1.95 eV (45 kcal/mole), which will lead to negligible thermal rate constants, and to small reaction cross sections except at the highest energies. This barrier does not change much on going to a larger basis set, so it is at least qualitatively correct. More work is necessary in the electronic structure calculations before a more accurate value of the barrier can be obtained. Also, as discussed in Section 3.1, the basis set used did not provide an accurate description of the OF product channel, and our fit naturally reflects this.

The thermochemical heat of reaction to form OH on surface II is within .1 eV of experiment, again indicating that it is sufficiently accurate for high energy collision studies.

In fitting potential surfaces, one of the best diagnostic tools for determining the usefulness of a fit is a plotting system. We made many plots in a variety of coordinates to assess the accuracy of the fit to the data in various regions of the surface and to examine regions where ab initio data was not calculated for unphysical behavior in the fit. This graphical study was made possible by a system of codes, developed at Chemical Dynamics, designed specifically for potential surface analysis. These programs allowed us to interactively examine an analytical function and make comparisons with ab initio points extracted from the data set.

We present several plots that illustrate the accuracy of our fit for Surface II and show the overall topology of this surface. Figures 3 and 4 show two cuts through the surface and compare the fit (solid line) to the computed ab initio points. It is apparent that the fitting function does a good job of representing the shape of the surface. Other cuts show similar good agreement. Figure 3 represents a cut for the oxygen atom approaching HF with HF near its equilibrium geometry. The potential is essentially repulsive. The attractive potential of Figure 4 occurs because when HF is stretched the formation of OH is favorable.

Figure 5 is a contour plot for the H-atom abstraction reaction. The barrier, or saddle point, for reaction is at an energy of 1.95 eV and represents an energetic barrier that must be crossed to form OH. There is a small exit channel barrier that is an artifact of our fit, caused by a sparcity of ab initio points in the exit channel. It should not have an effect on our vibrational excitation cross section predictions. A perspective plot of this region of the energy surface is given in Figure 6. This figure dramatically illustrates the energetic barrier to reaction, and

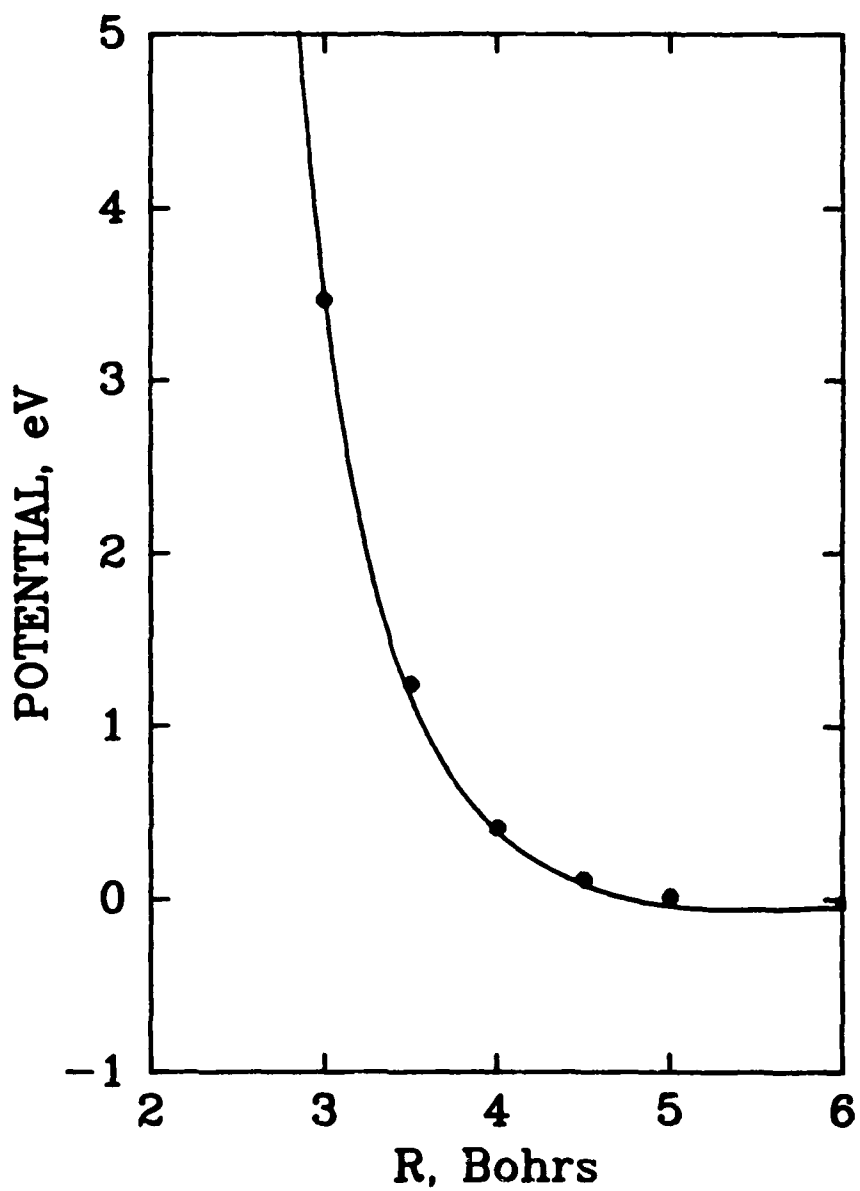


Figure 3. O+HF Potential Surface II for $R=1.733$ at a C.M. Angle of 60 Degrees. The Solid Curve is the Analytical Fit, and the Dots Represent the ab initio Data.

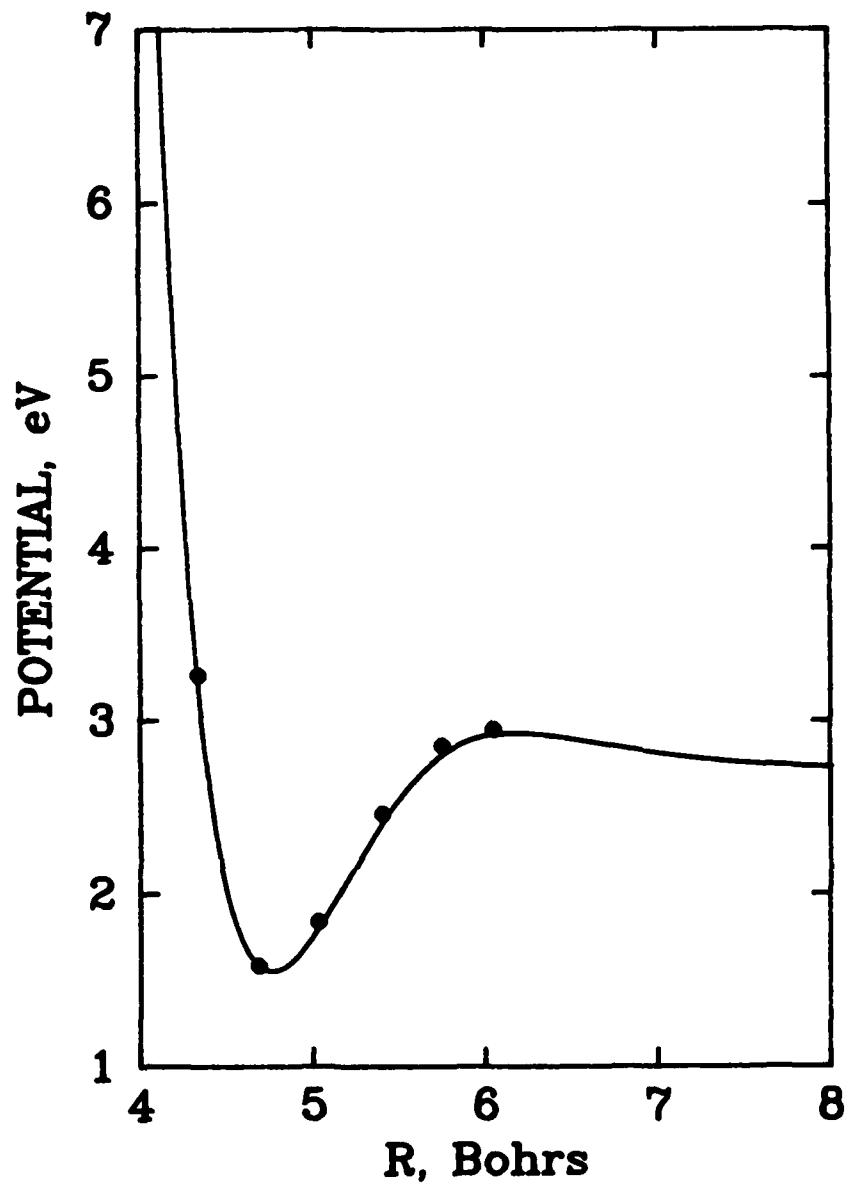


Figure 4. O⁺HF Potential Surface II for R=3.0 at a C.M. Angle of 60 Degrees. The Solid Curve is the Analytical Fit, and the Dots Represent the ab initio Data.

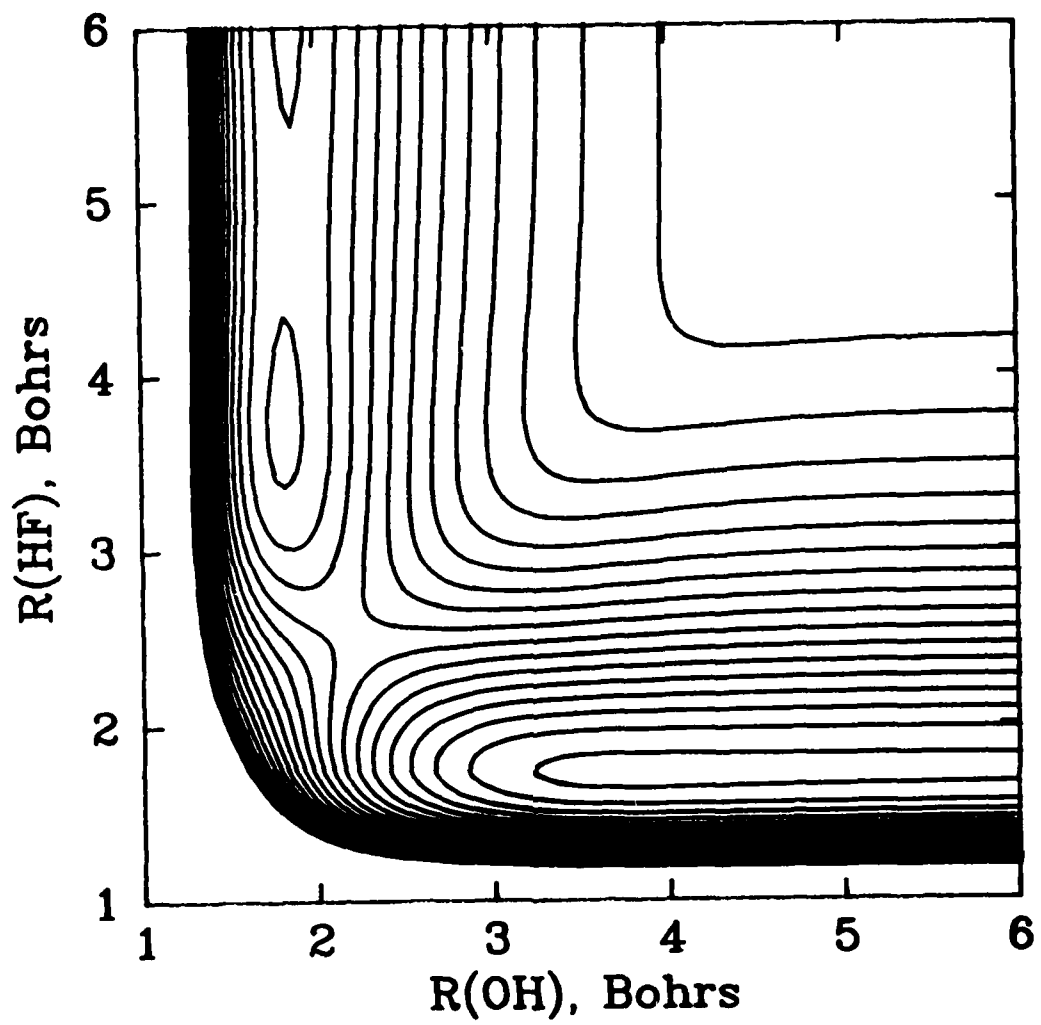


Figure 5. A Contour Plot of the $\text{O}+\text{HF}$ 0-Degree Surface II. Contour Values Range from 0 to 5 eV in Increments of 0.25 eV.

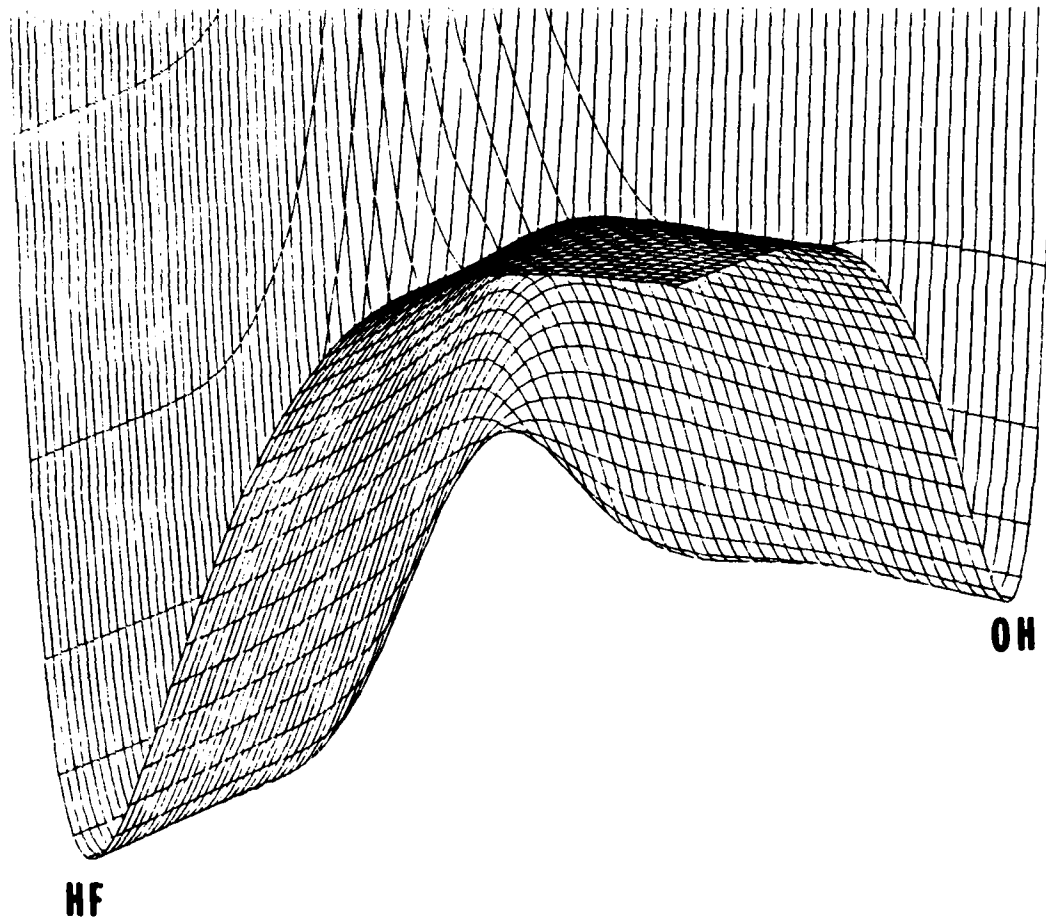


Figure 6. A Perspective Plot of the 0-Degree O+HF Surface II. The Region of the Plot Corresponds to Figure 5. The Energy Range Spanned is 0 to 6 eV.

the endothermicity to form OH.

3.3 CROSS-SECTIONS FOR EXCITATION OF HF BY O(³P)

Our preliminary dynamical studies of the O+HF system were done using a fit to the UHF potential energy surface (Surface I). Although this surface was fit to points near the HF equilibrium geometry and, thus, does not allow for reaction, it is sufficiently accurate for inelastic collision calculations and can be used to compare various inelastic dynamical theories.

We performed a set of calculations to determine the importance of quantum mechanical effects for this surface. The two methods employed were the quantum mechanical IOS method and the classical IOS analog. In the IOS approximation, as discussed previously, calculations are performed for fixed orientation of the diatomic molecule. In the quantum approach the close-coupling equations are solved for the vibrational motion, while in the classical method a set of classical trajectories for Hamilton's equations are computed. If the two methods yield similar results, we can exclude quantum mechanical effects for this system (at the velocities considered).

The results of these calculations are presented in Tables 4 through 6, for final vibrational states 1 through 3, respectively. The classical IOS results are presented for both a histogram final state analysis and for a moment analysis. The moment results are expected to be more reliable at low energies where the histogram cross sections are inaccurate. The agreement between quantum and classical IOS cross sections is quite satisfactory even at the lowest energies considered here. We therefore concluded that

TABLE 4. CROSS SECTIONS FOR EXCITATION OF HF($v=0$) TO HF($v=1$)
ON POTENTIAL ENERGY SURFACE I

Energy	Quantum IOS	Classical IOS		Classical 3D
		moment	hist.	hist.
2.0	2.4(-4)	3.6(-4)	-0-	2.6(-3)
2.5	2.4(-3)	2.7(-3)	-0-	2.8(-2)
3.0	1.3(-2)	1.3(-2)	4.2(-3)	6.4(-2)
3.5	4.2(-2)	5.0(-2)	4.8(-2)	7.6(-2)
4.0	7.8(-2)	8.7(-2)	9.0(-2)	2.0(-1)

* Cross Sections are in square Angstroms, relative energy in eV.
Values in parenthesis represent powers of ten.

TABLE 5. CROSS SECTIONS FOR EXCITATION OF HF($v=0$) TO HF($v=2$)
ON POTENTIAL ENERGY SURFACE I

Energy	Quantum IOS	Classical IOS		Classical 3D
		moment	hist.	hist.
2.0	3. (-8)	8. (-8)	-0-	-0-
2.5	8. (-6)	6. (-6)	-0-	-0-
3.0	4.5(-4)	3. (-4)	-0-	1.3(-3)
3.5	6.2(-3)	3.9(-3)	3.9(-3)	1.3(-2)
4.0	2.0(-2)	2.1(-2)	2.3(-2)	2.9(-2)

* Cross Sections are in square Angstroms, relative energy in eV.
Values in parenthesis represent powers of ten.

classical mechanics provides an accurate description of the dynamics.

We also include in these tables 3D classical trajectory results. It is apparent that there is significant disagreement between the IOS cross sections and the 3D cross sections. Because the HF molecule is polar, there is a significant amount of rotational excitation observed in the 3D collisions. Our IOS calculations showed a significant excitation probability only for a very restricted range of angles. Apparently the IOS method results in an underestimation of the cross section for this system. A factor of 2 to 3 error is often observed in IOS calculations. We know that the IOS approximation underestimates the $O+H_2O$ cross sections by at least this amount. A comparison of the IOS and 3D results for $O+HF$ is presented in Figure 7.

TABLE 6. CROSS SECTIONS FOR EXCITATION OF $HF(v=0)$ TO $HF(v=3)$
ON POTENTIAL ENERGY SURFACE I*

Energy	Quantum IOS	Classical IOS		Classical 3D
		moment	hist.	hist.
2.0	6. (-9)	3. (-9)	-0-	-0-
2.5	1. (-8)	1. (-7)	-0-	-0-
3.0	1. (-5)	3. (-7)	-0-	-0-
3.5	1.6(-3)	4.8(-4)	-0-	2.9(-3)
4.0	8.4(-3)	8.7(-3)	1. (-2)	7.4(-3)

* Cross Sections are in square Angstroms, relative energy in eV.
Values in parenthesis represent powers of ten.

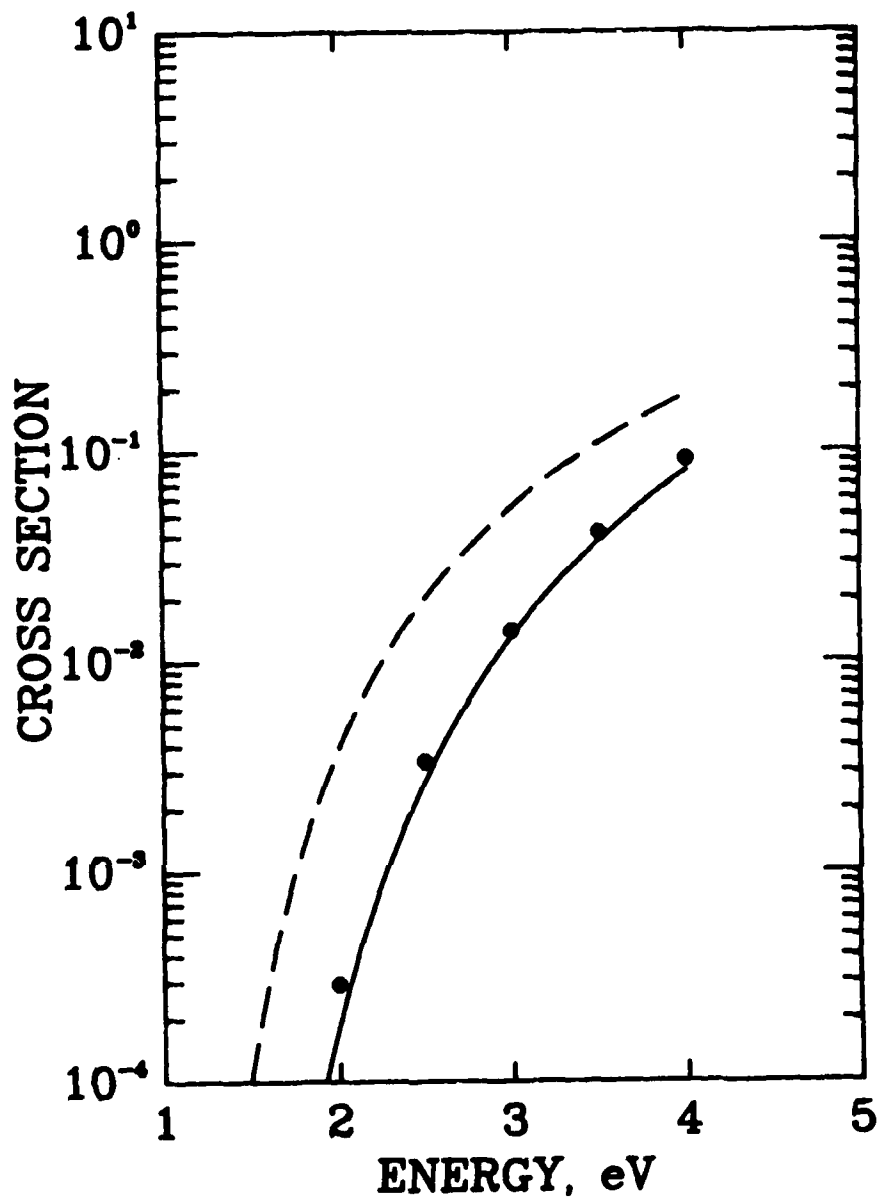


Figure 7. A Comparison of 3D and IOS Cross Sections for O+HF Surface I. The solid curve is the quantum IOS result, while the dots represent the classical IOS results. The dashed curve is the full 3D classical result, summed over final rotational states.

Full 3D classical trajectory calculations were performed for O+HF on surface II. This fit to the MCSCF ab initio calculations allows for the possibility of reaction. Calculations were done over an energy range of 1 to 6 eV, which corresponds to a relative velocity range of 4.7 to 11.4 km/sec. Three initial values of angular momentum of HF were considered. The results are given in Tables 7 through 9.

Below 1.5 eV we obtained no histogram results for vibrational excitation on this surface. We attempted several moment analyses to extrapolate the 3D results to low energies, and as of this time we do not consider any of them reliable. A continuous quantization method was very accurate at 6 eV (i.e., it agreed with the histogram result), but it appears to overestimate the low energy cross sections. It was thought that the use of a Morse oscillator model for the diatomics to compute the actions introduced a systematic error. However, we used an accurate numerical method for computing the action integral to test this hypothesis for HF, and the final results did not change significantly. For the present the histogram results are our current best estimates of the cross sections.

An analytic fit of the $v=1$ excitation cross section is given in the tables. This represents a weighted least squares fit to the $v=1$ data. Weights were chosen as energy times the number of trajectories run at each energy since the accuracy of the Monte Carlo method depends on these quantities. The $v=1$ cross section for HF starting in $v=0$, $J=10$ is given in Figure 8. The curve is the analytic function of Table 9. The quality of the fit to the cross section data is within the accuracy of the cross sections.

TABLE 7. CROSS SECTIONS FOR EXCITATION OF HF(J=0) ON SURFACE II*

E _{rel}	V _{rel}	Quantum Number v						
		1	2	3	4	5	6	7
2.0	6.6	.008	-0-	-0-	-0-	0	0	0
3.0	8.1	.027	-0-	-0-	-0-	-0-	-0-	-0-
4.0	9.3	.060	.003	-0-	-0-	-0-	-0-	-0-
5.0	10.4	.25	.033	.007	.003	-0-	-0-	-0-
6.0	11.4	.48	.066	.045	.004	.003	-0-	-0-

Analytical Fit for v=1 Cross Section

$$Q(E_{rel}) = A \exp[(a + bE + cE^2)/(E - E_0)]$$

A	a	b	c	E ₀
.0136219	-.290309	-2.02686	.892558	.683720

*Energy units are eV
 Velocity units are km/sec
 Cross Sections are in Å²

Error bars of one standard deviation are approximately 10% at 6 eV and 50% at 2 eV for v=1. Error bars on the other transitions scale approximately with the magnitude of the cross section, so that the smallest transitions have error bars of approximately the magnitude of the cross section. Entries marked with the symbol -0- indicate that no trajectories were found that correspond to the indicated final vibrational state. The notation 0 indicates the relative velocity is below the energetic threshold.

TABLE 8. CROSS SECTIONS FOR EXCITATION OF HF(J=5) ON SURFACE II *

E _{rel}	V _{rel}	Quantum Number v						
		1	2	3	4	5	6	7
2.0	6.6	.01	-0-	-0-	-0-	0	0	0
2.5	7.4	.05	-0-	-0-	-0-	-0-	-0-	-0-
3.0	8.1	.02	-0-	-0-	-0-	-0-	-0-	-0-
4.0	9.3	.07	.005	-0-	-0-	-0-	-0-	-0-
5.0	10.4	.35	.035	.004	.001	-0-	.0007	-0-
6.0	11.4	.47	.13	.02	.01	.01	.004	.005

Analytical Fit for v=1 Cross Section

$$Q(E_{rel}) = A \exp[(a + bE + cE^2)/(E - E_0)]$$

A	a	b	c	E ₀
.422336(-4)	-5.55648	5.33972	.684391	.626370

*Energy units are eV
 Velocity units are km/sec
 Cross Sections are in Å²

Error bars of one standard deviation are approximately 10% at 6 eV and 50% at 2 eV for v=1. Error bars on the other transitions scale approximately with the magnitude of the cross section, so that the smallest transitions have error bars of approximately the magnitude of the cross section. Entries marked with the symbol -0- indicate that no trajectories were found that correspond to the indicated final vibrational state. The notation 0 indicates the relative velocity is below the energetic threshold.

TABLE 9. CROSS SECTIONS FOR EXCITATION OF HF(J=10) ON SURFACE II*

E _{rel}	V _{rel}	Quantum Number v						
		1	2	3	4	5	6	7
2.0	6.6	.01	-0-	-0-	-0-	-0-	-0-	-0-
2.5	7.4	.047	-0-	-0-	-0-	-0-	-0-	-0-
3.0	8.1	.053	-0-	-0-	-0-	-0-	-0-	-0-
3.5	8.7	.14	.005	-0-	-0-	-0-	-0-	-0-
4.0	9.3	.17	.016	-0-	-0-	-0-	-0-	-0-
4.5	9.8	.36	.025	.003	.001	-0-	-0-	-0-
5.0	10.4	.25	.016	-0-	-0-	-0-	-0-	-0-
6.0	11.4	.53	.18	.06	.05	.02	.01	.004

Analytical Fit for v=1 Cross Section

$$Q(E_{rel}) = A \exp[(a + bE + cE^2)/(E - E_0)]$$

A	a	b	c	E ₀
.522703	-4.19727	-1.36899	.374942	.457320

*Energy units are eV
 Velocity units are km/sec
 Cross Sections are in Å²

Error bars of one standard deviation are approximately 10% at 6 eV and 50% at 2 eV for v=1. Error bars on the other transitions scale approximately with the magnitude of the cross section, so that the smallest transitions have error bars of approximately the magnitude of the cross section. Entries marked with the symbol -0- indicate that no trajectories were found that correspond to the indicated final vibrational state. The notation 0 indicates the relative velocity is below the energetic threshold.

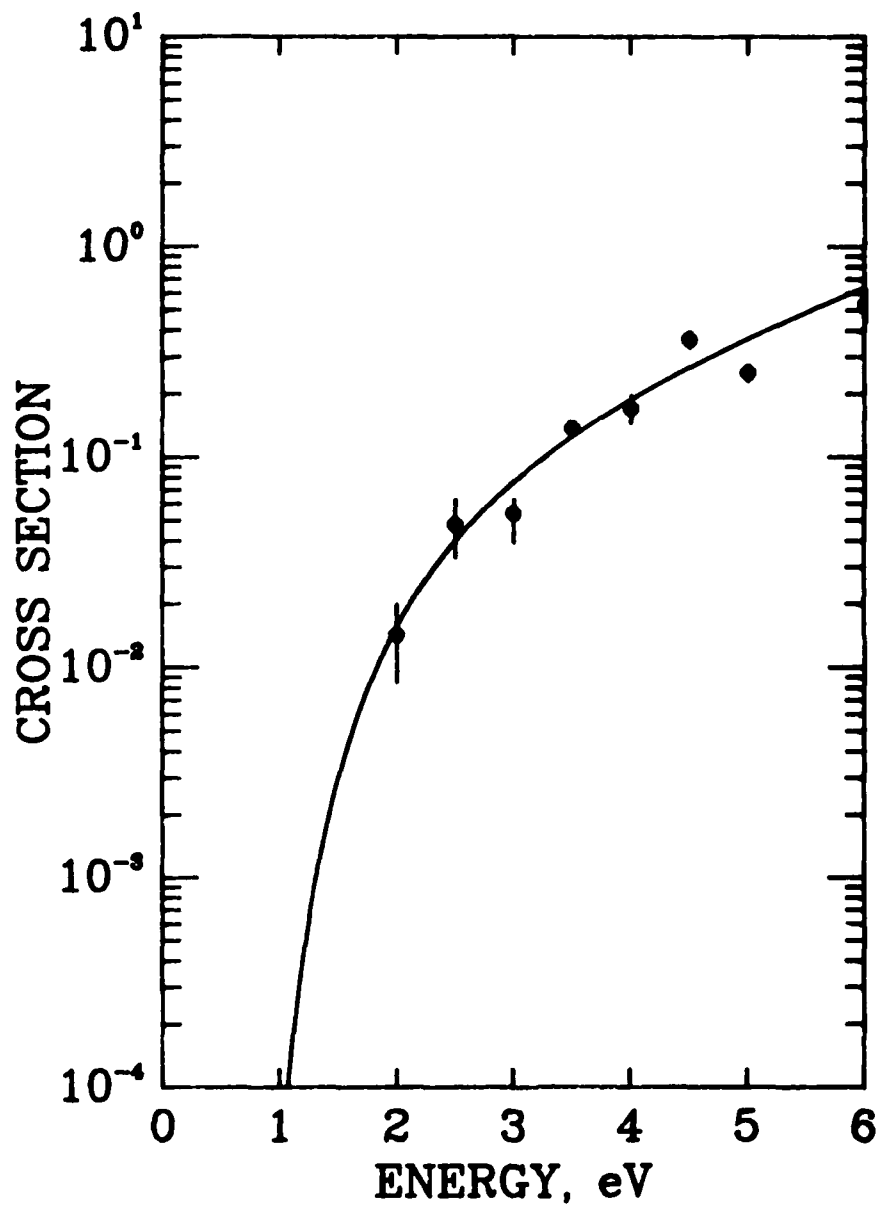


Figure 8. Cross Section for $v=1$ Excitation of $\text{HF}(J=10)$ for $\text{O}+\text{HF}$ Surface II.

Units are \AA^2 (10^{-16} cm^2). 2-Sigma (95%) deviations are shown with the vertical lines. The solid line is the fit (Table 9).

3.4 CHEMICAL REACTION IN $O(^3P) + HF$ COLLISIONS

Using the Chemical Dynamics VTST code, we performed variational transition state calculations for this surface for HF initially in the vibrational ground state. The reaction path was determined, and because of the high barrier to reaction, the thermal rate for forming OH is negligible. A saddle point at [R(OH)=2.21, R(HF)=2.59 Bohrs] with a barrier of 1.95 eV (45.0 kcal/mole) was found. Even so, high velocity collisions do lead to reaction. At 6 eV, the total reactive cross section to form OH is 0.2 \AA^2 .

We also examined HF with one quantum of vibrational energy, and looked for formation of OH in the ground and first excited vibrational states. For relative energies below 5 eV, the cross section for the reactive process to form OH(v=0) is less than .01 square Angstroms, while the cross section to form OH(v=1) is even smaller. The histogram cross sections are so small for the reactive processes they are unreliable. Collisions that are not vibrationally elastic tend to result in the collisional cooling of HF to v=0, or with somewhat greater probability, the excitation of HF to v=2. We concluded that reactive processes on the lowest adiabatic potential surface are unimportant. Even lowering the barrier to reaction (to correct for any error in the saddle point energy) is not likely to raise the high velocity reaction cross sections to significant magnitudes.

3.5 VIBRATIONAL RELAXATION IN $O(^3P) + HF$ COLLISIONS

Classical trajectory calculations were performed to obtain relaxation rates for $HF(v=1)$ colliding with atomic oxygen. Before attempting these calculations, we felt it was necessary to know the cross sections for collisional processes that involve $HF(v=1)$. Therefore, we performed a set of cross section calculations for the translational energy range of 2.5 to 5.0 eV. The predominant excitation/relaxation pathways are through $v=0$ and $v=2$, as expected. The reactive cross sections are very small, and were not accurately obtained in our calculations, although more reliable estimates of their magnitudes could be obtained by extending the calculations. At 5.0 eV translational energy, our calculations indicated both the reactive $v=1$ and $v=0$ cross sections to be less than $6 \times 10^{-19} \text{ cm}^2$. Thus, our conclusions from the theoretical calculations are consistent with the experiments of Quigley and Wolga⁴¹, in that atom exchange is not important in this system.

In Figure 9 we present cross sections for $HF(v=1)$ going to $HF(v=0)$. We performed a number of calculations to determine the energy (temperature) dependence of b_{max} on the cross sections and used these values of b_{max} in the Monte Carlo rate calculations. We felt this was necessary since the relaxation probabilities are very small in this system (even for translational temperatures on the order of 5,000 K) and classical trajectory calculations with histogram analysis are meaningless when the transition probabilities become very small.

In Figure 10 we present the rate constant for $O + HF(v=1)$ relaxing to the ground state as a function of translational temperature. We have not used an Arrhenius plot due to the high temperatures involved in the

calculations, since the calculations would be bunched together at small values of $1/T$. Because the low temperature transition probabilities are so small, it is not possible to obtain thermal (i.e., 300 K) rates for direct comparison with experiment. However, the translational temperatures of importance in plumes (corresponding to km relative velocities) are of the order of 15,000 K to over 20,000 K, so the calculations provide information in the relevant temperature regime.

We have included the 300 K experimental data point of Quigley and Wolga in Figure 10. It is apparent that the theoretical results fall off much too rapidly with decreasing temperature to extrapolate to the experimental value. Part of the reason for this is likely to be the inaccuracy of the quasiclassical trajectory method for low probability processes. However, this alone cannot explain the very large difference between the observed value and a reasonable extrapolation of our calculations to 300 K. It is possible that the experimentally observed relaxation rate is larger than predicted by our calculations because of a vibronic resonance effect.⁴¹ This results from nonadiabatic processes that are not included in our single-surface theory. Knowledge of the two lowest excited triplet surfaces and estimates of their couplings to the ground state surface could help resolve this problem. We conclude that our high temperature rate constants are probably accurate, and that a reasonable approach (for the present) to interpolating a useable rate constant is to make a linear fit of the 300 K experimental rate and our 20000 K calculated rate. Obviously, more work is required for this system to obtain an acceptably reliable rate constant over the entire temperature range of interest.

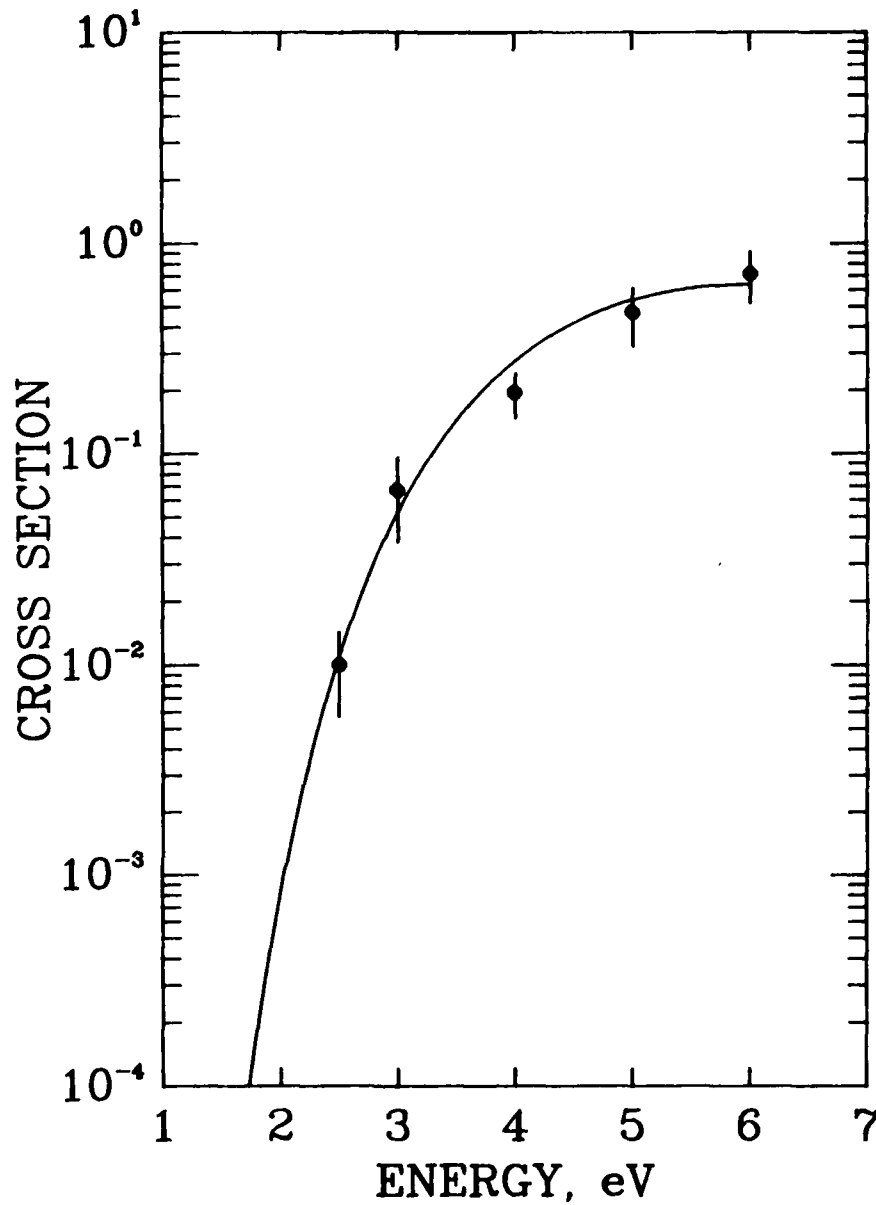


Figure 9. Cross Section for Relaxation of HF(v=1) to HF(v=0).

Units are \AA^2 (10^{-16} cm^2). 2-Sigma (95%) deviations are shown with the vertical lines. The solid curve is an analytical fit analogous to those for v=0 shown previously.

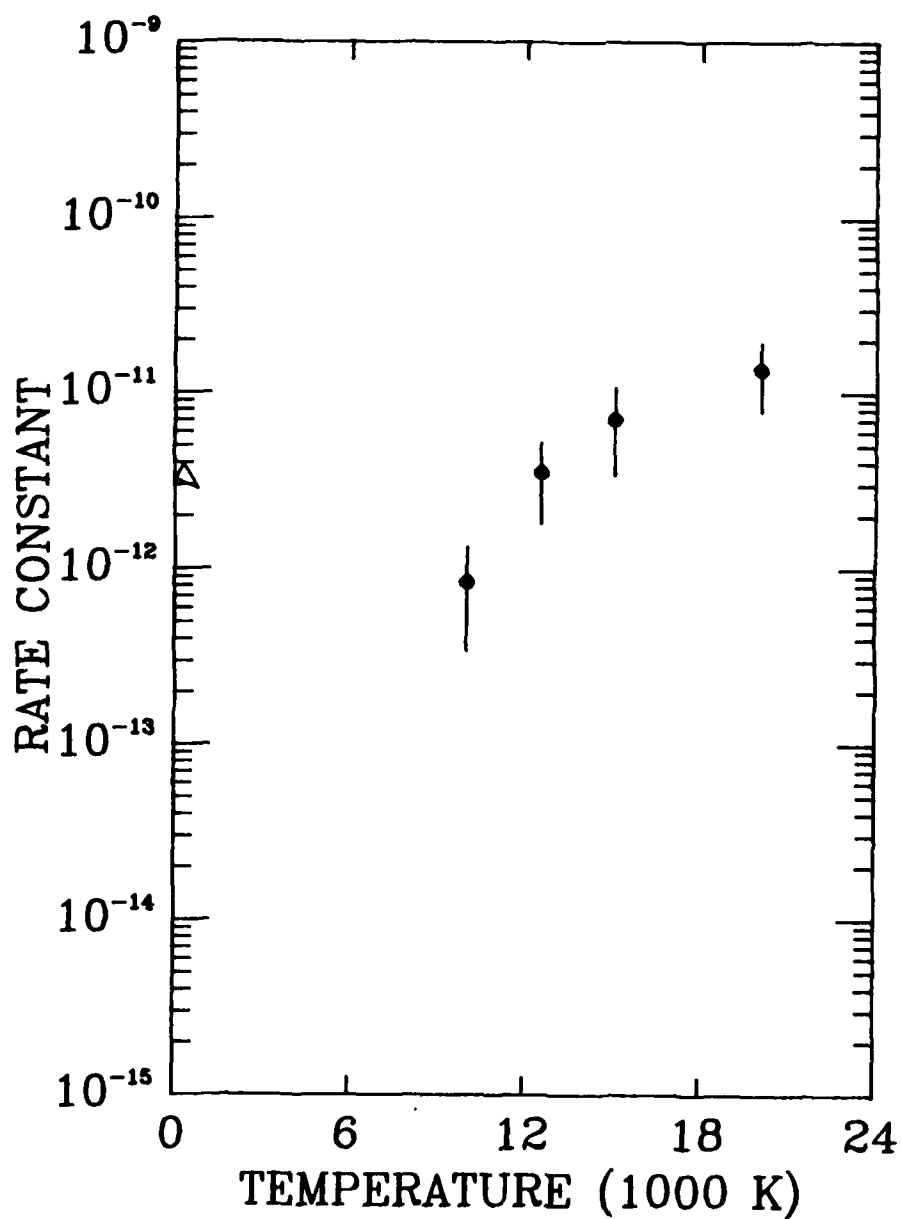


Figure 10. Rate Constant for Relaxation of HF(v=1) to HF(v=0).

Units are cm³/mol-sec. 2-Sigma (95%) deviations are shown by vertical lines. The triangle at 300 K represents the experimental result of Quigly and Wolga.⁴¹

Section 4

O + HCl COLLISIONS

4.1 POTENTIAL ENERGY SURFACE

The MCSCF surface for O + HCl was generated analogously to that for O + HF, with a few modifications. The basis set used for Cl was a [6s4p]/(12s9p) set used by Dunning⁴² and by McLaine and Chandler.⁴³ Calculations of the HCl diatomic curve with and without optimization of the core orbitals were performed. It was decided that the improvement in the well depth (about 10%) was worth the relatively small amount of computer time used for this optimization. No DZP calculations were performed. In Figure 11 we present a comparison of UHF-DZ and MCSCF-DZ curves with an experimental RKR curve. The shape of the MCSCF curve is superior to the UHF curve, as is the case for HF.

The configuration space used was chosen to be the 110 term case, in hopes of avoiding the problem encountered with OHF. The selection of points in this case was less rigid, in that the interesting areas, such as saddle points were investigated first, and points necessary to fill in the grid of various angles and R and r values were added later. Again, the shallowness of the potential for OCl made calculations in that region of the surface somewhat difficult. Over 147 points were generated. The surfaces are found to be somewhat similar, except that the formation of OH is much more thermoneutral in the O + HCl system.

4.2 ANALYTICAL REPRESENTATION OF THE O + HCl POTENTIAL SURFACE

This system is similar to O + HF, except that it is almost thermoneutral; the heat of reaction to form OH is .04 eV (0.9 kcal/mole).

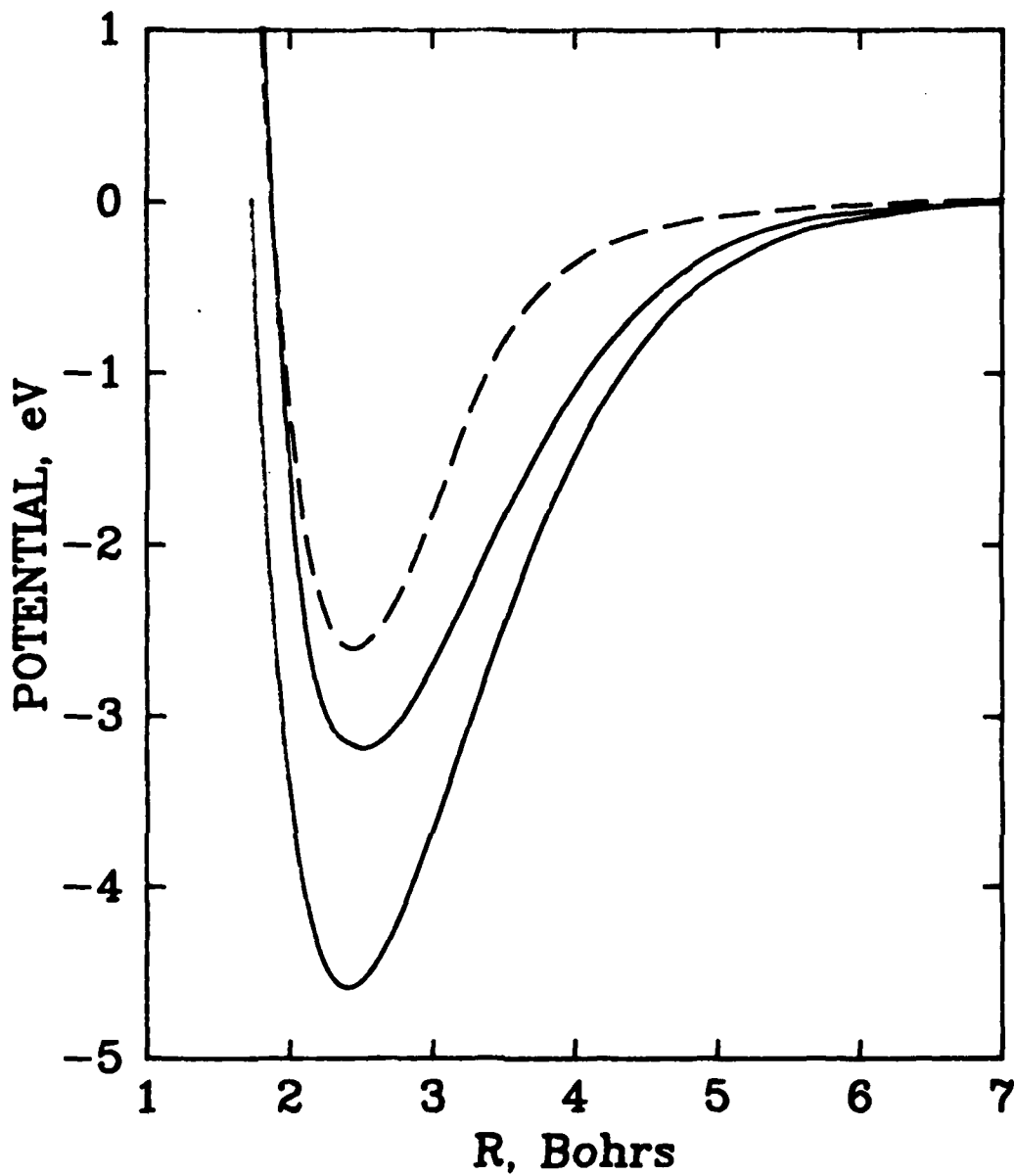


Figure 11. HCl Potential Curves for a DZ Basis. The dashed curve is the UHF potential. The upper and lower solid curves are the MC(5) and RKR Curves. The ab initio potentials are relative to the respective total energies at $R = 8$.

TABLE 10. PARAMETERS FOR O + HCl (³A") POTENTIAL ENERGY SURFACE I

	<u>TWO-BODY TERM</u>		
	OC1	OH	HCl
D ₀	.5769730 E+0	.3058360 E+1	.3195344 E+1
R ₀	.3467678 E+1	.1896137 E+1	.2519241 E+1
b ₁	.4435964 E+1	.2743570 E+1	.2252330 E+1
b ₂	.6214644 E+1	.1969780 E+1	.1537092 E+1
B ₃	.6403795 E+1	.7923473 E+0	.6332550 E+0
a ₁	.7389497 E+3	.2493282 E+3	.2702688 E+3
a ₂	.2489918 E+1	-.4320905 E+0	.1395276 E+1
a ₃	-.1628966 E+0	.2574459 E+0	-.1103783 E+0
a ₄	.2167729 E+1	.2028369 E+1	.1966759 E+1
	C ₄	.0	
	R ₄	.0	
	γ ₄	.0	
	C ₆	.0	
	R ₆	.0	
	γ ₆	.0	

* Units of energy are eV, units of distance are Bohrs.

TABLE 10 (cont.) PARAMETERS FOR O + HCl (³A'') POTENTIAL ENERGY SURFACE II

=====

THREE-BODY TERM

n	Term	Coefficient	n	Term	Coefficient
1	1.0	-.943469 E+2	19	$s_2 s_3^2$	-.387301 E+1
2	s_1	.128243 E+3	20	s_3^3	-.331752 E-3
3	s_2	-.828139 E+1	21	s_1^4	-.219578 E+1
4	s_3	.452639 E+2	22	s_2^4	-.691886 E+0
5	s_1^2	-.643143 E+2	23	$s_1^3 s_2$.353627 E+1
6	s_2^2	-.222754 E+2	24	$s_1^2 s_2^2$	-.593693 E+1
7	$s_1 s_2$.129324 E+2	25	$s_1 s_2^3$.315238 E+1
8	$s_1 s_3$	-.459071 E+2	26	$s_1^3 s_3$	-.140471 E+0
9	$s_2 s_3$.846001 E+1	27	$s_1^2 s_2 s_3$	-.123384 E+1
10	s_3^2	-.525112 E+1	28	$s_1 s_2^2 s_3$	-.414051 E+1
11	s_1^3	.144978 E+2	29	$s_2^3 s_3$.349680 E+0
12	s_2^3	-.509072 E+0	30	$s_1^2 s_3^2$	-.454789 E-1
13	$s_1^2 s_2$	-.240713 E+1	31	$s_2^2 s_3^2$	-.556131 E+1
14	$s_1 s_2^2$.826157 E+1	32	$s_1 s_2 s_3^2$.432320 E+1
15	$s_1^2 s_3$.158869 E+2	33	$s_1 s_3^3$	-.134004 E+1
16	$s_2^2 s_3$.315166 E+2	34	$s_2 s_3^3$.469098 E+0
17	$s_1 s_2 s_3$	-.183360 E+2	35	s_3^4	.410372 E+0
18	$s_1 s_3^2$.268899 E+1			

OCl: $\alpha_{10} = 0.20$ $R_{10} = 2.200$ $\beta_{10} = 0.050$
 OH: $\alpha_{20} = 0.30$ $R_{20} = 1.500$ $\beta_{20} = 0.050$
 HCl: $\alpha_{30} = 0.20$ $R_{30} = 1.600$ $\beta_{30} = 0.050$

=====

We expect, therefore, that reaction will be much more important in this system. The heat of reaction to form OCl is 1.7 eV (39 kcal/mole), so this channel is less favorable, although the cross section is not negligible at the energies considered. The barrier for this channel is large enough so that only the higher velocity collisions sample this channel.

The fitting of the O+HCl MCSCF ab initio data proceeded analogously to the O+HF fit. The parameters for the fit are given in Table 10. We decided not to use a long range interaction due to the insensitivity of the high energy cross sections to small long range interactions. The corresponding parameters are therefore zero.

For the surface fit, 142 ab initio points were selected. As for O + HF, a functional form allowing for reaction was used, and the rms error was .055 eV (1.3 kcal/mole). The barrier for formation of OH is .98 eV (22.6 kcal/mole) for this surface. This barrier is probably too high, due to basis set errors in the ab initio calculations, and more work needs to be done to determine it more accurately. This barrier is about half of the one for O + HF, and consequently we expect much more reaction in the dynamics. The smaller heat of reaction will also lead to a lower reaction threshold.

In Figures 12 through 15 we present plots illustrating the O+HCl potential energy surface. As Figures 12 and 13 indicate, the fit to the ab initio data is excellent. The contour plot for H-atom abstraction in Figure 14 shows a shallow well in the entrance channel that appears in the ab initio data. It is not an artifact of our fit. The high energy cross sections will not be sensitive to it.

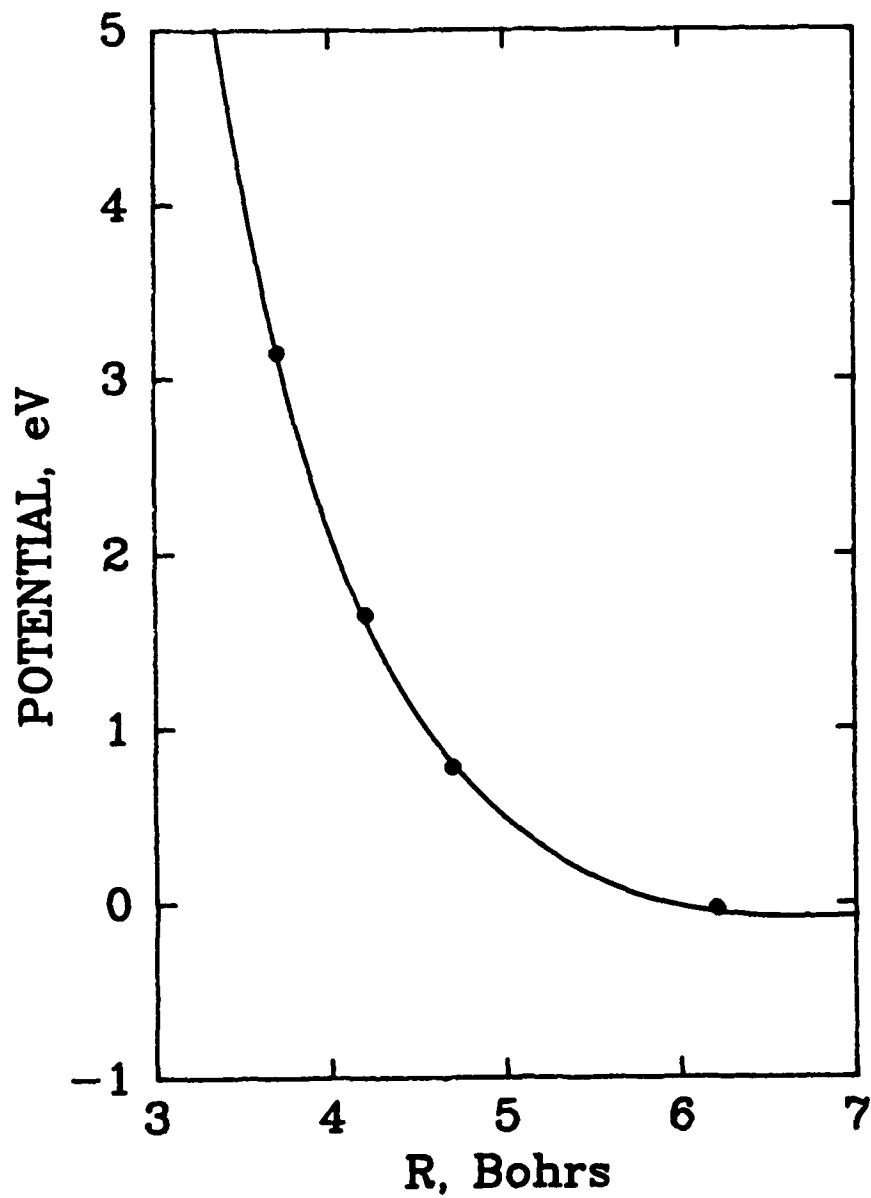


Figure 12. O^+HCl Potential Surface for $R=2.465$ at a C.M. Angle of 30 Degrees. The solid curve is the analytical fit, and the dots represent the ab initio data.

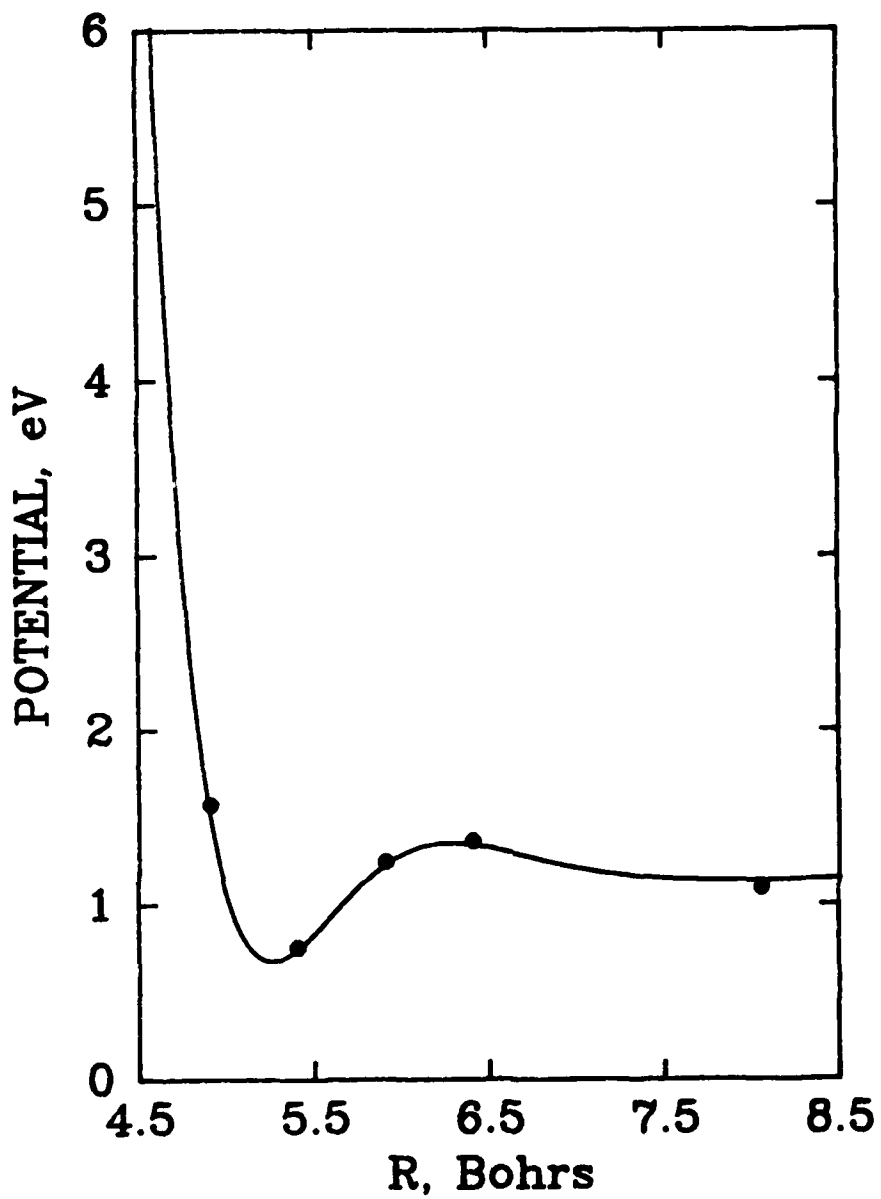


Figure 13. O+HCl Potential Surface for $R=3.45$ at a C.M. Angle of 0 Degrees. The solid curve is the analytical fit, and the dots represent the ab initio data.

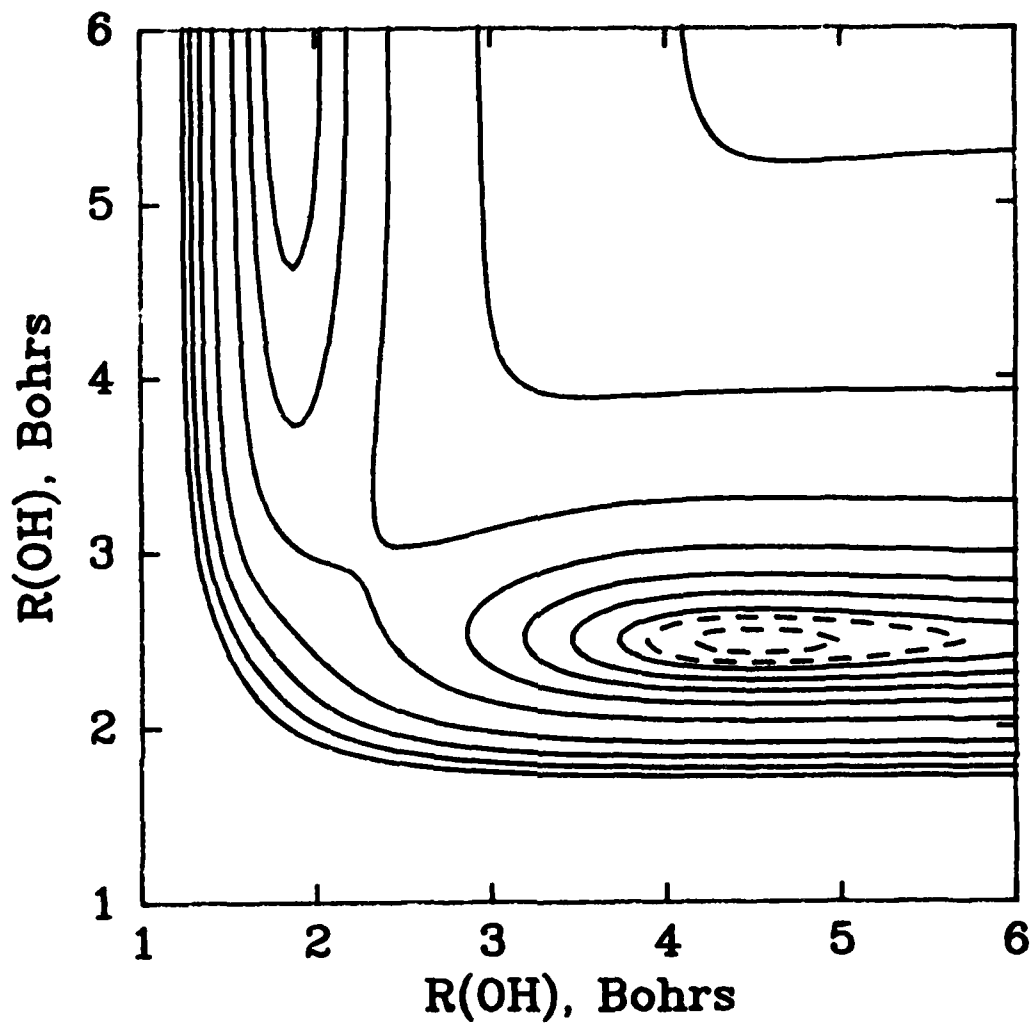


Figure 14. A Contour Plot of the O+HCl 0-Degree Surface I. Contour values are -.08, -.04, 0, .1, .25, .5, 1, 2, 3, 4, and 5 eV, with the negative contours shown as dashed lines.

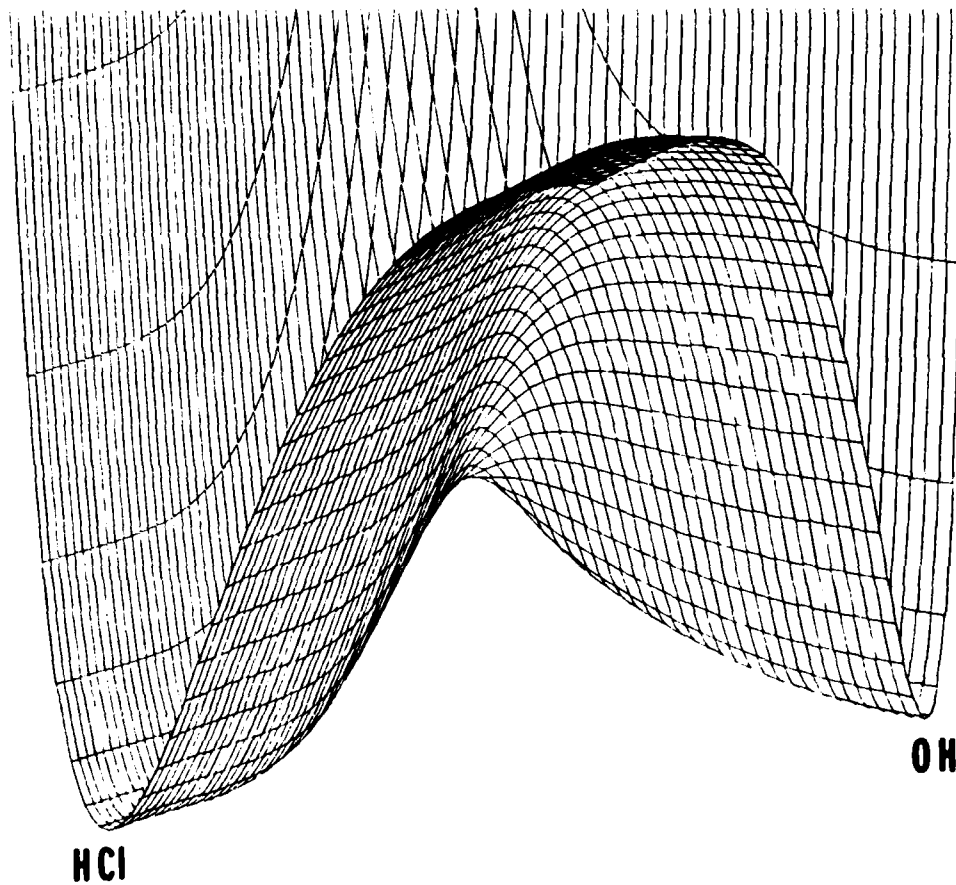


Figure 15. A Perspective Plot of the 0-Degree O+HCl Surface I. The Region of the Plot Corresponds to Figure 12. The Energy Range Spanned is 0 to 3.2 eV.

4.3 CROSS-SECTIONS FOR EXCITATION OF HCl BY O(³P)

Classical trajectory calculations were carried out over an energy range of 0.5 to 6 eV, corresponding to a relative velocity range of 3.0 to 10.2 km/sec. As expected from the energetics of the surface, the excitation thresholds for all processes are lower than for HF. At 5.9 km/sec the HCl v=1 excitation cross section is $.34 \text{ \AA}^2$ for HCl initially with angular momentum quantum number J=10, while the corresponding HF cross section is less than $.01 \text{ \AA}^2$. At the highest velocity considered, this cross section rises to 1.8 \AA^2 . The HF cross section is about 1/4 of this value.

Tables 11 through 13 present the results of our calculations for 3 values of initial J. Fits to the vibrational excitation cross sections are given for final v=1-3. For HF, we only provide a fit for v=1, due to the small values for the other cross sections. In Figure 16 we illustrate the J=10 cross sections from the analytic fits to the data. As for HF, the fits are accurate to within the errors inherent in the trajectory calculations.

4.4 CHEMICAL REACTION IN O(³P) + HCl COLLISIONS

VTST calculations were performed on this system as for O+HF. A saddle point occurs at [R(OH)=2.33, R(HCl)=2.99] Bohrs] with a barrier of 0.98 eV (2.25 kcal/mole). This barrier is approximately 1/2 that found for H-atom abstraction in O+HF. This system is endothermic by only .14 eV on this surface. These two properties will lead to much more reaction for this system than for O+HF.

Reaction cross sections are correspondingly larger. At 6 eV there is considerable OH formation. We also see OCl, although the cross section is smaller. We cannot provide quantitative estimates of the cross section for

TABLE 11. CROSS SECTIONS FOR EXCITATION OF HCl(J=0) ON SURFACE I*

		<u>Quantum Number v</u>						
E_{rel}	V_{rel}	1	2	3	4	5	6	7
2.0	5.9	.11	.005	-0-	-0-	-0-	-0-	-0-
2.5	6.6	.17	.022	.007	-0-	-0-	-0-	-0-
3.0	7.2	.48	.045	.021	.002	-0-	-0-	-0-
4.0	8.4	.53	.062	.026	.016	.01	-0-	-0-
5.0	9.3	1.08	.097	.068	.036	.015	.009	.005
6.0	10.2	1.60	.15	.085	.051	.018	.005	.003

Analytical Fits

$$Q(E_{rel}) = A \exp[(a + bE + cE^2)/(E - E_0)]$$

v	A	a	b	c	E_0
1	.0757023	-2.79790	1.00006	.385991	.468510
2	.0564515	-5.41613	1.36716	.0480587	.760230
3	.0541956	-7.96351	1.91882	-.0426581	1.035450

*Energy units are eV
 Velocity units are km/sec
 Cross Sections are in Å^2

Error bars of one standard deviation are approximately 10% at 6 eV and 50% at 2 eV for v=1. Error bars on the other transitions scale approximately with the magnitude of the cross section, so that the smallest transitions have error bars of approximately the magnitude of the cross section. Entries marked with the symbol -0- indicate that no trajectories were found that correspond to the indicated final vibrational state. The notation 0 indicates the relative velocity is below the energetic threshold.

TABLE 12. CROSS SECTIONS FOR EXCITATION OF HCl(J=5) ON SURFACE I*

E _{rel}	V _{rel}	Quantum Number v						
		1	2	3	4	5	6	7
2.0	5.9	.16	.021	-0-	-0-	-0-	-0-	-0-
2.5	6.6	.30	.064	.008	-0-	-0-	-0-	-0-
3.0	7.2	.32	.095	.024	.002	.001	-0-	-0-
4.0	8.4	.56	.16	.051	.012	.003	.005	-0-
5.0	9.3	1.13	.20	.065	.029	.024	.014	.013
6.0	10.2	1.47	.25	.096	.058	.028	.014	-0-

Analytical Fits

$$Q(E_{rel}) = A \exp[(a + bE + cE^2)/(E - E_0)]$$

v	A	a	b	c	E ₀
1	.772229	-1.84701	-.988499	.319375	.440150
2	8.08061	-2.76944	-2.23971	-.0576417	.732960
3	1.87208(5)	7.32361	-11.6931	.0560383	1.009260

*Energy units are eV
 Velocity units are km/sec
 Cross Sections are in Å²

Error bars of one standard deviation are approximately 10% at 6 eV and 50% at 2 eV for v=1. Error bars on the other transitions scale approximately with the magnitude of the cross section, so that the smallest transitions have error bars of approximately the magnitude of the cross section. Entries marked with the symbol -0- indicate that no trajectories were found that correspond to the indicated final vibrational state. The notation 0 indicates the relative velocity is below the energetic threshold.

TABLE 13. CROSS SECTIONS FOR EXCITATION OF HCl(J=10) ON SURFACE I*

E _{rel}	V _{rel}	Quantum Number v						
		1	2	3	4	5	6	7
2.0	5.9	.34	.041	.002	.001	-0-	-0-	-0-
2.5	6.6	.40	.049	.009	.008	-0-	-0-	-0-
3.0	7.2	.49	.088	.025	.014	-0-	-0-	-0-
4.0	8.4	.79	.14	.054	.032	.005	.002	-0-
5.0	9.3	1.18	.20	.058	.041	.02	.001	.001
6.0	10.2	1.80	.29	.11	.073	.03	.021	.017

Analytical Fits

$$Q(E_{rel}) = A \exp[(a + bE + cE^2)/(E - E_0)]$$

v	A	a	b	c	E ₀
1	5.83576	-.853798	-2.61815	.266106	.355590
2	.405522(+3)	3.38533	-8.62034	.264015	.651630
3	.151200(-5)	-14.1377	10.7302	.166057	.931160

*Energy units are eV
 Velocity units are km/sec
 Cross Sections are in Å²

Error bars of one standard deviation are approximately 10% at 6 eV and 50% at 2 eV for v=1. Error bars on the other transitions scale approximately with the magnitude of the cross section, so that the smallest transitions have error bars of approximately the magnitude of the cross section. Entries marked with the symbol -0- indicate that no trajectories were found that correspond to the indicated final vibrational state. The notation 0 indicates the relative velocity is below the energetic threshold.

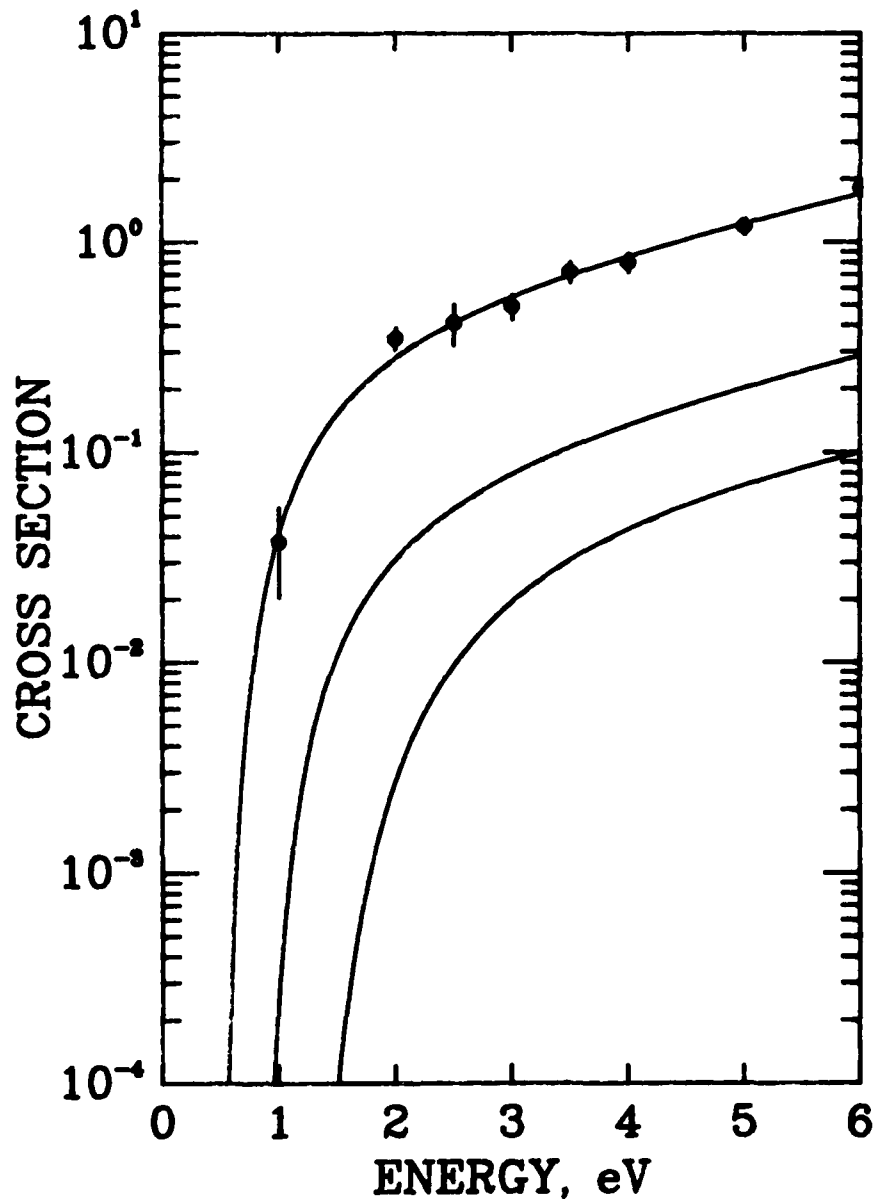


Figure 16. Cross Sections for Vibrational Excitation of HCl(J=10).

Units are $\text{\AA}^2 (10^{-16} \text{ cm}^2)$. The three curves correspond from top to bottom to $v=1, 2$ and 3 , respectively. The vertical lines represent 2-sigma (95%) deviations for the $v=1$ excitation.

forming OCl because our surface is only of qualitative utility for that channel. The theoretical methods employed here can be extended to provide a better description of that channel by using a larger basis set for the ab initio calculations.

In Figure 17 we present cross sections for reactive scattering to form OH for HCl(v=0). Due to basis set limitations in the electronic structure calculations, the threshold cross sections are not reliable (they are underestimated), but the high energy results are more meaningful. At the collision velocities of importance in plume modelling, OH formation should be a modestly important process. At 2.0 eV, the cross section for formation of OH(v=0) is approximately $3.6(-18)$ square Angstroms, and it increases to $1.1(-17)$ square Angstroms at 5 eV. The cross sections for formation of vibrationally excited OH are smaller. This is typical of an endothermic process, and in fact we expect the reaction cross sections to be larger for HCl with initial vibrational quanta.

4.5 VIBRATIONAL RELAXATION IN $O(^3P) + HCl$ COLLISIONS

As for HF, classical trajectory calculations were performed to obtain cross sections and relaxation rates for HCl(v=1). The energy dependence of b_{\max} was first determined, and used for the cross section calculations. The cross section for relaxation to HCl(v=0) rises from a value of $6(-19)$ square Angstroms at .6 eV to $5(-17)$ square Angstroms at 3 eV. The cross section for excitation to HCl(v=2) rises to a value of $7(-17)$ square Angstroms at the same translational energy. Reactive processes to form OH are small, even though we have one quantum of reagent vibration. Apparently more than one quantum of vibrational excitation is required to really drive the

reaction. Figure 18 presents our cross sections for collisions involving $\text{HCl}(v=1)$.

Rate constants for relaxation processes involving $\text{HCl}(v=1)$ are presented in Figure 19. As with HF, we essentially could obtain no meaningful data below a few thousand degrees K due to the considerable activation energies associated with these systems. Although experimental data for relaxation of HCl is available in the open literature⁴⁴⁻⁴⁵, it is for approximately 300 K. Due to the rapid fall off of probability (and reliability) with decreasing temperature, an Arrhenius extrapolation of our data is not fruitful. The plot of k versus temperature (instead of inverse temperature used in an Arrhenius plot) does extrapolate to within one deviation of MacDonald and Moore's 300 K value.⁴⁴ This results in a nonlinear temperature dependence on an Arrhenius plot, although that is not an unusual occurrence.

We also performed some calculations at 10000 K for rotationally excited $\text{HCl}(v=1)$, with $j = 3$ and $j = 5$. Within one standard deviation the relaxation rates to form $\text{HCl}(v=0)$ are the same as for $j = 0$. The same seems to hold for reactive cooling to form $\text{OH}(v=0)$, although with the limited number of trajectories that statement is not as strong due to the smaller probabilities for the reaction.

Some trajectories were run for $\text{HCl}(v=2)$ since experimentally we know that the rate to form $\text{HCl}(v=1)$ from this state is approximately four times that to form $\text{HCl}(v=0)$ from $\text{HCl}(v=1)$.⁴⁴ Our calculations tend to confirm this, although we were limited to high temperatures. In any case, the high temperature rate constants obtained in the present work are assumed to be reasonably accurate and are obtained in the temperature regime of interest.

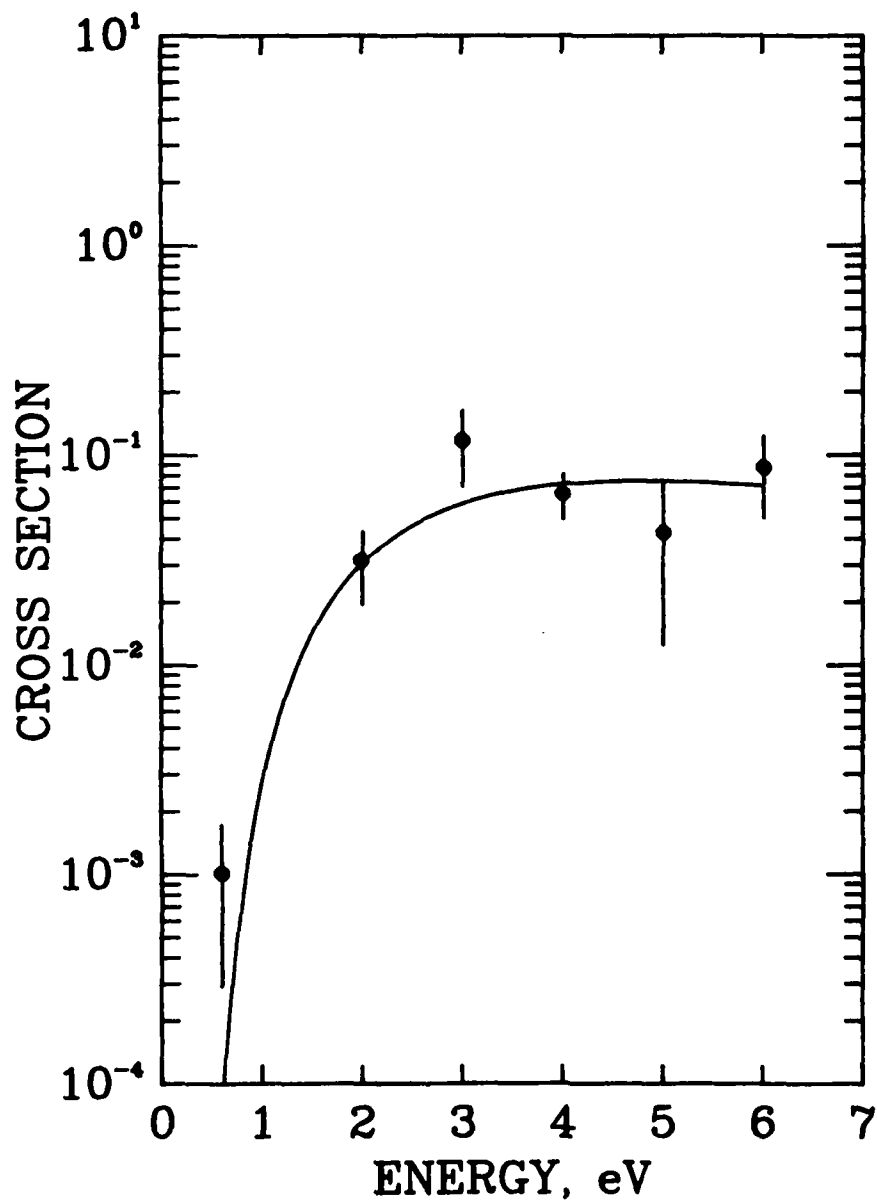


Figure 17. Reactive Cross Section to Form OH(v=0) From O + HCl(v=1).

Units are Å². 1-sigma deviations are shown.

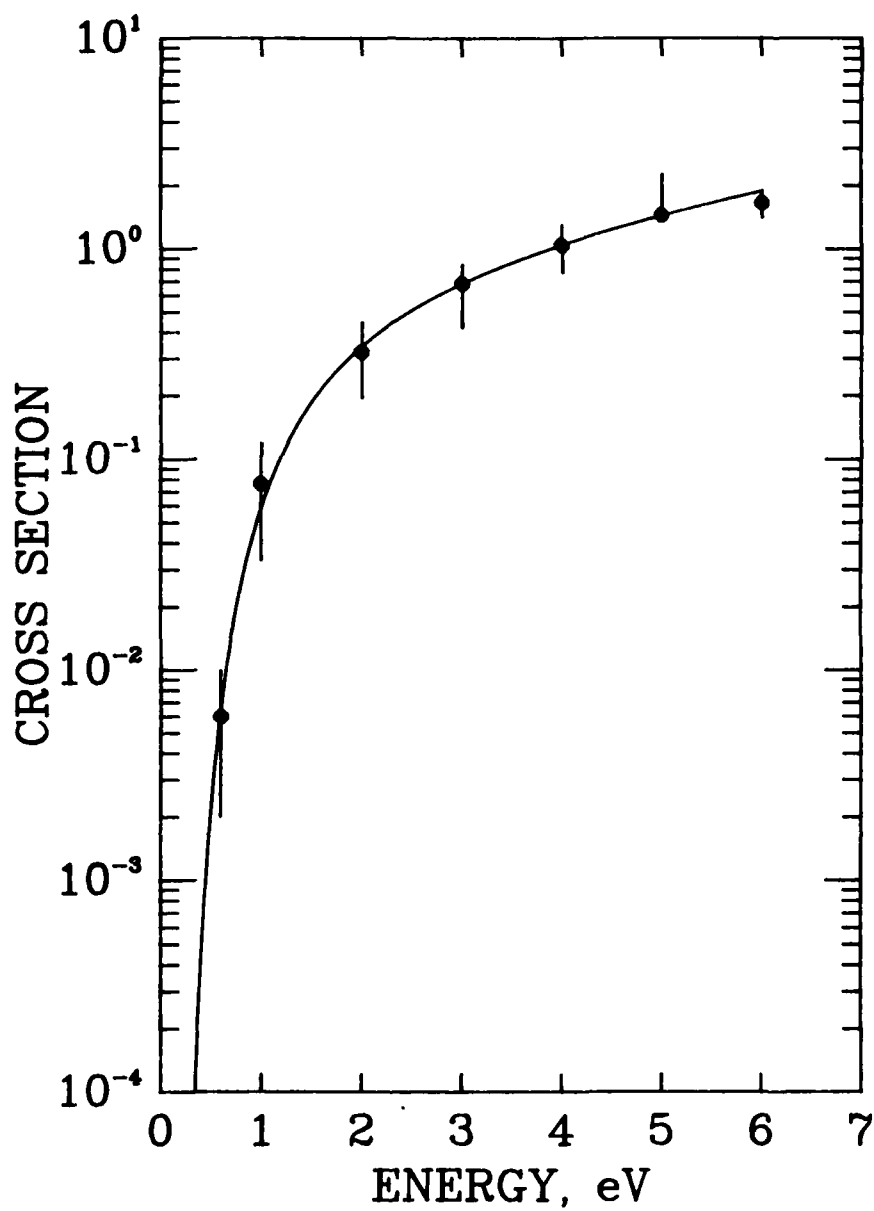


Figure 18. Cross Sections for Vibrational Relaxation of HCl($v=1$).

Units are \AA^2 . 2-Sigma deviations are shown.

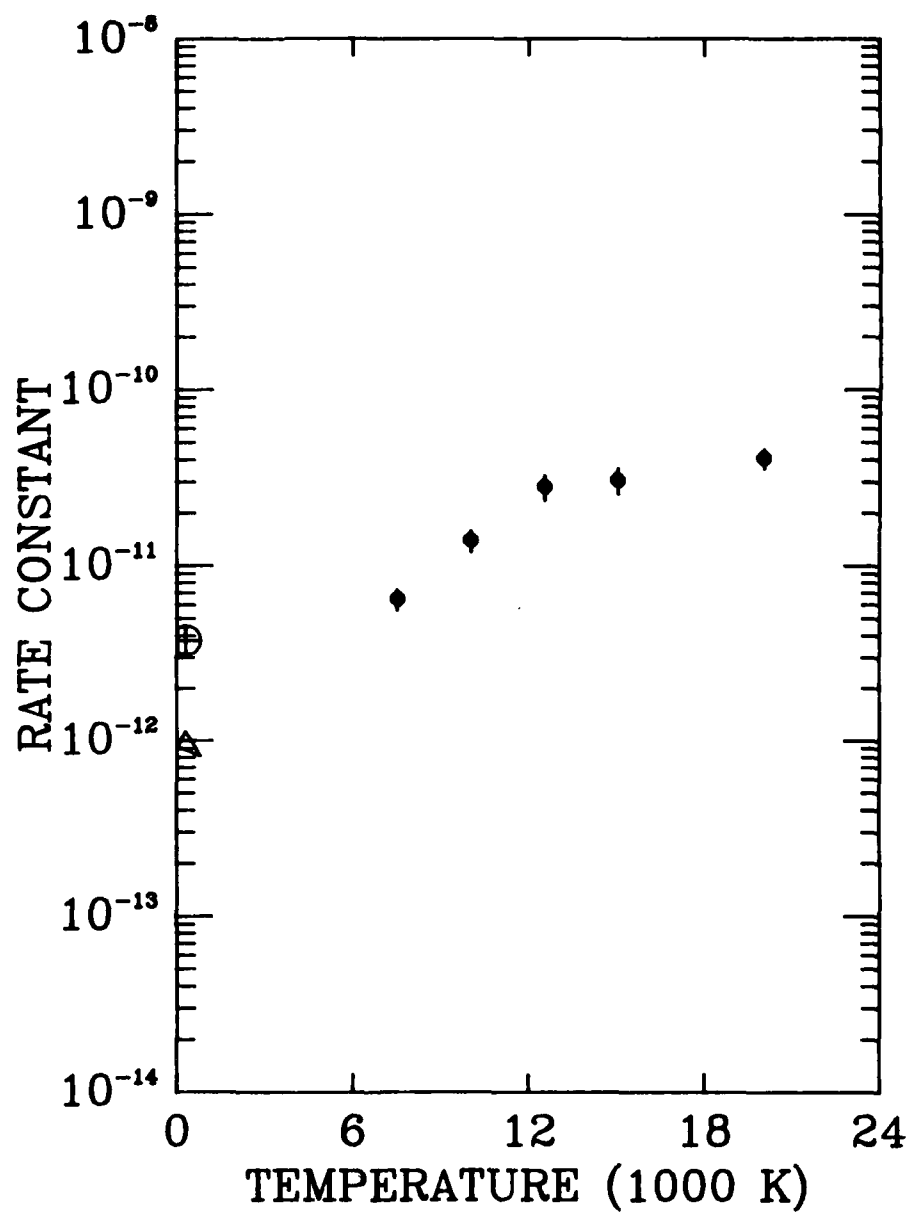


Figure 19. Rate Constant for Relaxation of HCl(v=1) to HCl(v=0).
 Units are cm³/mol-sec. 2-Sigma deviations are shown.
 The triangle is the experimental result of Macdonald and Moore,
 the circle the experimental result of Karny et. al. (Reference 44).

Section 5

O + CO COLLISIONS

5.1 Potential Energy Surface

Calculations for the A" surface of O + CO also used Dunning DZ basis sets. Here, including just the minimal orbitals and doubly occupying all of the 1s and 2s orbitals results in a space of 15 orbitals and 1,032 configurations for the full CI among the nondoubly occupied ones. This problem was judged to be infeasible. Therefore the configuration space was restricted to single and double excitations relative to the configuration having all except two electrons paired. This brought the configuration space down to a much more manageable 334 terms. The MCSCF CO potential corresponding to this case is compared to the experimental RKR curve in Figure 20.

This space is still adequate to describe the three-atom separated limit of the system since a double excitation from the base configuration (which occupies 12 orbitals leaving the anti-bonding orbitals from CO unoccupied) can unpair two more electrons, leaving two unpaired behind, for a total of six unpaired electrons, which can then be appropriately coupled to represent three triplet atoms. Essentially no difficulties in convergence were encountered for this MC. Apparently this can be attributed to a higher degree of "balance" in this calculation. That is, the number of valence orbitals in the space required the placing of 10 electrons in 9 orbitals. In fact, the analogous CO calculation, requiring 6 electrons in 6 orbitals has exactly one "correlating" orbital for each "active" orbital. This leads to a better-conditioned MC problem than the OHX cases, where there are 10 electrons to go into 7 orbitals, or the halogen halide cases

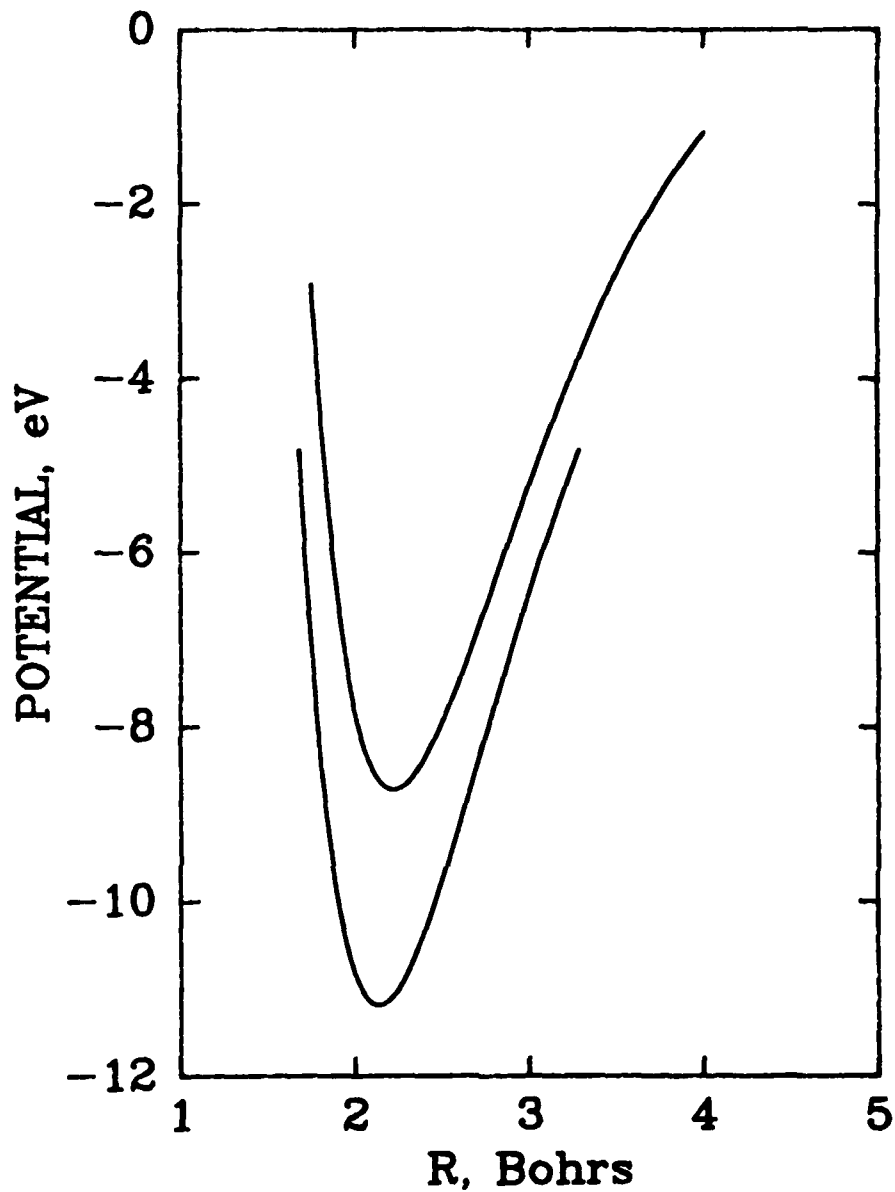


Figure 20. CO Potential Curve for a DZ Basis. The upper curve is the MC(55) potential, the lower is the RKR potential. The ab initio potential is relative to the total energy at $R = 10$.

where there are 6 electrons for 4 orbitals, or equivalently that there are no correlating orbitals for two of the active orbitals. However, it should be apparent that the rapidly expanding number of configurations resulting for the three-atom systems makes it difficult to add orbitals to the calculations.

We had hoped that the additional symmetry inherent in this system, as well as the expected high barrier to exchange would enable us to obtain a suitable fitted surface employing fewer computed data points than the OHX surfaces. However, we found that the barrier to exchange was not as high as expected. Furthermore, this surface apparently has a local minimum for the formation of a bent OCO triplet complex. Such features complicated the fitting procedure, requiring more ab initio points than anticipated. Approximately 70 points were computed for fitting the surface.

5.2 ANALYTICAL REPRESENTATION OF THE O + CO POTENTIAL SURFACE

The state chosen for study is the A" state. Because of the symmetry inherent in this system, only 70 ab initio points were required for the fit. The fitting procedure was complicated because the minimum energy path for the oxygen atom exchange occurs for nonlinear geometries. The surface also has a local minimum for the formation of a bent OCO triplet complex.

The fit used for the present dynamics calculations has an rms error of .238 eV (5.5 kcal/mole). This is considerably larger than we attained for the HF and HCl molecules interacting with oxygen, and reflects the more complex nature of the surface. We have managed to cut this in half using more complicated functional forms. Angle dependent Sato parameters were necessary to accommodate the nonlinear intermediate reaction path. The data

set contains points up to 7 eV, and, considering we are scattering at energies up to 6 eV, the present rms error in the fit can be considered adequate, although not optimal, at least for vibrational excitation studies. Parameters defining the fit are given in Table 14.

Figures 21 and 22 compare the fit to the data points. Figure 22 shows a bond angle bending potential to show the angular behavior that made the fit difficult. The accuracy of the fit is good considering the complexity of the surface. The use of angle-dependent Sato functions added considerable flexibility to our fitting function, and provided a sufficiently accurate fit without our having to use an additional polynomial term. We did try a 3-body term, but the improvement was only about 0.2 kcal/mole in the rms error. The improvement is small because symmetry in the O + CO system results in only 20 coefficients in the polynomial. By going to sixth-order we could have introduced enough additional flexibility to make the 3-body term useful, but there was insufficient ab-initio data to determine the additional parameters.

Figures 23 and 24 show contour and 3D perspective plots of the surface for a 127 degree approach (bond angle). This angle represents the angle of attack corresponding to the minimum energy path for the O+CO exchange reaction. Because of the complexity of the surface, a single plot is not sufficient to represent the minimum energy path over a very large range of R.

TABLE 14. PARAMETERS FOR O + CO ($^3A''$) POTENTIAL ENERGY SURFACE I

	TWO-BODY TERM	
	O ₂	CO
D ₀	.2616977 E+1	.8629377 E+1
R ₀	.2281882 E+1	.2203128 E+1
b ₁	.2881580 E+1	.3000490 E+1
b ₂	.2180270 E+1	.2643494 E+1
B ₃	.8883884 E+0	.7863756 E+0
a ₁	.4072468 E+4	.7459227 E+2
a ₂	-.2531790 E+0	.1628484 E+1
a ₃	.3762120 E-1	-.1022201 E+0
a ₄	.2032419 E+1	.1640921 E+1
Δ ₀	.4300060 E-1	-.2982237 E+0
d ₁	.1120325 E+0	-.1614153 E+0
d ₂	.1201922 E+0	.6862887 E+1
d ₃	-.4176183 E+0	-.7909080 E+1

* Units of energy are eV, units of distance are Bohrs.

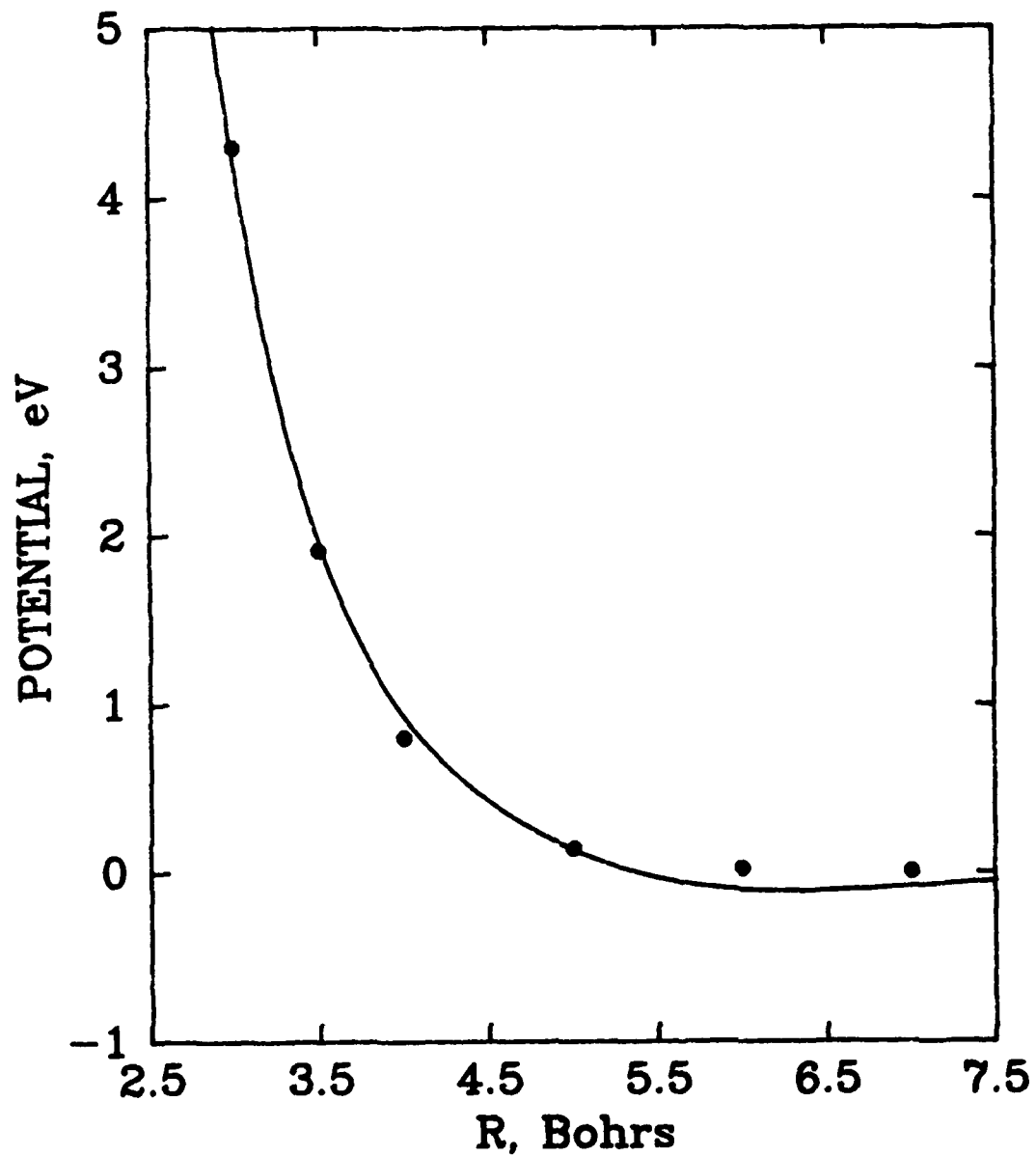


Figure 21. O+CO Potential Surface for $R=2.2$ at a C.M. Angle of 90 Degrees. The solid curve is the analytical fit, and the dots represent the ab initio data.

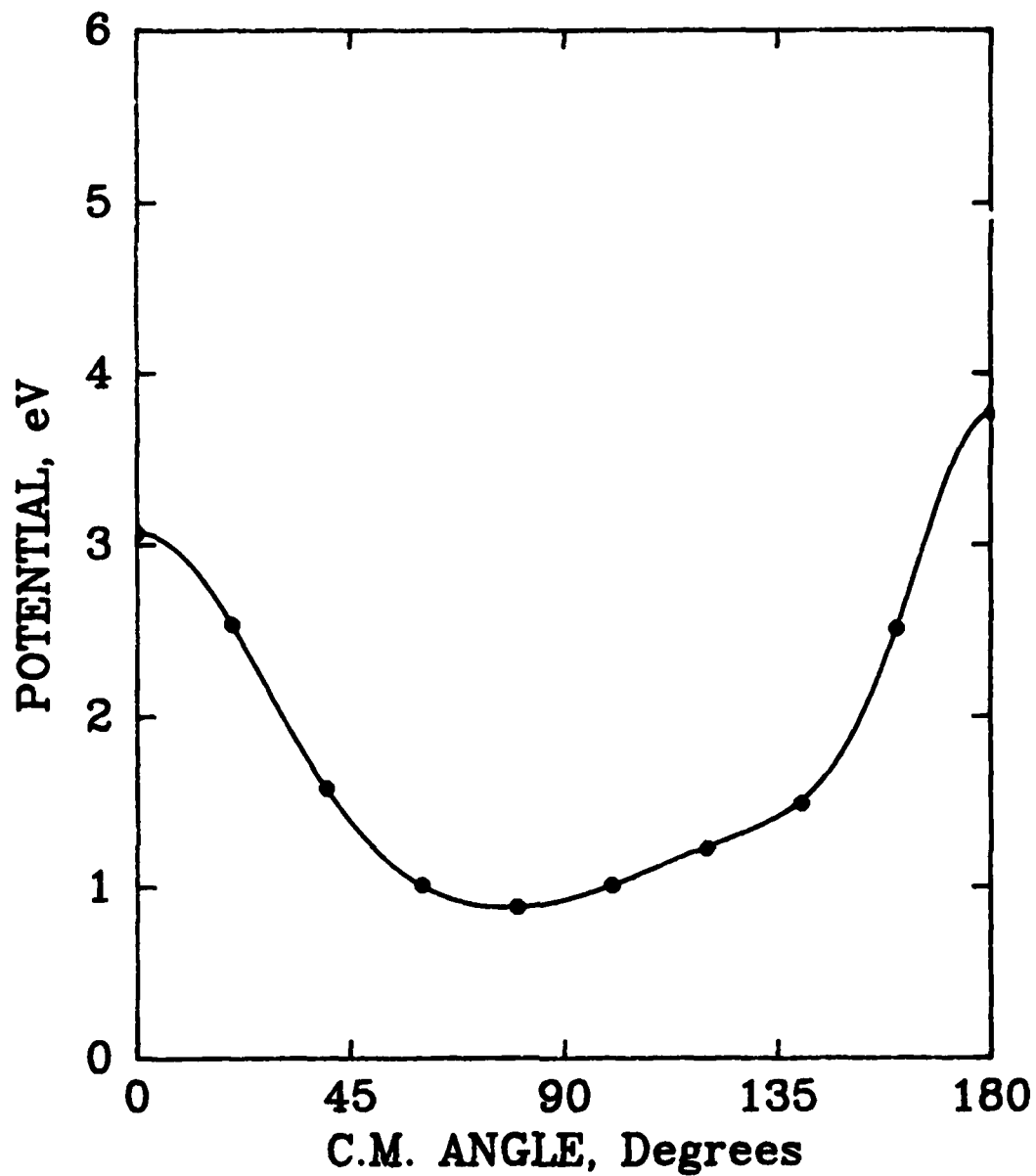


Figure 22. O+CO Bond Angle Bending Potential for $R(\text{CO})=2.2$, $R=4.0$. The distances are given in bohrs. The solid curve is the analytical fit and the dots represent the ab initio data.

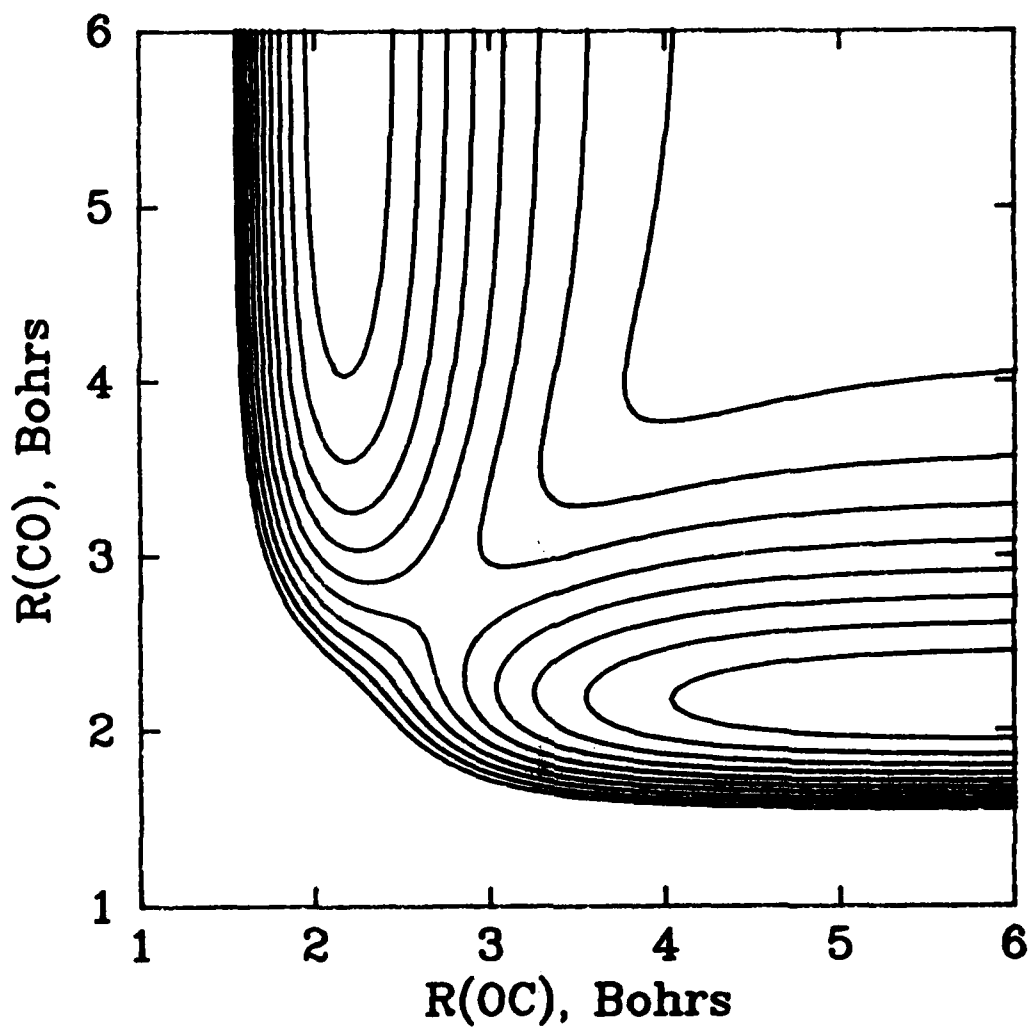


Figure 23. O+CO Surface Contour Plot for a Bond Angle of 127 Degrees. Contour values are to 10 eV in increments of 1 eV.

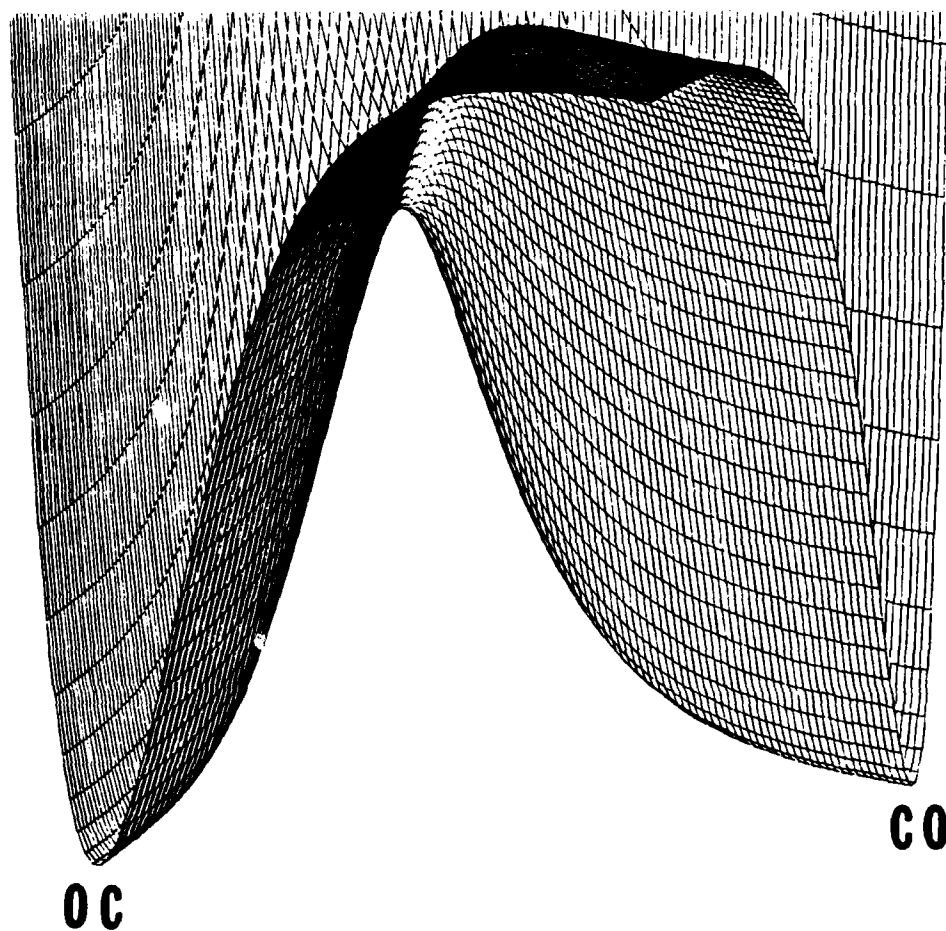


Figure 24. A Perspective Plot of the 127-Degree O+CO Surface. The Region of the Plot Corresponds to Figure 18. The Energy Range Spanned is 0 to 10. eV.

5.3 CROSS-SECTIONS FOR EXCITATION OF CO BY O(³P)

Trajectory calculations were done for this system over a velocity range of 3.8 to 10.7 km/sec, again for three initial angular momenta corresponding to J=0, 5, and 10. At 6 km/sec, the average final rotational quantum number increases from J=17 to J=20 for initial J=0 and J=10, respectively. At 10 km/sec the range is 18 to 21, indicating little dependence on relative velocity. There is appreciable rotational excitation at both velocities, with some final J values found above J=60.

The vibrational excitation cross sections are large at high velocities, but small at velocities below 7.5 km/sec. The results of this study for three angular momenta are given in Tables 15 through 17. The v=1 excitation cross section is presented in Figure 25. As for HF, the only cross section for which an analytical fit is given is v=1.

Of considerable interest is the amount of vibrational excitation found in CO formed by the exchange reaction, as compared to direct vibrational excitation. While the direct v=1 cross section is about 8 times as high at 10.7 km/sec as the cross section for forming v=1 by exchange, the cross sections for v greater than 1 are larger for the exchange reaction. Thus reaction is a dominant pathway for forming vibrationally excited CO molecules.

5.4 CHEMICAL REACTION IN O(³P) + CO COLLISIONS

VTST calculations have not been performed to date for this system due to complications caused by the nonlinear minimum energy path. Classical trajectory calculations show that the exchange reaction results in nonnegligible cross sections above 3 eV. Trajectory calculations of 12500 K

TABLE 15. CROSS SECTIONS FOR EXCITATION OF CO(J=0) ON SURFACE I*

E _{rel}	V _{rel}	Quantum Number v						
		1	2	3	4	5	6	7
3.0	7.5	.012	-0-	-0-	-0-	-0-	-0-	-0-
4.0	8.7	.31	.013	.004	-0-	-0-	-0-	-0-
5.0	9.7	.96	.017	.016	-0-	-0-	-0-	-0-
6.0	10.7	1.38	.27	.02	.04	.01	.01	-0-

Analytical Fit for v=1 Cross Section

$$Q(E_{rel}) = A \exp[(a + bE + cE^2)/(E - E_0)]$$

A	a	b	c	E ₀
.0627475	-50.3213	19.4138	-1.35746	.374180

*Energy units are eV
 Velocity units are km/sec
 Cross Sections are in Å²

Error bars of one standard deviation are approximately 10% at 6 eV and 50% at 2 eV for v=1. Error bars on the other transitions scale approximately with the magnitude of the cross section, so that the smallest transitions have error bars of approximately the magnitude of the cross section. Entries marked with the symbol -0- indicate that no trajectories were found that correspond to the indicated final vibrational state. The notation 0 indicates the relative velocity is below the energetic threshold.

TABLE 16. CROSS SECTIONS FOR EXCITATION OF CO(J=5) ON SURFACE I*

E _{rel}	V _{rel}	Quantum Number v						
		1	2	3	4	5	6	7
3.0	7.5	.021	-0-	-0-	-0-	-0-	-0-	-0-
4.0	8.7	.29	.005	-0-	-0-	-0-	-0-	-0-
5.0	9.7	.72	.07	.01	-0-	-0-	-0-	-0-
6.0	10.7	1.40	.15	.06	.03	-0-	-0-	-0-

Analytical Fit for v=1 Cross Section

$$Q(E_{rel}) = A \exp[(a + bE + cE^2)/(E - E_0)]$$

A	a	b	c	E ₀
4.48290	-32.4652	8.07237	-.635656	.368660

*Energy units are eV
 Velocity units are km/sec
 Cross Sections are in Å²

Error bars of one standard deviation are approximately 10% at 6 eV and 50% at 2 eV for v=1. Error bars on the other transitions scale approximately with the magnitude of the cross section, so that the smallest transitions have error bars of approximately the magnitude of the cross section. Entries marked with the symbol -0- indicate that no trajectories were found that correspond to the indicated final vibrational state. The notation 0 indicates the relative velocity is below the energetic threshold.

TABLE 17. CROSS SECTIONS FOR EXCITATION OF CO(J=10) ON SURFACE I*

E _{rel}	V _{rel}	Quantum Number v						
		1	2	3	4	5	6	7
3.0	7.5	.031	-0-	-0-	-0-	-0-	-0-	-0-
4.0	8.7	.43	.017	.018	-0-	-0-	-0-	-0-
5.0	9.7	.92	.047	.016	.002	-0-	-0-	-0-
6.0	10.7	1.25	.25	.05	.03	-0-	-0-	-0-

Analytical Fit for v=1 Cross Section

$$Q(E_{rel}) = A \exp[(a + bE + cE^2)/(E - E_0)]$$

A	a	b	c	E ₀
80.0615	-39.0031	9.57195	-1.17833	.352090

*Energy units are eV
 Velocity units are km/sec
 Cross Sections are in Å²

Error bars of one standard deviation are approximately 10% at 6 eV and 50% at 2 eV for v=1. Error bars on the other transitions scale approximately with the magnitude of the cross section, so that the smallest transitions have error bars of approximately the magnitude of the cross section. Entries marked with the symbol -0- indicate that no trajectories were found that correspond to the indicated final vibrational state. The notation 0 indicates the relative velocity is below the energetic threshold.

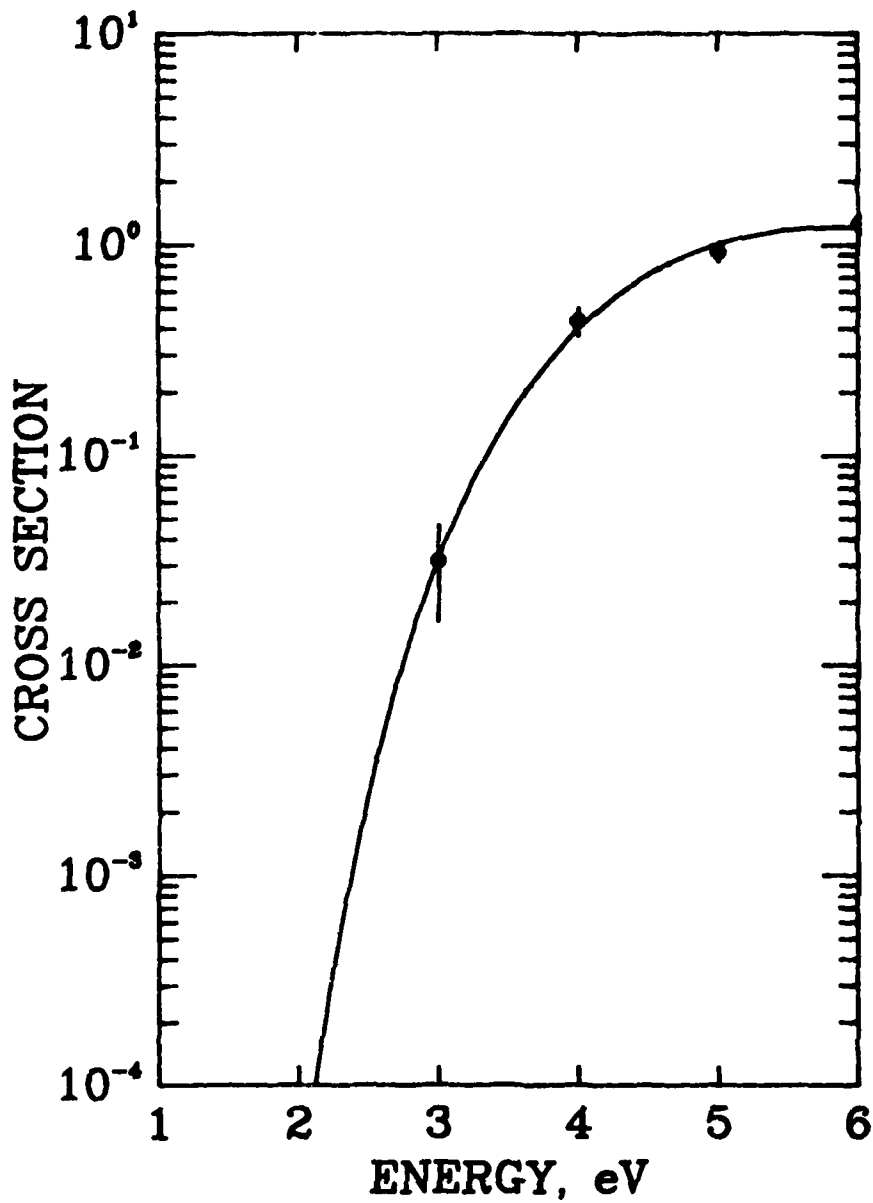


Figure 25. Cross Section for $v=1$ Excitation of $\text{CO}(J=10)$.

Units are Å^2 (10^{-16} cm^2). 2-sigma (95%) deviations are shown by the vertical lines.

AD-A145 198

COLLISIONAL EXCITATION CROSS SECTIONS(U) CHEMICAL
DYNAMICS CORP COLUMBUS OH M J REDMON ET AL. AUG 84
AFRPL-TR-84-030 F04611-82-C-0041

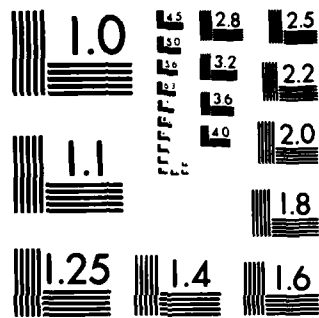
2/2

UNCLASSIFIED

F/G 20/8

NL





MICROCOPY RESOLUTION TEST CHART
NATIONAL BUREAU OF STANDARDS-1963-A

rate constants indicate that the reactive rates for forming CO by exchange vary from $5(-12)$ to $1(-12)$ $\text{cm}^3/\text{mol-sec}$ for final v from 0 to 4, respectively. There is considerable vibrational excitation of CO resulting from this process. The final rotational distribution is considerably hotter for the exchange reaction, with a final average J up to 70 at 6 eV. For direct (nonreactive) rotational excitation, the average J is 20 over a considerable initial velocity range.

5.5 VIBRATIONAL RELAXATION IN $\text{O}(^3\text{P}) + \text{CO}$ COLLISIONS

Cross sections for quenching of $\text{CO}(v=1)$ are shown in Figure 26, and rate constants for this process are given in Figure 27. Although the direct process is more efficient, the exchange reaction enhances the cooling process. As with HF and HCl, it was not possible to obtain low temperature rate constants due to the very high thresholds for relaxation. While the rates for quenching of CO are smaller than for HCl, they are considerably larger than for HF.

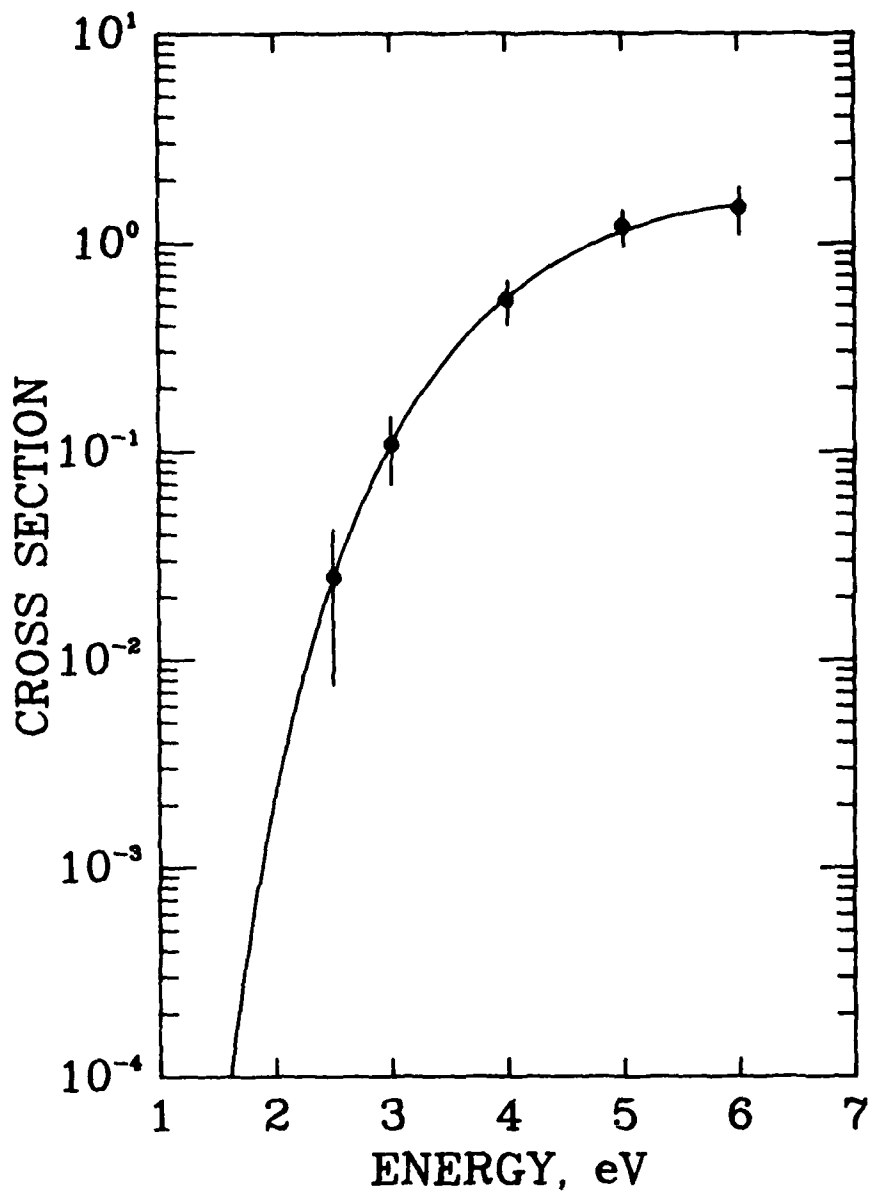


Figure 26. Cross Section for Vibrational Relaxation of CO(v=1)
 Units are Å². 2-Sigma deviations are shown.

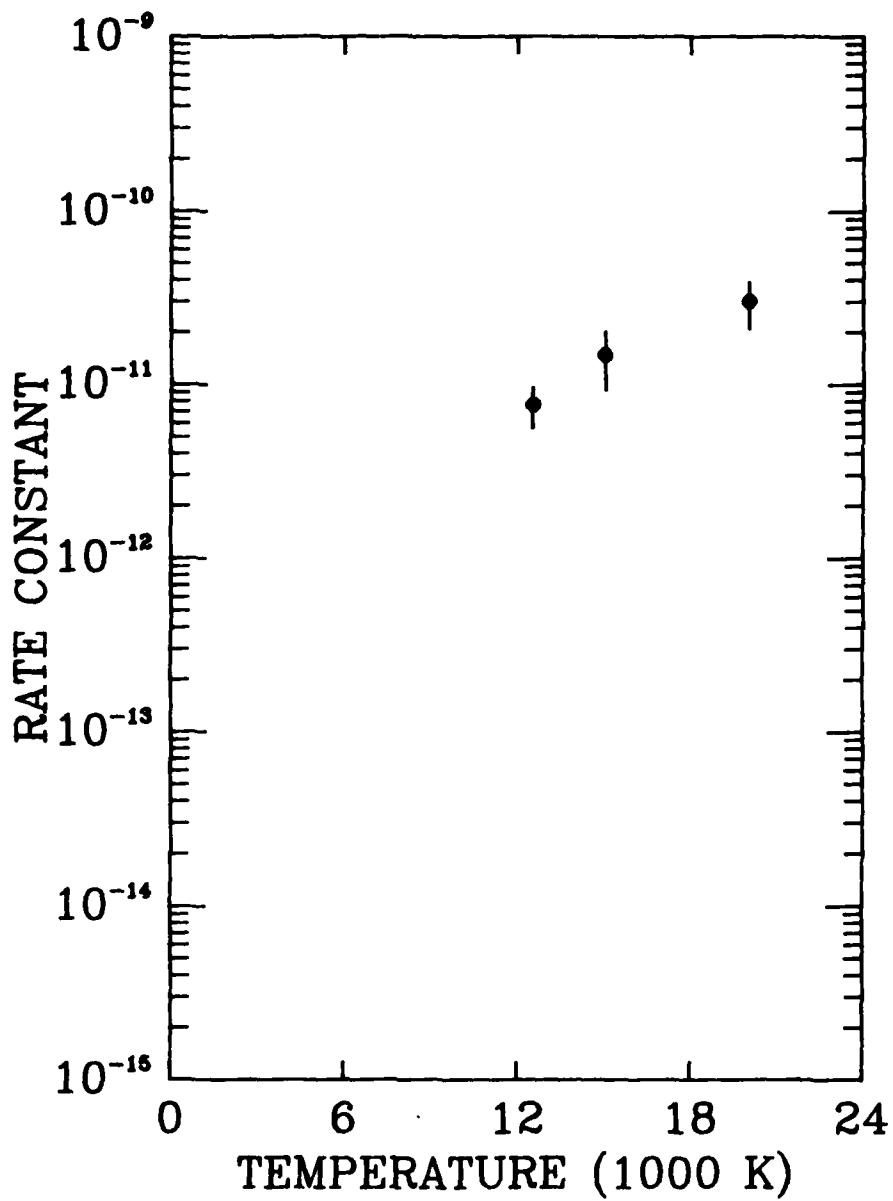


Figure 27. Rate Constant for Relaxation of CO(v=1)

Units are $\text{cm}^3/\text{mol}\cdot\text{sec}$. 2-Sigma deviations are shown.

Section 6

DYNAMICAL STUDIES OF $O(^3P) + CO_2$ COLLISIONS

In our previous work on this system with the classical trajectory method^{3,13} we found that excitation of the (001) mode was difficult to obtain by direct collisional excitation from the ground state. Subsequent quantum IOS calculations⁴⁶ predicted considerably larger cross sections, although we recently showed⁴⁷⁻⁴⁸ that most of the discrepancy between the classical and quantal results can be attributed to basis set errors in the quantal calculations. The remaining difference of about a factor of two can be attributed to difficulties in obtaining the very small classical probabilities. In any event we feel the (001) excitation cross section of Reference 47 is currently the most reliable estimate of this transition. The cross section for direct excitation of the (001) state of CO_2 by collision with an atomic partner is small and any experiments that indicate otherwise are simply measuring radiation from other transitions. We previously suggested¹³ that low resolution experiments can be observing radiation from combination bands that overlap the 4.3 micron band, such as from (NN'1) states of CO_2 . This premise has received experimental support from the recent work of Flynn and co-workers⁴⁹ at Columbia. In their work with hot hydrogen atoms, they find that direct collisions with hydrogen "do not produce detectable amounts" of (001) or (002) excitation. They attribute the observed radiation to the rapid accumulation of quanta in combination levels that subsequently produce (001) population. Our calculations on CO_2 are completely in agreement with this mechanism.

The direct computation of a relaxation rate for the (001) state of CO_2 is not practical within the classical trajectory method due to the long

lifetime of that state, just as calculations of excitation cross sections are difficult. We have therefore made use of the results of our quantum IOS calculations⁴⁷, have fit the cross section for the relaxation of (001), and directly computed the energy integral for the rate. The results are shown in Figure 28. The rates above a few thousand degrees are considered reliable, but the low temperature rates probably suffer from errors resulting from the required extrapolation of the cross section to threshold. The use of two different extrapolation methods and three different interpolation schemes produces 300 K rate constants that differ by an order of magnitude. However, the same comparison of rates computed at 5000 K show the difference is reduced to less than one percent, so that the rate integral at least is accurate for the high temperature rates that we report.

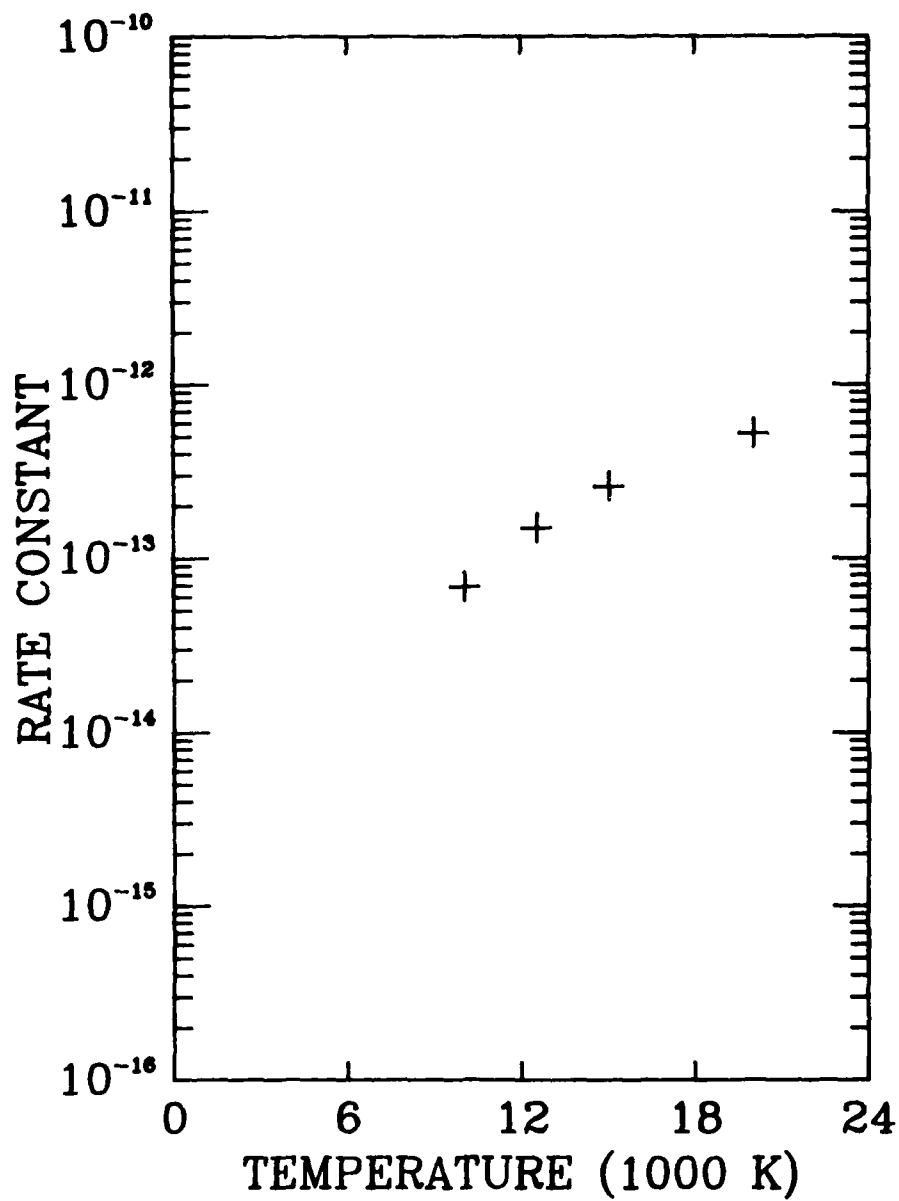


Figure 28. Rate Constant for Relaxation of $\text{CO}_2(001)$

Units are $\text{cm}^3/\text{mol}\cdot\text{sec}$

Section 7

DYNAMICAL STUDIES OF $O(^3P) + H_2O$ COLLISIONS

We have extended the calculations of collisional excitation of H_2O reported previously^{3,14} by computing many thousands of additional trajectories to decrease the Monte Carlo error. The results for the (001) excitation are shown as the dashed curve in Figure 29. The maximum in the cross section curve reported previously is not apparent. That maximum resulted from poor statistics in the cross section data. Within the Monte Carlo sampling error, however, the result is unchanged.

The cross section for relaxation of the (001) state was computed during the present contract, and is shown as the full curve in Figure 29. The potential surface used was obtained on the previous contract³. The computed points are also shown, along with the sampling error. Rate constants were computed by direct integration of the energy integral and are presented in Figure 30. Low temperature results are not shown since they are not expected to be accurate due to noise in the low energy cross section data. The cross section below 0.5 eV is probably overestimated due to noise in the action calculations.

We originally planned to perform new quantum chemistry calculations to extend the surface to allow for reaction, but the difficulties encountered in converging the 3-atom calculations meant that not enough time remained to do so. We did modify the four-atom trajectory code to permit the study of state-to-state reaction dynamics, and obtained an analytical function suitable for studying reaction. Our attempts to fit the surface without resorting to ab-initio calculations (we had already greatly exceeded our computing budget) did not yield a sufficiently reliable surface. Given

sufficient resources this part of the program can be completed.

The H_2O trajectory calculations are very time consuming, taking approximately 70 cpu seconds per trajectory on our computer system. This is a result of the complexity of the potential. To obtain a reasonably converged rate constant, thousands of trajectories are required. We have attempted to make the calculation of the (001) relaxation rate as efficient as possible, and by doing so (through optimizing b_{max}) we have sacrificed accuracy for other transitions. We have computed the rate for relaxation on the lowest adiabatic electronic state of H_2O . This means that we will miss any relaxation mechanism involving the other two triplet states that might be important at low temperatures. The theoretical results are probably reliable for the high temperatures reported.

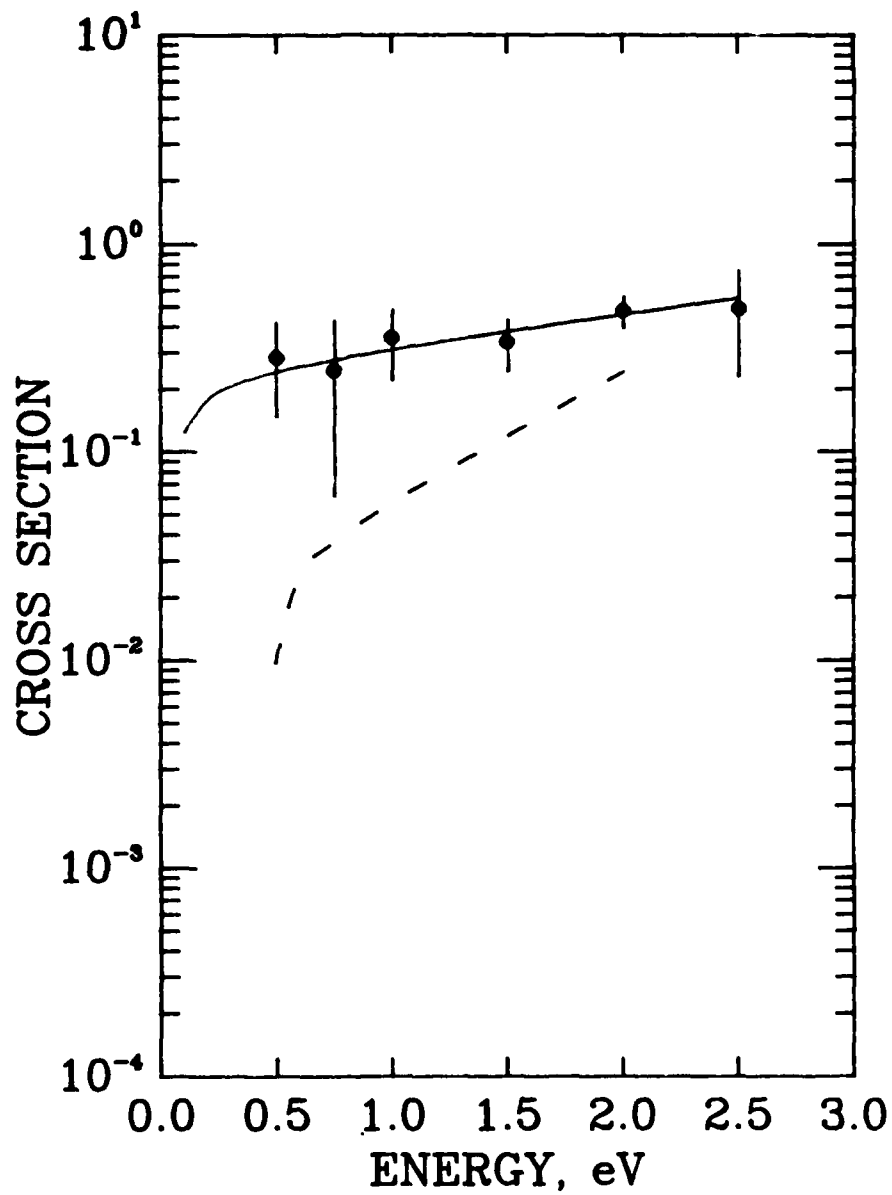


Figure 29. Cross Section for Vibrational Energy Transfer in $\text{H}_2\text{O}(001)$
Units are \AA^2

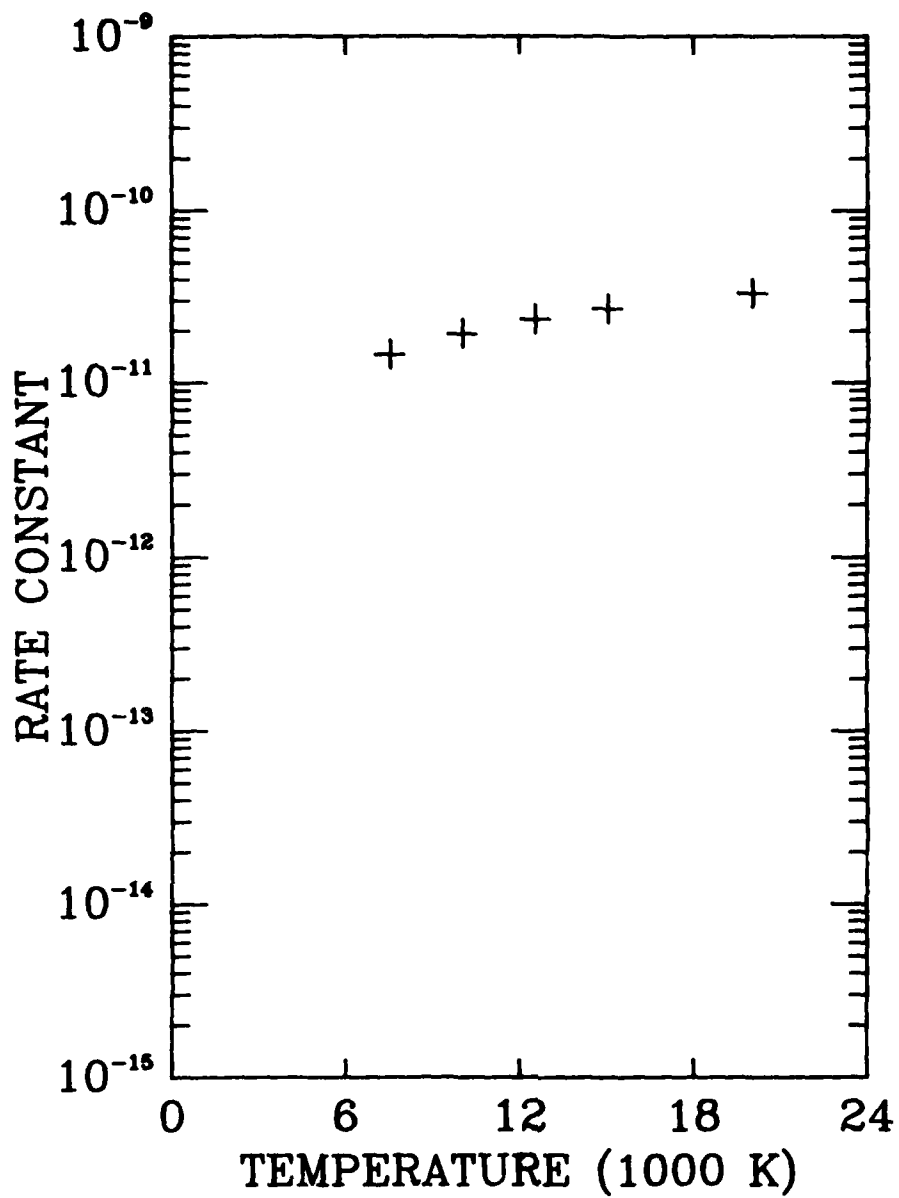


Figure 30. Rate Constant for Relaxation of H₂O(001)

Units are cm³/mol-sec

Section 8

CONCLUSIONS

During this contract vibrational excitation cross sections were obtained for HF, HCl and CO colliding with atomic oxygen. Potential energy surfaces were obtained with the multi-configuration self-consistent-field (MCSCF) method. Accurate analytical fits to the computed points were made for use in the dynamics calculations. The rms error in the fits approaches 1 kcal/mole, which is better than the error expected in the ab initio points from the limited basis set and lack of complete electron correlation. Although absolute energies are often in error, the important quantity for energy transfer calculations is the variation of the potential energy with geometry, and experience shows that computed gradients are sufficiently accurate. The goal for overall accuracy in the cross sections was a factor of two. We believe this has been achieved for the processes with large transition probabilities, i.e., for those with cross sections on the order of one \AA^2 .

One aspect of collisional excitation involving triplet oxygen that was ignored in the present calculations is the role of other electronic states in the dynamics. In particular, there are two other electronic surfaces that correlate with the same separated atom limit ($O(^3P)$ removed to an infinite distance from the molecule). The assumptions in the current approach are that these surfaces are similar and that the computed scattering cross section would be independent of which state was studied. When a factor of two error is acceptable, these assumptions are probably sufficiently valid for high velocity inelastic scattering. This judgment is supported by recent experiments for vibrational relaxation of HF and DF

(which should be sensitive to vibronic effects due to electronically nonadiabatic coupling of electronic states) that indicated the magnitude of these effects to be on the order of a factor of two.⁴¹

The assumptions are less tenable for reaction since each of the three reactant electronic states correlates with a different OH product state. However, it is often the case that only the lowest channel is energetically accessible. Therefore the present calculations are expected to yield good results for vibrational excitation of the reagent molecule, but only qualitative information on the products of reaction. The present methods are applicable to studying each of the three surfaces. The results could then be averaged for input to the plume modelling codes, which do not yet include all of the species responsible for the observed signature, much less explicitly treat individual contributing states. Present dynamics codes cannot simultaneously address all three states. The development of a single dynamical model including accurate treatment of the coupling of the electronic surfaces is an area of active research.

While it is possible to model potential surfaces for vibrational relaxation studies in terms of pair interactions that only approximate the true surface and do not allow for chemical rearrangement, the nature of our computed surfaces indicates that potentials must be designed to include the possibility of reaction. We found that high velocity collisions could force the molecule into vibrational displacements so extended that geometries near saddle points for reaction were sampled, even though the outcome of the trajectory was nonreactive. When a trajectory encounters such "softer" areas of a surface, the energy transfer can be considerably different than that of an otherwise similar collision on a more impulsive surface, such as

one represented by a simple sum of pairwise interactions. The potential surface contour and 3D perspective plots in this report show the variations in the shape of these surfaces in regions where reaction can occur. Thus, while the cross sections for reaction in these systems are approximate, particularly at the lower energies, reactive trajectories were obtained during the current vibrational cross section calculations, and indicate the extent to which reaction is important for collisions involving atomic oxygen.

In comparing the relative importance of vibrational excitation for the three diatomic systems studied, we find that HCl has a lower excitation threshold and, therefore, a larger cross section for a given relative velocity. CO is next in importance. A similar trend holds for vibrational relaxation, as is expected from considerations of microscopic reversibility. A comparison at 8.7 km/sec shows that the $v=1$ cross section for HF is $.14 \text{ \AA}^2$, while for CO the value is $.43 \text{ \AA}^2$, and for HCl this cross section is approximately (by interpolation) $.91 \text{ \AA}^2$. At relative velocities greater than 10 km/sec this ordering still holds; the HF cross section reaches only $.5 \text{ \AA}^2$, while both the HCl and CO cross sections attain values of over 1 \AA^2 . These values are for an initial J of 10, but the trends are the same for the other two J values studied.

Our studies indicate that the 4.3 micron radiation of interest in plume modelling does not result from direct excitation of the (001) state of CO_2 ; it must originate in combination bands ($\text{NN}'1$) instead. Our calculated (001) relaxation rates are small, and our conclusions are strongly supported by the recent experiments of Flynn and coworkers⁴⁹. It must be understood that our work on CO_2 only eliminates the (001) state as an important contributor

to plume radiation. The combination states very likely are important at appropriate wavelengths. To our knowledge these states have not been included in previous or present plume modelling codes.

The results presented in this report indicate the large amount of information available from modern ab initio theoretical chemistry. Many transitions for which results were obtained during this project are not reported here simply due to the large amount of data involved. The reliability of the reported data is proportional to the magnitude of the transition, the larger probability processes being more accurately described. In many instances weaker processes could be predicted more reliably by doing more work. We had to obtain potential surfaces for three systems, and the amount of computer resources available subsequently limited the scope of the dynamical calculations. For example, rotational transitions are not reported, but with additional work they could be obtained quite reliably.

The primary deficiency of the dynamical methods used in this program involves the computation of final actions (quantum numbers) for low energy trajectories. This is particularly troublesome for the four-atom systems. Research presently in progress is leading to improved techniques, and within a year we expect to be able to obtain more accurate near-threshold cross sections. Averaging of cross section data over rotational distributions is desirable. Information is needed for transitions involving combination states of H_2 and CO_2 and for the other electronic surfaces for all of the systems studied. Newer theoretical methods that are being developed can be effectively used to improve the quantity and quality of cross section data required for plume modelling.

Section 7

REFERENCES

1. K. H. Wilson and C. E. Smith, "A Definitive Explanation of High Altitude Enhancement", TR LMSC-L030440.
2. M. G. Dunn, G. T. Skinner, and C. E. Treanor, "Infrared Radiation from H₂O, CO₂, or NH₃ Collisionally Excited by N₂, O, or Ar," AIAA Journal 13, 803 (1975); C. E. Kolb, M. Camac, R. B. Subbaro, and T. B. Anderson, "Experimental Studies of Collisional Excitation of Infrared Active Vibrational Stretch Modes in CO₂ and H₂O With an Intersecting, Hyperthermal Molecular Beam Apparatus", AFRPL-TR-75-2.
3. R. J. Bartlett and M. J. Redmon, "Collisional Excitation of H₂O and CO₂ by O(³P) Atoms," AFRPL-TR-81-27, February 1981.
4. J. C. Slater, Phys. Rev. 35, 210 (1930), Quantum Theory of Matter (McGraw-Hill, New York, 1968); V. Fock, Z. Physik 61, 126 (1930); D. R. Hartree, Proc. Cambridge Phil. Soc. 24, 89 (1928), The Calculation of Atomic Structures (Wiley, New York, 1957); C. C. J. Roothaan, Rev. Mod. Phys. 32, 179 (1960).
5. P.-O. Lowdin, Adv. Chem. Phys. 2, 207 (1959).
6. I. Shavitt, Methods of Electronic Structure Theory (Modern Theoretical Chemistry, Vol. 3) ed. by H. F. Schaefer (Plenum, New York, 1977) p. 189; B. O. Roos and P. E. M. Siegbahn, *ibid.*, p. 277; R. F. Hausman, Jr. and J. Paldus, The Unitary Group for the Evaluation of Electronic Energy Matrix Elements (Lecture Notes in Chemistry, Vol. 22) ed. by J. Hinze (Springer-Verlag, New York, 1981) p. 1; I. Shavitt, *ibid.*, p. 51.
7. K. A. Bruekner, Phys. Rev. 97, 1353 (1955), *ibid.* 100, 36 (1955) J. Goldstone, Proc. R. Soc. (London) Ser. A 239, 267 (1957); H. P. Kelly, Adv. Chem. Phys. 14, 129 (1969); R. J. Bartlett, Ann. Rev. Phys. Chem. 32, 359 (1981); B. H. Brandow, Rev. Mod. Phys. 39, 771 (1967).
8. R. J. Bartlett and I. Shavitt, Int. J. Quantum Chem. S11, 165 (1977).
9. I. Shavitt and L. T. Redmon, J. Chem. Phys. 73, 5711 (1980); L. T. Redmon and R. J. Bartlett, *ibid.* 76, 1938 (1982); M. G. Sheppard and K. F. Freed, *ibid.* 75, 4525 (1981); G. Hose and U. Kaldor, Phys. Scr. 21, 357 (1980).
10. A. C. Wahl and G. Das, Applications of Electronic Structure Theory (Modern Theoretical Chemistry, Vol. 3) ed. by H. F. Schaefer (Plenum, New York, 1977); Recent Developments and Applications of Multi-Configuration Hartree-Fock Methods (NRCC Proceedings, Vol. 10) ed. by M. Dupuis (Report LBL-12157, Lawrence Berkeley Laboratory, University of California, Berkeley, 1981); R. L. Shepard, I. Shavitt, and J. Simons, J. Chem. Phys. 76, 543 (1982).

11. P. J. Kuntz, in Dynamics of Molecular Collisions, Part B, Wm. H. Miller, ed., Plenum, N.Y. (1977).
12. M. J. Redmon and G. C. Schatz, "An Analytical Fit to an Accurate Ab Initio (1A_1) Potential Surface for H₂O," Chem. Phys. 54, 365 (1981).
13. G. C. Schatz and M. J. Redmon, "A Quasiclassical Trajectory Study of Collisional Excitation in O(3P)+CO₂," Chem. Phys. 58, 195 (1981).
14. M. J. Redmon, B. C. Garrett, and G. C. Schatz, "Theoretical Studies of Vibrational Excitation in Collisions of O(3P) With H₂O (1A_1)," Preprint.
15. G. A. Watson, ed., Numerical Analysis, Lecture Notes in Mathematics 630, Springer-Verlag (1977).
16. H. Rabitz, J. Chem. Phys. 57, 1718 (1972).
17. G. Zarur and H. Rabitz, J. Chem. Phys. 59, 943 (1973); 60, 633 (1974).
18. R. T Pack, J. Chem. Phys. 60, 633 (1974).
19. P. McGuire and D. J. Kouri, J. Chem. Phys. 60, 2488 (1974).
20. A. DePristo and M. H. Alexander, J. Chem. Phys. 63, 3552 (1975); 63, 5327 (1975); and 64, 3009 (1976).
21. S. I. Chu and A. Dalgarno, Proc. R. Soc. (London) A342, 191 (1975).
22. V. Khare, J. Chem. Phys. 68, 4631 (1978).
23. G. Bergerson, J. M. Launay and C. Leforestier, Chem. Phys. Lett. 59, 129 (1978).
24. G. A. Parker and R. T. Pack, J. Chem. Phys. 68 1585 (1978).
25. R. Goldflam, S. Green and D. J. Kouri, J. Chem. Phys. 67, 4149 (1977).
26. There are many references for the rotational IOS approximation. See, e.g., M. A. Brandt and D. G. Truhlar, Chem. Phys. Lett. 23, 48 (1973); R. T Pack, J. Chem. Phys. 60, 623 (1974); D. Secrest, J. Chem. Phys. 62, 710 (1975); J. M. Bowman and S. C. Leasure, J. Chem. Phys. 66, 288, 4724(E) (1977); R. Goldflam, S. Green, and D. J. Kouri, J. Chem. Phys. 67, 4149 (1977); G. A. Parker and R. T Pack, J. Chem. Phys. 68, 1585 (1978); V. Khare, D. J. Kouri, J. Jellinek, and M. Baer in: Potential Energy Surfaces and Dynamics Calculations, D. G. Truhlar, ed., (Plenum, New York, 1981) 475; J. Jellinek and M. Baer, J. Chem. Phys. 76, 4883 (1982); and references therein.
27. L. Monchick and E. A. Mason, J. Chem. Phys. 35, 1676 (1961); R. J. Cross and D. R. Herschbach, J. Chem. Phys. 43, 3530 (1965).
28. J. C. Light and R. B. Walker, J. Chem. Phys. 65, 4272 (1976); N. M. Harvey

- and D. G. Truhlar, Chem. Phys. Lett. 74, 252 (1980); E. B. Stechel, T. G. Schmalz, and J. C. Light, J. Chem. Phys. 74, 412 (1981).
29. See for example, D. G. Truhlar and J. T. Muckerman, Atom-Molecule Collision Theory: A Guide for the Experimentalist, R. B. Bernstein, ed., (Plenum, New York, 1979), p. 505.
 30. D. G. Truhlar, B. P. Reid, D. E. Zurawski, and J. C. Gray, J. Phys. Chem. 85, 786 (1981).
 31. R. A. Fifer, 17th Symposium (International) on Combustion, The Combustion Institute, 1979, pp. 587-599; and R. A. Fifer and H. E. Holmes, 16th JANNAF Combustion Meeting, Sept. 1979 (CPIA, 1980).
 32. D. G. Truhlar and B. C. Garrett, Accounts Chem. Res. 13, 440 (1980).
 33. B. C. Garrett and D. G. Truhlar, J. Phys. Chem. 83, 1079 (1979); 84, 682(E) (1980).
 34. B. C. Garrett and D. G. Truhlar, J. Amer. Chem. Soc. 101, 4534, 5207 (1979).
 35. B. C. Garrett, D. G. Truhlar, A. F. Wagner, and T. H. Dunning, J. Chem. Phys. 78, 4400 (1983).
 36. R. T. Skodje, D. G. Truhlar, and B. C. Garrett, J. Chem. Phys. 77, 5955 (1982).
 37. B. C. Garrett and D. G. Truhlar, "A least-action variational method for calculating multi-dimensional tunneling probabilities for chemical reactions," J. Chem. Phys., in press.
 38. T. H. Dunning, Jr., J. Chem. Phys. 53, 2823 (1970).
 39. S. Huzinaga, J. Chem. Phys. 42, 1293 (1965).
 40. L. T. Redmon, G. D. Purvis, and R. J. Bartlett, J. Am. Chem. Soc. 101, 2856 (1979).
 41. G. P. Quigley and G. J. Wolga, J. Chem. Phys. 63, 5263 (1975).
 42. T. H. Dunning, Jr., Chem. Phys. Lett. 7, 423 (1970).
 43. A. D. McLaine and G. S. Chandler, J. Chem. Phys. 72, 5639 (1980).
 44. R. G. Macdonald and C. B. Moore, J. Chem. Phys. 68, 513 (1978).
 45. Z. Karny, B. Katz, and A. Szoke, Chem. Phys. Lett. 35, 100 (1975).
 46. N. M. Harvey, Chem. Phys. Lett. 88, 553 (1982).
 47. B. C. Garrett, Chem. Phys. 00, 0000 (1984).

48. M. J. Redmon, B. C. Garrett, and L. T. Redmon, "Theoretical Predictions of Excitation Cross Sections for Collisions of HF, HCl, CO, H₂O, and CO₂ with O(³P)", Proceedings of the 14th JANNAF Plume Technology Conference at China Lake, CA (CPIA, 1984).
49. J. O. Chu, C. F. Wood, G. W. Flynn, and R. E. Weston, Jr., Chem. Phys. 80, 1703 (1984).

END

FILMED

10-84

DTIC